CHARACTERIZING CYTOKINE TRANSPORT IN HEMOADSORPTION BEADS USED TO TREAT SEPSIS

by

Jeremy David Kimmel

B.S. Cornell University, 2003

M.S. Polytechnic University, 2006

Submitted to the Graduate Faculty of the

Swanson School of Engineering in partial fulfillment

of the requirements for the degree of

Doctor of Philosophy

University of Pittsburgh

2011

UNIVERSITY OF PITTSBURGH

SWANSON SCHOOL OF ENGINEERING

This dissertation was presented

by

Jeremy David Kimmel

It was defended on

May 11th 2011

and approved by

Simon C. Watkins, Ph.D.
Professor, Departments of Cell Biology & Physiology and Immunology

John A. Kellum, M.D., FACP, FACM
Professor, Departments of Critical Care Medicine and Bioengineering

William R. Wagner, Ph.D.
Professor, Departments of Surgery, Bioengineering, and Chemical & Petroleum Engineering

Dissertation Director: William J. Federspiel, Ph.D.
Professor, Departments of Bioengineering, Chemical & Petroleum Engineering, and Critical Care Medicine

CHARACTERIZING CYTOKINE TRANSPORT IN HEMOADSORPTION BEADS USED TO TREAT SEPSIS

Jeremy David Kimmel, Ph.D.

University of Pittsburgh, 2011

Extracorporeal blood purification is a promising therapeutic modality for sepsis, a potentially fatal, dysfunctional immune disorder caused by infection. During sepsis, dysregulation of the innate immune system leads to excessive release of inflammatory mediators known as cytokines into the bloodstream. Removal of cytokines from the circulating blood may attenuate hyper-inflammatory signaling and promote immunologic homeostasis. We are developing an extracorporeal blood purification device to remove cytokines from the blood using biocompatible, porous, polymeric beads. Hemoadsorption therapy using our device has demonstrated improved survival in a murine sepsis model, and may serve as a novel adjuvant therapy to improve patient outcomes in the setting of severe sepsis and septic shock.

We developed a mathematical model to characterize cytokine adsorption dynamics within the device, and used confocal laser scanning microscopy (CLSM) to quantify cytokine transport within single sorbent beads. Finite element modeling was utilized to estimate model parameters based on best fits to CLSM data, and the fitted model was used to simulate cytokine adsorption behavior under clinically relevant conditions. We investigated intraparticle cytokine transport under competitive and non-competitive adsorption conditions, and demonstrated that effects due to coadsorption of serum solutes are likely negligible under physiologic cytokine concentrations.

CLSM results indicate that less than 20% of available sorbent surface area is utilized for cytokine adsorption.

Tumor necrosis factor (TNF) is a pleiotropic, pro-inflammatory cytokine, and serves as a primary initiator of systemic inflammation during sepsis. Removal of TNF within the device is slow, putatively due to hindered diffusion of the large TNF molecule (51kD) within the sorbent pores. We induced deoligomerization of trimeric TNF into its monomeric subunits, and demonstrated significantly accelerated capture of monomerized TNF within the device, compared to native TNF. We investigated small molecules capable of facilitating TNF deoligomerization, and proposed techniques to immobilize such molecules on the sorbent surface. Functionalized sorbent beads capable of locally dissociating TNF at the bead surface may significantly accelerate capture of TNF from the circulating blood. This concept could be expanded to enhance capture of oligomeric biomolecules using size exclusion filtration materials for a variety of disease states.

TABLE OF CONTENTS

LIST OF TABLES

LIST OF FIGURES

ACKNOWLEDGEMENTS

First and foremost, I would like to thank my mentor and dissertation advisor, Dr. William J. Federspiel, for his unwavering support and guidance throughout my graduate work at the University of Pittsburgh. Through his mentorship, I have learned the diligence and critical thinking skills necessary to become a successful scientist. He taught me that research sometimes takes you down unexpected paths, yet these challenges and setbacks are often what lead to remarkable scientific progress. I am excited to use all that I have learned while working with Dr. Federspiel, to help advance the field of bioengineering, and innovate new medical technologies that will improve patients' lives.

I would also like to thank my thesis committee members: Dr. William Wagner, Dr. John Kellum, and Dr. Simon Watkins, for their leadership and direction. They have been instrumental in helping to develop the work presented in this dissertation. In the hectic world of academic research, I greatly appreciate the time and energy they have dedicated to support my work.

I would like to extend my deepest appreciation to the members of the Medical Devices Laboratory for being great colleagues and friends. I was fortunate to be surrounded by an extraordinary group of graduate students, undergraduate students, and staff. Their willingness to share ideas, collaborate on projects, and brainstorm new directions provided constant support in my work. I am especially thankful for a great group of undergraduate students who were

instrumental in facilitating the research presented in this dissertation: namely Chris Lacko and Emma Harbert. I wish you both great success in your future endeavors.

I am indebted to various labs and collaborators throughout the university who were kind enough to share their time, expertise, and equipment with me. I greatly appreciate the staff at the Center for Biologic Imaging, Dr. Russell Delude, and Dr. Robert Parker for their support.

I would like to acknowledge my funding sources: the National Institutes of Health (Grant # HL080926-02) and Public Health Services (Grant # T32-HL07612403). Special thanks to Dr. Sanjeev Shroff, who appointed me as a predoctoral trainee in the Cardiovascular Bioengineering Training Program. His guidance and support have been instrumental in my graduate work.

Finally, I would like to thank my family and friends for their support and encouragement over the past years. Through the ups and downs of graduate school, a solid support framework has been essential for my professional and personal successes. I greatly appreciate my family's unwavering confidence and guidance. I hope that I have made them proud. Lastly, and most importantly, I am indebted to my loving wife, and best friend, Jen. Despite her enormous responsibilities as a medical resident during my graduate studies, she has been a source of constant support and dedication. I would never have been successful in this endeavor without her love and courage. We're a team in the best sense of the word, and she inspires me in all aspects of my life. I love you from the bottom of my heart.

1.0 INTRODUCTION

Sepsis is a serious medical condition characterized by systemic inflammation caused by infection, and affects more than 750,000 individuals per year in the US, with a mortality rate of 30% [1]. The pathophysiology of sepsis is complex and not entirely understood, but is believed to be related to the activity of multiple interdependent humoral mediator pathways [2]. Therapies aimed at blocking single mediators within the network of pathological processes, such as TNF antagonists [3], IL-1 antagonists [4], and anti-endotoxin antibodies [5], have failed to improve clinical outcomes. One promising strategy for the treatment of sepsis is nonspecific removal of inflammatory cytokines from the circulating blood [6]. Cytokines are ubiquitous inflammatory mediators that are substantially up-regulated during sepsis [7]. Elevated levels of circulating cytokines such as IL-6 and TNF are highly associated with increased risk of death [8]. Nonspecific removal of both pro-inflammatory (e.g. IL-6, TNF) and anti-inflammatory (e.g. IL-10) cytokines may provide a beneficial clinical effect by promoting overall down-regulation of systemic inflammation, and assisting the body in regaining immunologic homeostasis [9].

Our group is developing an extracorporeal hemoadsorption device to remove cytokines from the circulating blood using a novel, biocompatible, sorbent bead technology (CytoSorb™, CytoSorbents™, Inc.). CytoSorb hemoadsorption beads are polystyrene-divinylbenzene porous particles with a biocompatible polyvinyl-pyrrolidone coating. Adsorption to the internal pore surface is accomplished by a putative combination of nonspecific hydrophobic interactions, and

size exclusion of large molecular weight solutes such as albumin and immunoglobulins. This "semi-selective" approach is effective for broad-spectrum removal of cytokines and other small and middle molecular weight inflammatory mediators involved in the pathophysiology of sepsis. Kellum, *et al*. demonstrated rapid clearance of cytokines and increased mean survival time in a murine endotoxemia model using CytoSorb hemoadsorption beads [6]. Peng and colleagues further demonstrated short-term [10] and long-term [11] mortality benefit of CytoSorb hemoadsorption therapy in a murine cecal ligation and puncture (CLP) model of sepsis.

The first goal of the work presented in this dissertation was to characterize cytokine capture dynamics within the hemoadsorption beads (Chapters 3 & 4). Our group previously investigated cytokine removal dynamics within the cytokine adsorption device (CAD) by measuring temporal changes in cytokine concentrations in a reservoir during *in vitro* recirculation experiments [12]. However, this technique offered only macro-scale assesments of cytokine removal within the entire device, and did not provide insight into cytokine transport mechanisms within the beads. In this work, we sought to directly quantify adsorption behavior within single sorbent beads, and test the hypothesis generated from a mathematical model that minimal sorbent surface area participates in cytokine adsorption. We utilized fluorescently-tagged cytokines and confocal laser scanning microscopy (CLSM) to quantify transport within the hemoadsorption beads, and characterized the adsorption behavior in both single-component and multi-component solutions. Results from these studies will be used to optimize bead and device properties to maximize cytokine removal efficiency. Additionally, our mathematical model will be incorporated into large-scale inflammatory systems models to predict effects of cytokine removal dynamics on downstream physiological pathways.

The second goal of this dissertation was to develop techniques to accelerate removal of tumor necrosis factor (TNF) within the CAD (Chapters 5 & 6). TNF is a large oligomeric cytokine (51kD) that is an important initiator of systemic inflammatory processes [13], and high levels of circulating TNF have been directly correlated with increased mortality rates in sepsis [8]. TNF is on the cusp of molecular weight ranges excluded by the sorbent pore structure, hence, TNF removal is slow within the device. We sought to accelerate TNF capture through dissociation of oligomeric TNF into its smaller monomeric subunits, thereby enhancing diffusional rates into the sorbent pores, and increasing overall removal of TNF. We also examined small molecules capable of dissociating TNF that could be tethered to the sorbent surface as a localized mechanism for TNF deoligomerization within the device. This concept presents a novel technique for manipulating the quaternary structure of molecules to facilitate faster removal by size exclusion materials, while retaining an optimal pore structure for exlusion of necessary large proteins and cells.

Finally, we discuss future applications based on the concepts presented in this dissertation. The role of anti-TNF or anti-cytokine strategies for the treatment of sepsis remains elusive. However, blood purification is an attractive therapeutic modality for the removal of endogenous solutes as well as foreign toxins in a variety of disease states [14]. The primary results presented in this work: (1) mathematical modeling of protein transport within hemoadsorption beads, and (2) strategies to modulate the quaternary strucure of large solutes to accelerate capture within size exclusion filtration materials, may have applications outside the realm of sepsis. We hope that the concepts presented in this dissertation help to advance the field of sorbent blood purification, and lead to safe and effective technologies for the treatment of the critically ill.

2.0 BACKGROUND

2.1 SEPSIS

Sepsis can broadly be defined as a systemic inflammatory response to infection. It is the leading cause of death in the intensive care unit (ICU) [1], with mortality rates ranging from 27% to 54% in the case of septic shock [15]. Sepsis is estimated to affect at least 750,000 people per year in the United States, with total annual costs approaching $20 billion [1]. This rate of incidence is projected to increase by 1.5% per annum due to the growing elderly population [1]. Although clinicians and scientists have made significant advances in our understanding of the pathophysiology of sepsis over the past decades, there has been limited success of new treatment strategies. Sepsis remains one of the most elusive medical problems facing our society, and new therapeutic approaches are urgently needed.

2.1.1 Pathophysiology

Sepsis is a complex, dysregulatory immunologic state, characterized by interdependent changes in coagulatory, circulatory, and immunological systems. Although infection is typically the initial cause of sepsis, deleterious physiological effects have been linked to reaction of the innate immune system, not simply from the pathogen itself [16]. A generalized schematic of the progression of sepsis is shown in Fig. 1. The body mounts a normal response to infection

through recruitment of immune cells and increased production of inflammatory mediators. Various pathogenic products such as pathogen-associated molecular patterns (PAMPS) and lipopolysaccharide (LPS) trigger immune cell activation through complex receptor signaling (toll-like receptors, etc.) [17]. In response, these cells up-regulate production of pro-inflammatory mediators such as TNF, IL-1, and IL-6 [18]. Subsequent signaling pathways increase nitric oxide-mediated endothelial permeability [19], activate the coagulation cascade [20], and trigger production of anti-inflammatory cytokines (IL-10, IL-1ra) [21]. The synergistic effects of these physiological events at a systemic level induce vascular hypotension, tissue hypoxia, coagulopathy, and direct cell necrosis/apoptosis. Sepsis can be considered an exaggerated and dysfunctional response of the innate immune system to infection. Complex positive feedback signaling networks send the body into a vicious cascade of pathological events, ultimately leading to multiple organ failure, and often death.

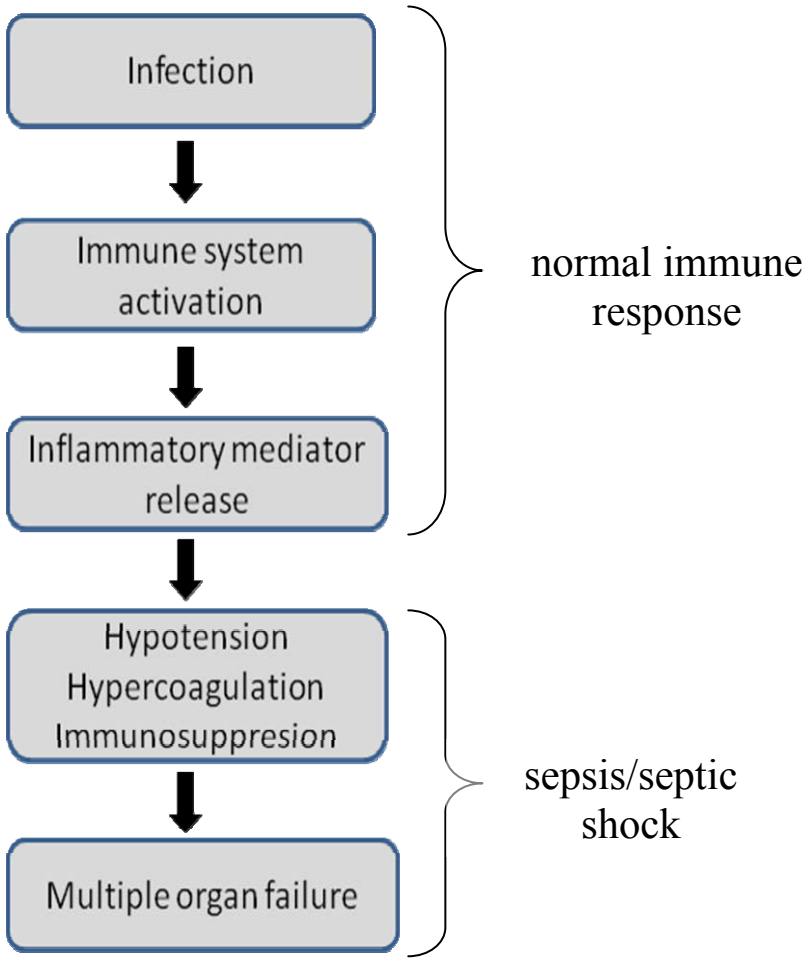

Figure 1: Generalized schematic of sepsis progression.

2.1.2 Clinical Indications & Definitions

In 2001, a consensus report was published by North American and European intensive care societies to formally delineate the various stages of sepsis [22]. Their goals were to assist with patient recruitment for clinical trials, and generate a more robust understanding of the pathophysiology and etiology of systemic inflammatory diseases. Table 1 summarizes the consensus definitions.

Table 1: Standard definitions of the clinical stages of systemic inflammation and sepsis, from the 2001 International Sepsis Definitions Conference.

Systemic inflammatory response syndrome (SIRS)	• Body temperature >38.5˚C or <35.0˚C • Heart rate >90 beats per min • Respiratory rate >20 breaths per min, or arterial CO_2 tension <32mmHg • White blood cell count >12,000/mm^3 or <400/mm^3
Sepsis	SIRS and documented infection
Severe sepsis	Sepsis and at least one sign of organ dysfunction
Septic shock	Severe sepsis and acute circulatory failure (mean arterial pressure <60mmHg)

2.1.3 Hypercytokinemia

Sepsis is characterized by excessive and sustained release of inflammatory cytokines in the tissues and circulating blood, a condition known as hypercytokinemia [23]. Immune cell activation via toll-like receptor pathways causes up-regulated production of nuclear factor κB (NFκB), a primary transcription factor which controls release of pro-inflammatory mediators such as TNF, HMGB-1, and various interleukins [18]. Abundant release of pro-inflammatory cytokines in response to the initial pathogenic assault is followed by counterproduction of anti-inflammatory cytokines such as IL-10 and IL-1 receptor antagonist [24]. Positive feedback signaling between these two pathways results in sustained and uncontrolled mediator production, thought to be a significant contributor to downstream organ damage and mortality [25].

Numerous pharmacologic interventions have been developed to attenuate the initial pro-inflammatory response, such as corticosteroids [26], TNF antagonists [3], anti-endotoxin

antibodies [5], and IL-1 receptor antagonists [4]. Although animal models demonstrated benefit from use of such interventions, human clinical trials have largely been unsuccessful [27-28]. One hypothesis for the clinical failure of pro-inflammatory inhibitors is that the concept essentially ignores significant pathophysiological contributions from the counterregulatory anti-inflammatory response [29]. Evidence has suggested that an over reactive anti-inflammatory response to the initial pathogen-induced pro-inflammatory state results in significant immunosupression [23]. The majority of septic patients often survive the initial infectious insult, only to succumb to nosocomial infection days or weeks later [30].

A hypothetical example of sepsis-induced immunologic dysregulation is illustrated in Fig. 2. In one patient (solid line), the initial hyperimmune response to infection is followed by a brief state of hypoimmunity, although the body eventually returns to a homeostatic level and survives. In a different patient, the hyperimmune response is followed by sustained immunosupression, either leading to recovery or death. This prolonged state of "immunoparalysis" often leads to death via severe nosocomial infections [31] or reactivation of dormant viruses [32]. The complex interplay between hyper and hypo immune states during sepsis has been a primary challenge in the development of effective mediator-targeted therapies [27]. Whereas one patient in the hyperimmune phase may benefit from pro-inflammatory inhibitors, immunostimulation therapy for patients experiencing a prolonged anti-inflammatory state may be beneficial. Difficulties in establishing treatment strategies are further compounded due to variable timing of patient presentation; i.e. the cytokine cascade is often fully activated by the time patients seek hospital care [8]. Thus, point-of-care data on patient-specific immunologic trajectories would be beneficial for tailoring appropriate immuno-modulatory therapies.

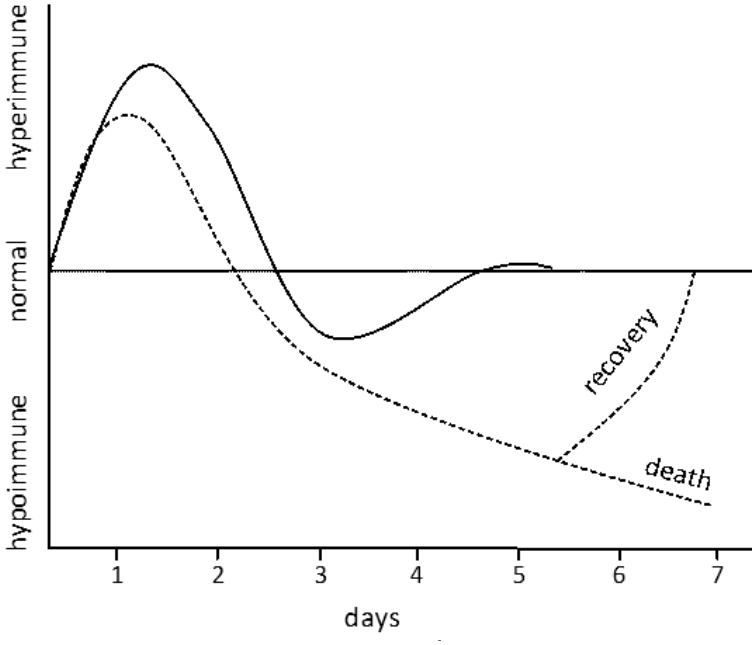

Figure 2: Immunologic responses in the setting of severe sepsis. Adapted from Hotchkiss, *et al.* [29]

2.2 CURRENT TREATMENT STRATEGIES

2.2.1 Intensive Care Management

Sepsis and septic shock treatment in the intensive care unit (ICU) is primarily focused on three goals: (1) hemodynamic support, (2) eradication of the infectious agents, and (3) adequate organ perfusion and function [33]. Clinical guidelines published by the Surviving Sepsis Campaign aimed to define standards of care in severe sepsis and septic shock [34]. Their recommendations included: broad-spectrum antibiotic therapy, crystalloid or colloid fluid resuscitation, vasopressor guidelines, inotropic therapy, and other adjuvant therapies.

Rivers *et al.* published a landmark study in 2001, demonstrating improved clinical outcomes using early-goal directed therapy upon patient admission to the emergency department [35]. This work was predicated on evidence that global tissue hypoxia is a key factor preceding development of multi-organ failure and death [36]. They demonstrated that a goal-oriented resuscitation strategy focused on oxygen delivery and demand, implemented within the first six hours of emergency department admission, significantly improved morality outcomes in patients with severe sepsis or septic shock. Early-goal directed therapy (EGDT) has now been accepted as standard of care for the initial treatment of sepsis [34].

2.2.2 Pharmaceuticals

Numerous pharmacologic interventions have been evaluated for their efficacy in the treatment of sepsis. As previously discussed, strategies to blunt the pro-inflammatory response have largely been unsuccessful in improving patient outcomes, despite promising results from preclinical models [37]. As our understanding of the pathophysiology of sepsis has grown over the past decades, the role of sepsis-induced immunosupression has gained traction as an important factor in mortality/morbidity [38]. Immunostimulation therapy using interferon-γ improved survival in a subgroup of patients with sepsis [39], however, other immune system activating agents such as granulocyte colony stimulating factor (GC-SF) [40-41] have generated disappointing clinical results.

Therapies aimed at attenuating sepsis-induced hypercoagulation have shown mixed results in clinical trials. Anticoagulant agents such as antithrombin III [42] and tissue factor pathway inhibitor [43] failed clinical trials. Activated protein C (drotrecogin alpha) demonstrated significant mortality reduction in a large, controlled trial [44], and is currently the

only FDA approved drug for the treatment of sepsis. However, enormous controversy surrounded the results of the trial [45], and a second study investigating APC in patients with severe sepsis and low risk of death was terminated early due to lack of mortality benefit [46]. According to the Surviving Sepsis Campaign guidelines, use of recombinant APC should be limited to patients at high risk of death and low risk for bleeding complications [34].

2.3 BLOOD FILTRATION

Despite significant advances in our understanding of the underlying cellular and molecular mechanisms during sepsis, therapies targeting specific immunologic mediators have largely been unsuccessful [27]. Due to the complex interplay of various competing and often synergistic pathophysiological pathways, non-specific removal of multiple mediators from the blood may serve as novel therapy by promoting global immunologic homeostasis [47]. A multitude of extracorporeal blood filtration modalities have been developed in recent years, many of which have demonstrated potential benefit in preclinical and clinical trials of severe sepsis [14, 47-48]. Japan, in particular, has embraced blood filtration as a clinical tool in the treatment of sepsis and other critical care diseases [49], although further large scale trials are necessary for widespread acceptance of these technologies [50].

Many hypotheses have been proposed regarding the effects of blood filtration during systemic inflammatory disorders. Honoré and Matson [51] suggested that removal of cytokines from the blood leads to cytokine depletion in the tissues, due to concentration gradients between the two compartments. Ronco and colleagues [52] postulated that cytokine removal during the early pro-inflammatory phase could stop the inflammatory cascade, and limit subsequent organ

damage. Peng and colleagues [53] suggested that blood filtration modulates function of inflammatory cells, with significant effects on leukocyte trafficking and bacterial clearance from the tissues.

2.3.1 Endotoxin Removal using Polymyxin B

Lipopolysaccharide (LPS) is a bacterial endotoxin found in the cell membrane of Gram-negative bacteria. High concentrations of endotoxin in the circulating blood have been associated with increased mortality rates in severe sepsis [54], and LPS has been shown to be an important trigger of the pro-inflammatory innate immune response [55]. Hence, there is significant interest in systemic removal of LPS from the blood as a potential treatment for Gram-negative sepsis [56]. Polymyxin B is an antibiotic that binds and neutralizes endotoxin, although clinical use has been limited due to acute toxicity [57]. However, immobilization of polymyxin B on solid supports within an extracorporeal device has been shown to remove endotoxin without leaching polymyxin B into the circulating blood [58].

Endotoxin removal using a polymyxin B blood filtration device (Toraymyxin) has been used widely in Japan since 1994. However, widespread use of the device has been limited due to lack of large scale clinical trials. In 2005, the first European randomized controlled trial (RCT) reported results using polymyxin filtration in sepsis [59]. They demonstrated improvement in cardiac function and hemodynamics status, but found no significant changes in either endotoxin concentration or 28-day mortality. More recently, a multicenter RCT in Italy reported improvement in hemodynamic parameters and reduction in 28-day mortality using polymyxin B hemoperfusion in the setting of severe sepsis or septic shock [60]. However, the study has been criticized due to significance of the clinical endpoints, and the fact that the trial was stopped

early due to a ruling by the hospital ethics committee [61]. Additional trials are currently underway using polymyxin B hemoperfusion [62-63], and further analysis of safety and clinical benefit are necessary for widespread acceptance of the technology.

2.3.2 Hemofiltration

Hemofiltration refers to convective removal of solutes from the blood using semi-permeable membranes. Selectivity is based on solute molecular size – large solutes are excluded from entering the porous membrane, while smaller solutes pass through the membrane pores and into a separate fluid channel. Hemofiltration is a promising adjuvant treatment modality for sepsis due to the non-specific nature of solute removal. As previously discussed, therapies aimed at blocking individual pro- or anti-inflammatory mediators have not demonstrated clinical efficacy. Broad-spectrum removal of multiple immunologic mediators (e.g. cytokines, chemokines) may have a beneficial effect by modulating the excessive innate immune responses towards a state of homeostasis.

Standard "renal dose" continuous hemofiltration [25-30 mL/kg/hr] appears to be ineffective in the treatment of sepsis [64-65]. However, high volume hemofiltration (HVHF) [>35 mL/kg/hr] has shown promise as a therapeutic tool due to accelerated rates of mediator clearance from the plasma, compared to conventional hemofiltration [66]. Numerous clinical studies have demonstrated beneficial effects of HVHF on hemodynamic parameters [67-68] and expected mortality [69-70], although further large scale RCTs are necessary to support clinical efficacy of HVHF in the treatment of sepsis and septic shock [47]. In recent years, additional hemofiltration technologies have been developed, such as cascade hemofiltration [71], coupled plasma filtration adsorption (CPFA) [72], high cut-off hemofiltration/hemodialysis [73], and

high-adsorption hemofiltration [74]. Although stand-alone hemofiltration therapies such as those described above may prove to be safe and effective for the treatment of severe sepsis, synergistic effects of combined technologies (e.g. high volume + high adsorption hemofiltration) may elucidate new concepts for blood filtration in the critically ill [75].

2.3.3 Hemoadsorption

Hemoadsorption refers to removal of blood solutes through direct adsorption to sorbent materials, typically through hydrophobic, electrostatic, or van der Waals' interactions [76]. In contrast to hemofiltration, hemoadsorption offers two important advantages: (1) extremely high material surface area, and (2) self-regulating solute removal via concentration dependent diffusion. Due to highly interconnected porous networks, sorbent materials offer far greater surface area than standard hollow fiber hemofiltration membranes. This distinction is critical given recent evidence that cytokine removal using hemofiltration is predominantly due to adsorption on the filter surface [77]. As a result of limited surface area of standard hemofilters, cytokine removal efficiency rapidly decreases over time due to saturation of the filter [78]. An additional benefit of sorbent-based blood filtration is self-regulating solute removal, i.e. rate of removal is dependent on solute concentration in the blood. In contrast to convective removal using hemofiltration, diffusion-mediated hemoadsorption provides a regulated removal mechanism, which may be more effective in modulating blood mediator levels towards homeostasis.

Although sorbent blood filtration has existed for decades, recent innovations in sorbent biocompatibility and tunable pore structure have piqued interest in using hemoadsorption as an adjuvant therapy for severe sepsis [76]. CTR (Kaneka Corporation) is a sorbent comprised of

cellulose beads functionalized with a hydrophobic ligand, and has been shown to effectively remove small and middle molecular weight molecules such as cytokines and bacterial toxins *in vitro* [79]. Additionally, hemoadsorption therapy using CTR significantly reduced mortality rates in an endotoxemic rat model [79]. CytoSorb™ (CytoSorbents, Inc.) are polystyrene-divinylbenzene sorbent beads with a biocompatible polyvinyl-pyrrolidone coating. Kellum and colleagues demonstrated rapid cytokine removal and improved survival in an endotoxemic rat model using CytoSorb hemoadsorption therapy [6]. Furthermore, they utilized a physiologically relevant cecal ligation & puncture (CLP) septic rat model, and demonstrated reduction in circulating cytokines, improved mean arterial pressure, and improved short-term survival compared to sham treatment [10].

3.0 INVESTIGATING CYTOKINE ADSORPTION DYNAMICS USING CONFOCAL LASER SCANNING MICROSCOPY

A robust understanding of cytokine capture within the hemoadsorption device is necessary to optimize device performance. Aspects such as clinical operational parameters and downstream physiological effects *in vivo* are predicated on cytokine removal dynamics within the device. Our group previously characterized cytokine removal using simple mass balance methodology: temporal changes in cytokine concentration in a reservoir were measured during *in vitro* recirculation capture using small sorbent cartridges, where mass of cytokine removed from the reservoir was assumed to be captured by the sorbent beads [12]. Although this technique offered a generalized model of cytokine removal dynamics, we sought to directly measure cytokine adsorption within single sorbents beads as direct validation of model predictions.

Kellum, *et al.* demonstrated rapid clearance of cytokines and increased mean survival time in a murine sepsis model using CytoSorb hemoadsorption beads [6]. They measured cytokine removal using cytokine-rich blood from rats challenged with endotoxin, in an *ex vivo* circuit containing a hemoadsorption column packed with 10g of CytoSorb beads. A similar circuit and endotoxin challenge was used for *in vivo* experiments to determine effects from hemoadsorption therapy on the inflammatory response and survival. IL-6, IL-10, and TNF were rapidly removed by the device, with <50% of the initial concentrations present after 1hr of recirculation. Despite significant cytokine removal rates observed in the study, a model analysis

performed by our group predicted that cytokine adsorption is limited to the outer ~15μm of the sorbent particle over a clinically relevant time period (4-6 hours). Given the large diameter of CytoSorb beads (450μm), this prediction suggested that less than 20% of the sorbent surface area participates in cytokine adsorption. To test this hypothesis, we utilized confocal laser scanning microscopy (CLSM) to quantify adsorption of fluorescently labeled cytokine within single sorbent beads. CLSM was first applied to studies of adsorption in sorbent materials by Ljunglöf and Hjorth [80], and provides a powerful tool for direct visualization and quantification of fluorescently labeled proteins adsorbed within sorbent particles. Numerous authors have utilized CLSM to study protein uptake phenomena in packed-bed chromatography sorbents [21, 81-87]. Hubbuch, *et al.* [88] provides an extensive review of CLSM as an analytical tool in chromatographic research.

In this study, CLSM was used to quantify IL-6 adsorption dynamics in CytoSorb hemoadsorption beads, and to compare intraparticle spatial adsorption profiles to predictions of our previous mathematical model [12]. Our application of CLSM differs from previous sorbent CLSM studies in two important aspects: 1) CytoSorb beads are significantly larger than sorbents typically characterized using CLSM (450μm compared to 90μm average particle diameter, respectively) [88]; and 2) physiological cytokine levels found in human sepsis are significantly smaller than protein concentrations typically used in sorbent applications (~pg/ml compared to ~mg/ml, respectively) [6, 88]. Accordingly, in our study we developed new strategies to minimize signal attenuation within the bead, to study cytokine-fluorophore degree of labeling, and to examine effects of bulk cytokine concentration on adsorption.

3.1 MATERIALS & METHODS

3.1.1 Materials

Lyophilized recombinant human IL-6 (MW = 21kD, >95% purity) and DyLight™ 549 fluorescent labeling kits were purchased from Thermo Scientific (Rockford, IL). DyLight 549 is an N-hydroxysuccinimide (NHS) ester activated fluorophore (MW = 982Da) that reacts with primary amines on the target protein to form stable, covalent bonds. The DyLight 549 fluorophore has an excitation and emission maxima of 562nm and 576nm, respectively. Bovine serum albumin (MW = 66kD, >96% purity) was used as a negative control, and was purchased from Sigma Aldrich (St. Louis, MO). Low molecular weight impurities were eliminated by running BSA (1mg/ml) in 10mM PBS through a Superdex™200 gel permeation column (AKTAexplorer FPLC, GE Healthcare) at 0.1ml/min flow rate. The 66kD major protein component was collected and used for all subsequent BSA fluorescent labeling.

3.1.2 Fluorescent Labeling

Lyophilized recombinant human IL-6 (20µg) was reconstituted in 0.5ml 10mM PBS and fluorescently labeled with the DyLight 549 fluorophore as follows: 15µg dried fluorophore was reconstituted in 100µl 10mM PBS and 8µl 0.67M sodium borate buffer, as recommended by the manufacturer. Reconstituted fluorophore (either 50µl or 5µl) was added to 250µl reconstituted IL-6 in PBS and incubated in the dark for 60min. Unreacted fluorophore was removed using resin spin columns provided by the manufacturer. Protein-fluorophore degree of labeling (DOL)

could not be directly measured due to low cytokine concentrations used in this study. The FPLC purified BSA was fluorescently labeled in the same manner as IL-6.

3.1.3 Bead Preparation

CytoSorb hemoadsorption beads were provided by CytoSorbents, Inc. (Monmouth Junction, NJ). CytoSorb beads are polystyrene-divinylbenzene porous particles (450μm avg. particle diameter, 67% porosity, 1.02g/cm^3 density, 0.8-5nm pore diameter, 850m^2/g surface area) with a biocompatible polyvinyl-pyrrolidone coating. Fluorescently labeled IL-6 was incubated with CytoSorb beads as follows: Labeled IL-6 was diluted in 10mM PBS with BSA (10mg/ml) added as a stabilizing protein, to yield final IL-6 concentrations of approximately 1μg/ml, 0.1μg/ml, and 0.01μg/ml. 1mg CytoSorb bead mass was added to each 1ml aliquot, and samples of each IL-6 concentration were placed on a rocker shielded from light for 2, 5, and 18 hours, at ambient temperature. Labeled BSA was added to 1mg CytoSorb bead mass in 1ml PBS to yield a BSA concentration of approximately 20μg/ml. BSA samples were placed on a rocker shielded from light for 2, 5.5, and 21.5 hours, at ambient temperature. At the end of each incubation time point, beads were removed from the corresponding sample, and manually sliced in half using a thin razor blade. Beads that were sliced exactly or as close to the particle centerline as possible were selected for CLSM analysis. Sliced beads were placed sliced side down on a glass cover slip in a droplet of PBS, and imaged using CLSM, as follows.

3.1.4 Confocal Microscopy

A schematic of the confocal setup with a sliced CytoSorb bead is illustrated in Fig. 3. An Olympus FluoView^{TM} FV1000 confocal microscope outfitted with a UPlanSApo 20X/.75 oil objective and a HeNe laser (543nm excitation, 572nm emission) was used for all confocal imaging. During image capture, the microscope objective was focused such that the confocal plane was localized within the bead, close to the sliced edge to minimize signal loss through the bead. Images were acquired by horizontal scan at 1024x1024 pixel resolution, corresponding to 0.621μm pixel size. Digital images of sliced beads were analyzed using ImageJ software (National Institutes of Health), and intraparticle signal intensity profiles were generated by quantifying a horizontal segment of the image across the diameter of each bead (4 - 5 beads were imaged at each incubation time point). Beads incubated in PBS/BSA buffer without fluorescently labeled IL-6 were sliced and imaged as a control, and background signal was found to be negligible.

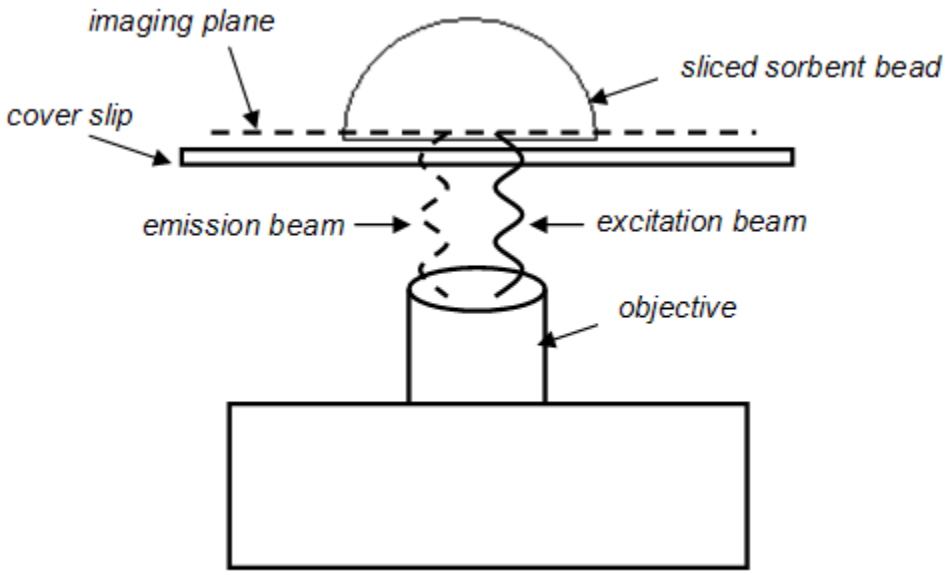

Figure 3: Schematic of a sliced CytoSorb bead in the confocal microscope setup.

3.1.5 Data Analysis

DiLeo, *et al.* developed a simple model analysis to study cytokine adsorption dynamics within CytoSorb hemoadsorption beads [12]. The model predicts the following intraparticle cytokine adsorption profile:

$$\frac{q(r,t)}{q_o} = 1 - erf\left[\sqrt{\frac{\rho\alpha}{4t}}(R-r)\right] \qquad \text{(Eq. 1)}$$

where $q(r,t)$ is the mass of cytokine adsorbed on the internal pore surface per unit bead mass, q_o is the mass of cytokine adsorbed on the particle surface, ρ is the bead mass density, and R is radius of the bead. The model is concentration dependent, where adsorbed cytokine (q) is proportional to free cytokine (c) through the Langmuir adsorption isotherm, $q = {}^{q^{\max} Kc}/_{1+Kc}$. The mathematical model contains one unknown parameter, $\alpha = {}^{q^{\max} K}/_{D}$, where q^{max} and K are

Langmuir adsorption isotherm parameters, and D is the effective diffusion coefficient of the cytokine within the porous bead matrix. In our application, signal intensity generated by fluorescently labeled IL-6 within the sorbent particle is predominantly due to adsorbed rather than free cytokine, due to the large sorbent surface area and low bulk cytokine concentrations. Accordingly, the value of α was estimated at each incubation time point by fitting Eq. 1 to intraparticle IL-6 CLSM fluorescence intensity curves using nonlinear least squares regression in Matlab^{TM}, with $\rho = 1.02 g/cm^3$. Intraparticle signal intensity profiles for each bead were normalized by dividing the signal intensity value at each pixel by the maximum signal intensity value found at the edge of each bead. Student's t-test was used to evaluate any statistical differences between the fitted α values.

3.2 RESULTS

3.2.1 IL-6 Adsorption Profiles

A CLSM image illustrating adsorption of fluorescently labeled IL-6 within a CytoSorb hemoadsorption bead after 5 hours incubation is shown in Fig. 4. IL-6 adsorption is limited to the outer most pores where a thin ring of fluorescence is observed penetrating into the bead from the bead surface. No signal is detected near the center of the particle.

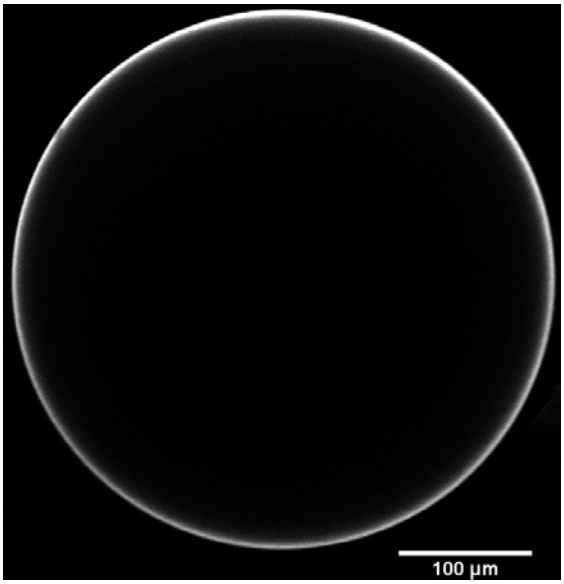

Figure 4: CLSM image of a CytoSorb bead after 5hr incubation with fluorescently labeled IL-6.

Intraparticle intensity profiles for IL-6 at 2hr, 5hr, and 18hr incubation at 1μg/ml are illustrated in Fig. 5(a). Intensity is normalized by the maximum intensity found at the bead surface (I_{max}), where $I_{max} \sim q_o$ from Eq. 1. Normalized intensity is greatest at the bead surface ($I/I_{max} = 1$), and quickly decays as IL-6 diffuses into the sorbent and adsorbs to the pore walls. The protein front slowly moves through the particle over time, yet even after 18hr incubation time, IL-6 does not penetrate farther than 30μm into the bead. Intraparticle intensity profiles for labeled BSA at 2hr, 5.5hr, and 21.5hr incubation are illustrated in Fig. 5(b). In contrast to the behavior observed for IL-6, BSA does not continually penetrate into the bead over time. The mathematical model (Eq. 1) was fit to the IL-6 CLSM curves at each time point, as shown by the solid lines in Fig. 5(a). Good agreement exists between the model fits and the CLSM data ($R^2 > 0.98$ for all fits). Fig. 6 illustrates fitted values for the model parameter α at each time point. The α values were not statistically different between any two IL-6 incubation time points ($p > 0.1$).

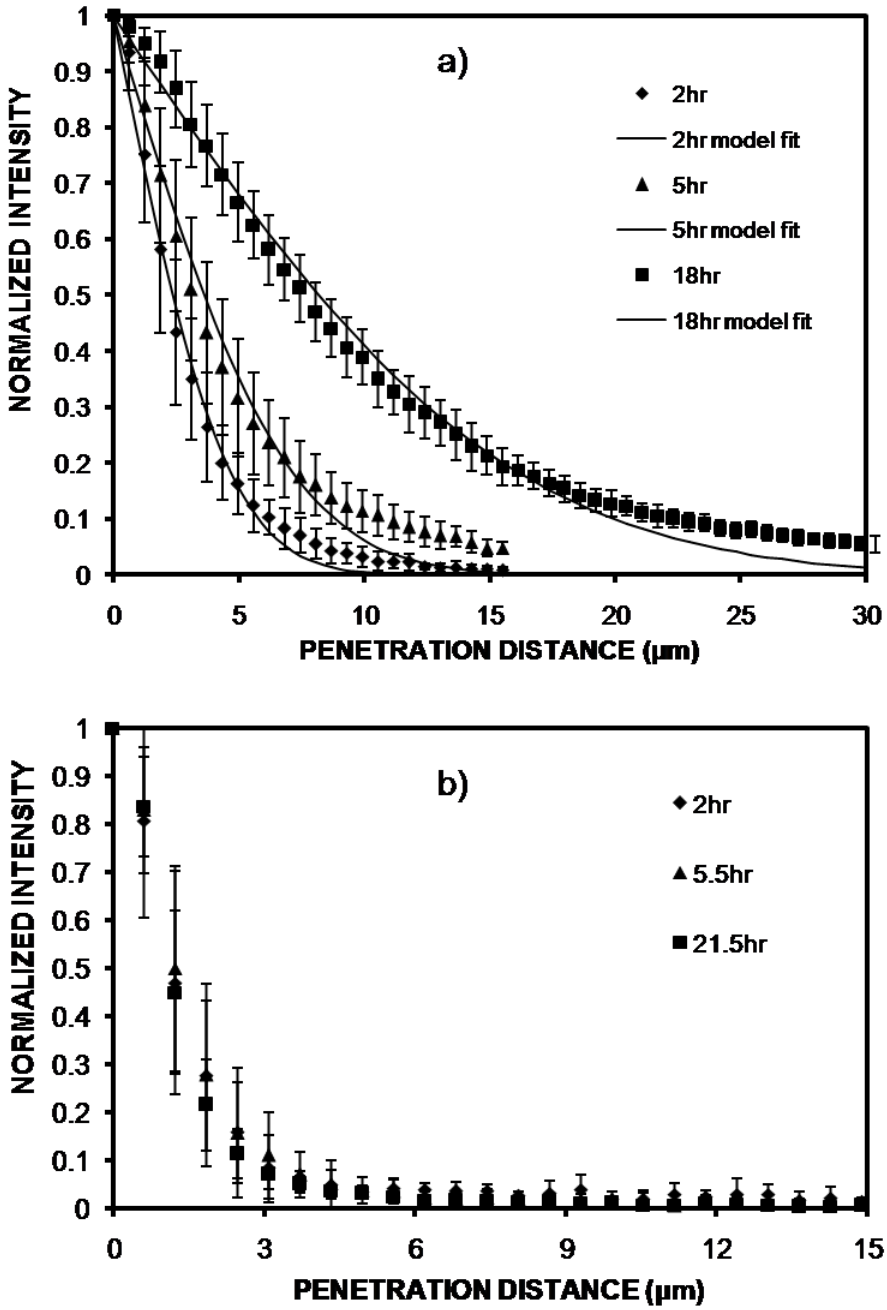

Figure 5: (a) Normalized IL-6 CLSM intraparticle intensity profiles at 2hr, 5hr, and 18hr incubation times, with corresponding nonlinear regression model fits. (b) Normalized BSA CLSM intraparticle intensity profiles at 2hr, 5.5hr, and 21.5hr incubation times.

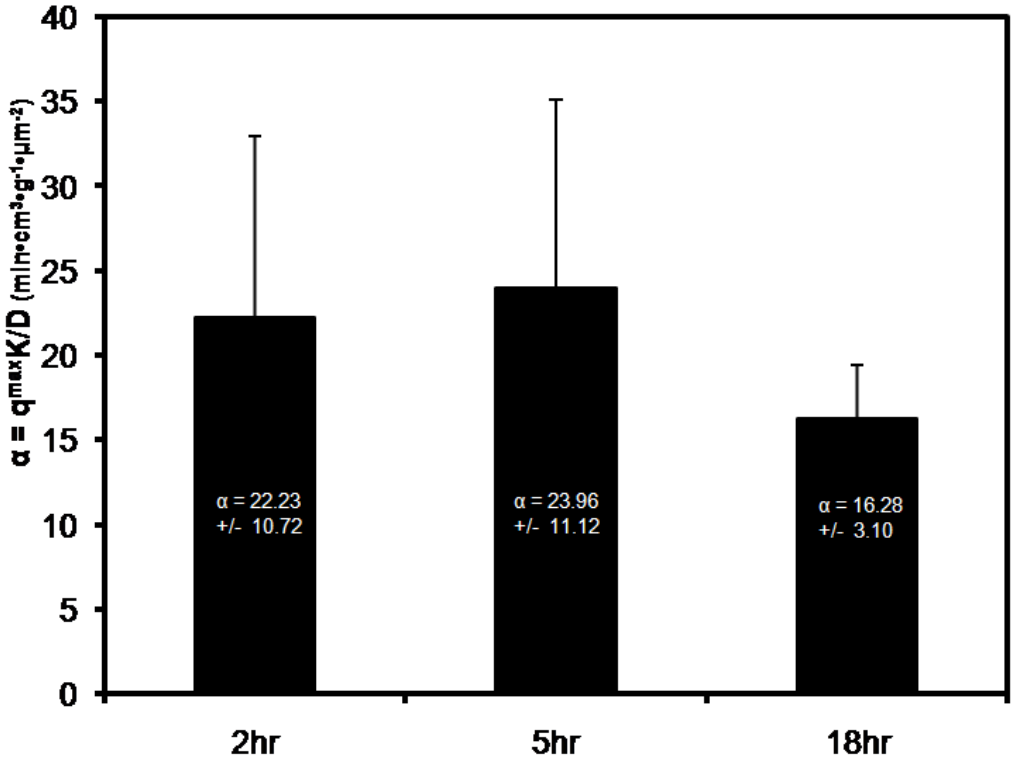

Figure 6: α values estimated by best fit of the model to IL-6 CLSM intensity profiles. The α values were not statistically different ($p > 0.1$) for any two incubation time points tested.

3.2.2 Effect of Bulk IL-6 Concentration

Labeled IL-6 concentrations were varied to confirm that normalized adsorption profiles were independent of bulk IL-6 concentration. Fig. 7(a) illustrates intraparticle IL-6 intensity profiles for CytoSorb beads incubated for 5hr with 1μg/ml, 0.1μg/ml, and 0.01μg/ml labeled IL-6. Similar penetration curves were observed for all concentration values tested. Intensity profiles were fit to the mathematical model (Eq. 1), and α was estimated by best fit of the model to the CLSM data (Fig. 7(b)). The α values were not statistically different between any two bulk IL-6 concentrations tested ($p > 0.49$).

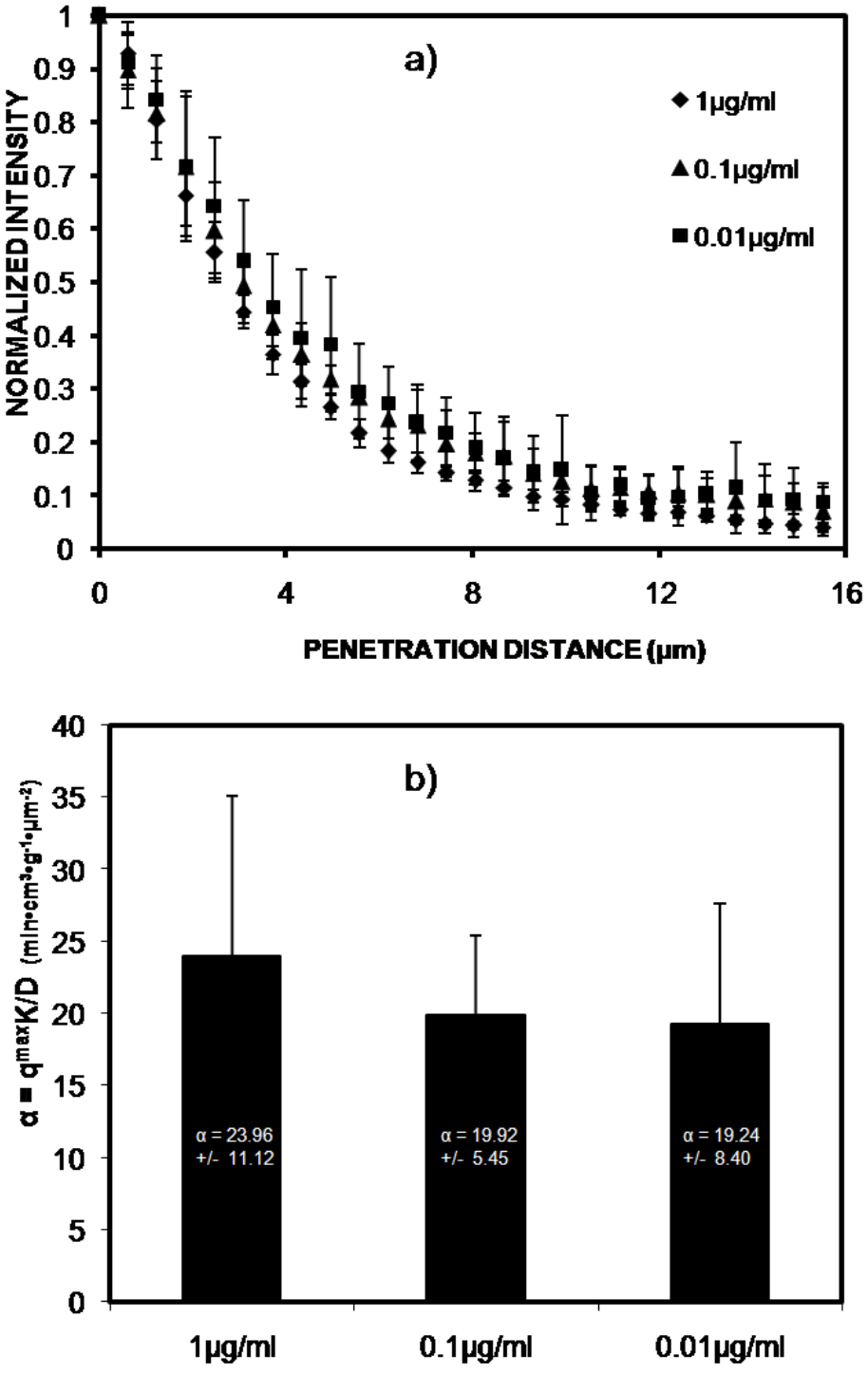

Figure 7: (a) Intraparticle intensity profiles for various concentrations of labeled IL-6 incubated for 5 hours with CytoSorb beads. (b) Corresponding α values were not statistically different for any two IL-6 concentrations tested ($p > 0.49$).

3.2.3 Effect of Fluorophore Labeling on IL-6 Adsorption

We tested whether the degree of labeling (DOL) affected IL-6 adsorption by reducing the DOL during the fluorophore-cytokine conjugation step. The DOL was decreased by reducing the volume of fluorophore added to IL-6 during conjugation [89]. Fig. 8 illustrates the maximum intensity values at the bead surface after 5hr incubation with IL-6 labeled using either 5µl or 50µl fluorophore. Beads incubated with IL-6 conjugated with less fluorophore demonstrated lower maximum intensity values. This indicates a lower DOL for IL-6 samples conjugated with 5µl fluorophore since the same IL-6 concentration and imaging parameters were used for both DOL conditions. As demonstrated in Fig. 9(a), the low DOL (5µl fluorophore) and the high DOL (50µl fluorophore) IL-6 intensity profiles are similar after 5hr incubation. The curves were fit to the mathematical model (Eq. 1) to determine α values (Fig. 9(b)). The α values were not statistically different between the two DOL conditions ($p > .25$).

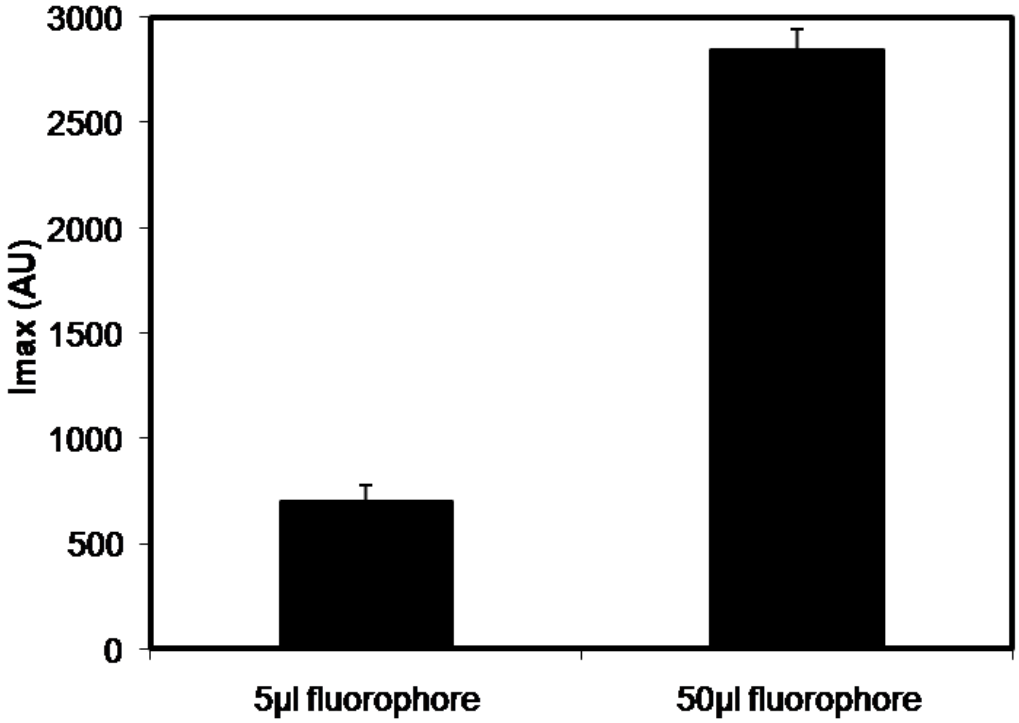

Figure 8: Comparison of maximum intensity values at the bead surface under different IL-6 labeling conditions.

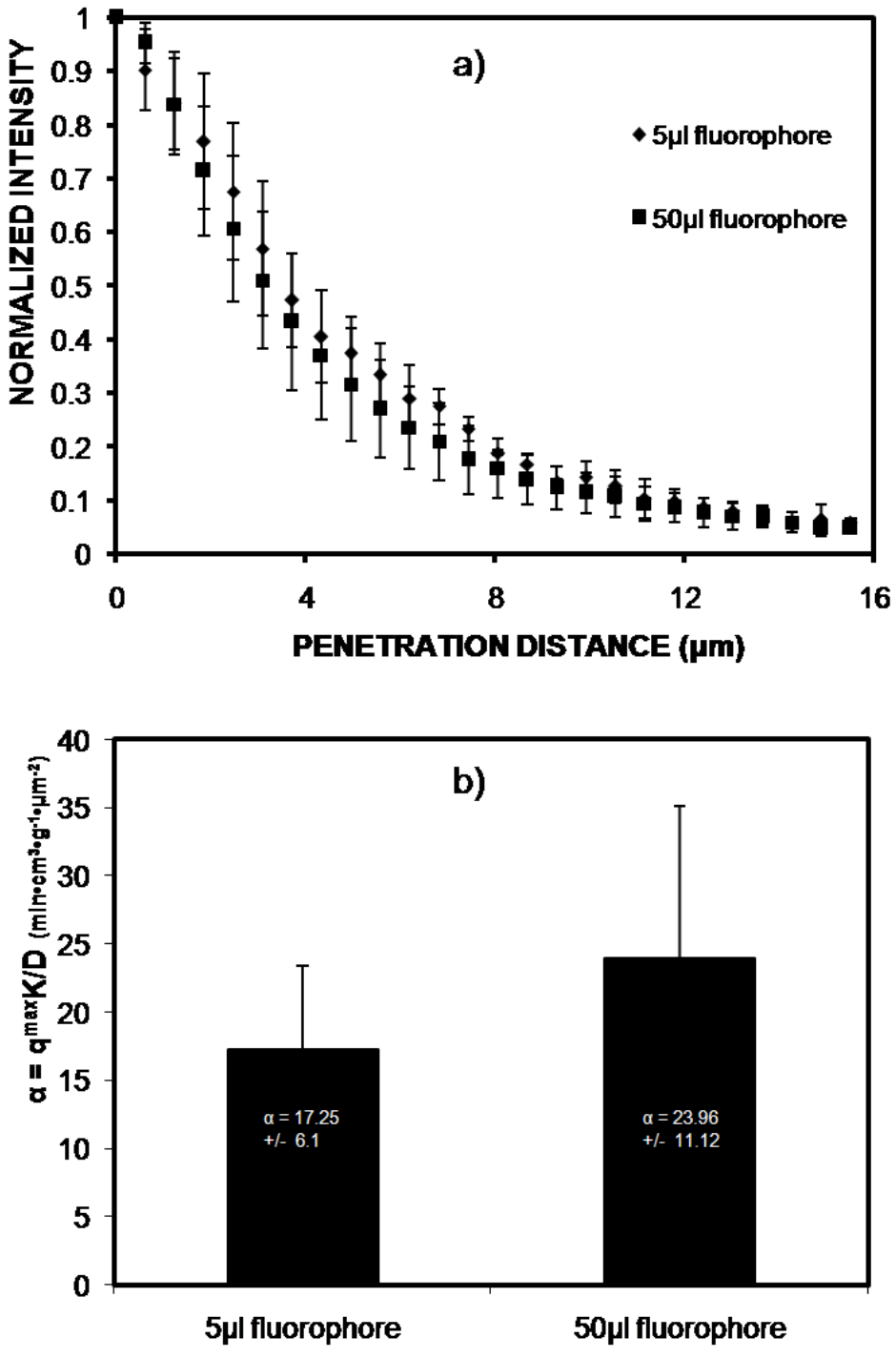

Figure 9: (a) Normalized IL-6 intraparticle intensity profiles for 5µl and 50µl labeling conditions after 5hr incubation with CytoSorb beads. (b) Corresponding α values were not statistically different (p > .25) between the DOL conditions.

3.3 DISCUSSION

The goal of this work was to examine the dynamics of cytokine adsorption within single sorbent particles using confocal laser scanning microscopy (CLSM). Results indicate that IL-6 adsorption dynamics can be modeled using classical adsorption/diffusion mechanisms, and a single model parameter, $\alpha = q^{\max} K / D$, can characterize interactions between IL-6 and CytoSorb beads, where q^{max} and K are Langmuir adsorption isotherm parameters, and D is the effective diffusion coefficient within the porous matrix. After 5hr incubation with sorbent beads, IL-6 adsorption was limited to the outer 15μm of the pore structure, which represents use of less than 20% of available surface area for adsorption. The CytoSorb pore structure was designed to exclude large molecular weight solutes such as albumin and immunoglobulins. We confirmed that BSA (66kD) does not penetrate appreciably into the sorbent due to size exclusion of BSA from the internal pore structure.

In our previous work in which the mathematical model was developed [12], we fit our model to *ex vivo* data on cytokine removal from septic rat blood circulated through a hemoadsorption device containing the same CytoSorb beads [90]. We have also fit the mathematical model to *in vitro* studies of cytokine removal from spiked serum circulated through CytoSorb cartridges [91]. In these recirculation experiments, as opposed to batch incubation experiments performed in this study, the same mathematical model yields a parameter, Γ, given by:

$$\Gamma = q^{\max} K \; D$$

The Langmuir parameters, q^{max} and K, cannot be practically measured in CytoSorb beads due to the large amount of recombinant cytokine needed. We can estimate, however, an

intraparticle IL-6 diffusion coefficient by dividing Γ by α, which yields D^2. Using $\Gamma = 1.05 \times 10^{-4}$ $cm^2 \bullet ml \bullet min^{-1} \bullet g^{-1}$ for IL-6 in the *in vitro* recirculation studies, and α = 20.8 $min \bullet cm^3 \bullet g^{-1} \bullet \mu m^{-2}$ from this study, the IL-6 effective diffusion coefficient is estimated as 3.7×10^{-9} cm^2/s. Assuming a free IL-6 diffusion coefficient of 1.0×10^{-6} cm^2/s and hydrodynamic radius of 2nm from similarly sized molecules [92-93], theoretical hindered diffusion models [94-96] predict intraparticle diffusion coefficients within the range of our estimated value, given the approximate pore size of CytoSorb beads (0.8-5nm).

The CLSM technique presented here differs from typical CLSM studies due to the large size of CytoSorb beads, and the low protein concentrations necessary to mimic cytokine levels found in human sepsis. In typical CLSM studies, signal attenuation by the sorbent material is either neglected or corrected using mathematical light attenuation models [21, 97]. Given the large size of CytoSorb beads compared to other sorbents (450μm vs. 90um, respectively), signal attenuation could not be neglected nor adequately corrected by these attenuation models. Accordingly, we needed to eliminate signal attenuation by slicing the beads in half prior to imaging. Slight variations in sliced bead geometry from the slicing technique may have resulted in variability observed in the CLSM adsorption profiles, however, we would not expect small geometric variations to significantly affect average penetration behavior given the small penetration depths relative to particle diameter. In typical CLSM studies, the steric effect of fluorophore conjugation on protein adsorption is assumed negligible because of large sorbent pore sizes relative to protein size [98]. Given the small size of CytoSorb pores compared to other sorbents, we wanted to assess whether steric effects due to fluorophore conjugation might alter cytokine intensity profiles. The DOL could not be measured directly due to low cytokine concentrations used, but we lowered IL-6 DOL by reducing the molar excess of fluorophore

during the conjugation step, and demonstrated that IL-6 adsorption was unaffected. This result indicates minimal interference from fluorophore conjugation, and we would expect unlabeled IL-6 to perform in a similar manner.

Typical *in vivo* IL-6 levels in human sepsis are less than 0.001μg/ml [6]. We could not obtain adequate signal to noise levels of intensity at this bulk IL-6 concentration. Theoretically, normalized intensity profiles for IL-6 adsorption should be independent of bulk IL-6 concentration when adsorption is occurring in the linear portion of the Langmuir adsorption isotherm. We found no statistical difference in adsorption behavior as measured by the α parameter for bulk IL-6 concentrations of 1μg/ml, 0.1μg/ml and 0.01μg/ml. Accordingly, the adsorption dynamics of IL-6 at physiological levels is unlikely to differ from that reported here.

CLSM results indicate that IL-6 adsorption dynamics agree with predictions of our mathematical model, and that IL-6 adsorption is confined to the outer 15μm of the CytoSorb sorbent over a clinically relevant time period. Given this observation, less than 20% of available sorbent surface area is utilized for cytokine adsorption. For the current large size of CytoSorb beads, the surface area for diffusion into the beads relative to bead volume is small for a given mass of beads. Smaller CytoSorb beads may provide significantly faster cytokine capture by maximizing available surface area for diffusion per bead mass. We are currently developing and testing smaller CytoSorb beads to accelerate cytokine capture in a hemoadsorption device.

****The work in this chapter was published as:** Kimmel JD, Gibson GA, Watkins SC, Kellum JA, Federspiel WJ. IL-6 adsorption dynamics in hemoadsorption beads studied using confocal laser scanning microscopy. *Journal of Biomedical Materials Research: Part B.* 2010, 92B(2): 390-6.

4.0 MODELING COMPETITIVE ADSORPTION WITHIN HEMOADSORPTION BEADS

In Chapter 3, we presented a study of intraparticle IL-6 adsorption dynamics in PBS/BSA buffer, and CLSM results agreed with predictions of a single component adsorption/diffusion model [99]. PBS/BSA buffer was used as a simple protein solution, where cytokine adsorption behavior could be studied without potential confounding effects such as competitive adsorption of plasma solutes, interactions with soluble cytokine receptors, etc. In order to more closely mimic physiologic conditions in this study, we sought to characterize intraparticle cytokine adsorption dynamics in serum. Specifically, we wanted to confirm the assumption generated in our earlier modeling work that coadsorption of serum solutes within the beads does not significantly affect cytokine removal dynamics under clinically relevant cytokine levels [12].

Preliminary results from CLSM work in serum could not be predicted by our single component model presented in Chapter 3. We hypothesized that the observed intraparticle cytokine adsorption behavior was due to coadsorption of serum solutes, and therefore extended our original model to include competitive adsorption effects. Inclusion of multicomponent adsorption necessitated more complex modeling approaches, since an analytical solution to the model equations could not be obtained as was the case in our original model development [99].

Many authors have investigated protein transport within sorbent materials, typically utilizing commercial chromatography sorbents (ion exchange, affinity, hydrophobic interaction,

etc.) and simple, well characterized protein solutions [21, 83, 100-101]. While these techniques offer insight for optimization and scale-up for certain industrial applications, they are not suitable for analysis of complex feed solutions such as whole blood or plasma used in a hemoadsorption device [102]. Recent developments in sorbent-based blood purification modalities indicate a need for further understanding of mass transport within these materials [76, 103-104]. Specifically, clinically relevant analyses are necessary to characterize mass transport under physiologic conditions, a criterion that is not addressed in traditional chromatography studies where parameters such as pH, protein concentration, and ionic strength can be manipulated.

Multicomponent protein adsorption has been investigated in various types of chromatography sorbents by others [102, 105-110]. Martin, *et al.* [110] developed a two-component pore diffusion model to predict intraparticle concentration profiles in ion exchange SP Sepharose FF beads, and validated the model using batch and shallow-bed adsorption experiments. Gallant [105] described multi-component adsorption in ion exchange particles using the steric mass action model (SMA) [111], and observed displacement of low affinity protein and salt components by a higher affinity protein. Bak, *et al.* [102] utilized a complex feedstock (rabbit antiserum) to investigate removal of antibodies by various affinity-based sorbents. They developed a lumped parameter model and quantified Langmuir kinetics through equilibrium and batch adsorption studies.

In this study, confocal laser scanning microscopy (CLSM) was used to quantify intraparticle adsorption dynamics of fluorescently labeled IL-6 in serum, and results were compared to predictions of a competitive adsorption model. We present for the first time a study of intraparticle mass transport using CLSM in whole serum. Quantifying cytokine adsorption dynamics within the hemoadsorption beads is technically challenging due to (1) low cytokine

concentrations typically found in sepsis (< 1ng/ml), and (2) difficulties of performing CLSM in whole serum due to autofluorescence of adsorbed serum solutes. In this work, we used supraphysiologic IL-6 concentrations necessary to achieve adequate CLSM signal to noise ratios, and fit a multicomponent model to the observed IL-6 intraparticle intensity profiles. The fitted model was then used to simulate physiologic IL-6 concentrations which were below the detection limit of the CLSM technique, to determine if competitive adsorption effects were relevant under clinical conditions.

4.1 MATERIALS & METHODS

4.1.1 Materials

Recombinant human IL-6 (MW = 21kD, >95% purity) and an NHS-activated fluorophore (DyLight^{TM} 549, MW = 982Da) were purchased from Thermo Scientific (Rockford, IL). IL-6 was conjugated with the fluorophore as follows: 15µg dried fluorophore was reconstituted in 100µl 10mM PBS and 8µl 0.67M sodium borate buffer. 50µl reconstituted fluorophore was added to 250µl IL-6 (40µg/ml) in PBS and incubated in the dark for 60min. Unreacted fluorophore was removed using resin spin columns provided by the manufacturer. CytoSorb beads were provided by CytoSorbents, Inc. (Monmouth Junction, NJ). CytoSorb beads are polystyrene-divinylbenzene porous particles (450µm avg. particle diameter, 67% porosity, 1.02g/cm^3 density, 0.8-5nm pore diameter, 850m^2/g surface area) with a biocompatible polyvinyl-pyrrolidone coating.

4.1.2 Confocal Laser Scanning Microscopy

Confocal laser scanning microscopy (CLSM) was used to quantify intraparticle adsorption profiles within the sorbent beads. Labeled IL-6 was spiked into horse serum (Invitrogen, Camarillo, CA) to achieve cytokine concentrations of ~1μg/ml. 1ml aliquots of IL-6 in horse serum or horse serum alone were incubated with 1.5mg CytoSorb beads for 2.5hr, 5hr, and 21hr on a rocker at ambient temperature. At the specified time points, beads were removed from solution, sliced in half using a thin razor blade, and placed in a droplet of PBS on a cover slip for CLSM analysis. An Olympus FluoView^{TM} FV1000 confocal microscope outfitted with a UPlanSApo 20X/.75 oil objective and a HeNe laser (543nm excitation, 572nm emission) was used for all confocal imaging. During image capture, the microscope objective was focused such that the confocal plane was localized within the bead, close to the sliced edge to minimize signal loss through the bead (Fig. 3). Images were acquired by horizontal scan at 1024x1024 pixel resolution, corresponding to 0.621μm pixel size. Digital images of sliced beads were analyzed using ImageJ software (National Institutes of Health), and intraparticle intensity profiles were generated by quantifying a rectangular segment of the image across the diameter of each bead (4 – 5 beads were imaged at each incubation time point). Refer to Kimmel *et al.* [99] (Chapter 3) for further details regarding the CLSM technique.

Baseline autofluorescence profiles from adsorbed serum solutes at each time point were quantified by averaging CLSM intraparticle intensity values for 4 – 5 beads incubated only with serum. This procedure was repeated using different serum/bead samples, and intensity data was found to be repeatable using the same microscope and laser parameters. Mean baseline serum intensities were subtracted from mean IL-6 intensities at each radii point to separate serum autofluorescence signal from IL-6 fluorophore signal. Resulting intraparticle intensity data were

normalized by the maximum intensity within each particle (I/I_{max}), and spatial position was normalized by the average particle radius (r/R).

4.1.3 Theoretical Model Development

Mass transport within the sorbent beads is mediated by diffusion into the porous structure, and physical adsorption to the interior polymer surface via hydrophobic interactions. The governing equation for adsorption/diffusion of species *i* within a single sorbent bead is:

$$\rho \frac{\partial q_i}{\partial t} = D_i \frac{1}{r^2} \frac{\partial}{\partial r}\left(r^2 \frac{\partial c_i}{\partial r} \right)$$

where $q_i(r,t)$ is the mass density of adsorbed species *i* per bead mass, at radial position, r, in the bead. D_i is the effective intraparticle diffusion coefficient of species *i*, and $c_i(r,t)$ is the mass concentration of species *i* within the liquid phase of the sorbent pores. The following assumptions are made: (1) film diffusion effects are negligible, (2) concentration in the liquid phase of the pores is much smaller than concentration in the adsorbed phase, (3) intraparticle adsorption is fast compared to diffusion, such that local equilibrium applies, (4) adsorption is modeled using the multicomponent Langmuir isotherm, where $q_i = \frac{q_i^{\max} K_i c_i}{1 + \sum_j K_j c_j}$. A nondimensional form of the governing equation is created using:

$$r^* = r / R \qquad q_i^* = q_i / q_i^{max} \qquad c_i^* = c_i / c_i^{in} \qquad t^* = t / t_s$$

where R is the average particle radius, q_i^{max} is the maximum adsorbed mass of specie *i* per bead mass, c_i^{in} is the initial bulk concentration of specie *i*, and t_s is a time scale corresponding to the experimental conditions used in the study. Dropping asterisks and combining parameters:

$$\alpha_i \frac{\partial q_i}{\partial t} = \frac{1}{r^2}\frac{\partial}{\partial r}\left(r^2 \frac{\partial c_i}{\partial r}\right)$$

where $\alpha_i = \frac{\rho q_i^{\max} R^2}{D_i c_i^{in} t_s}$.

Mass transport of serum components (lumped for simplicity as a single species, *a*) and cytokine (species *b*) are modeled in a two component competitive adsorption system:

$$\alpha_a\left(q_{aa}\frac{\partial c_a}{\partial t} + q_{ba}\frac{\partial c_b}{\partial t}\right) = \frac{1}{r^2}\frac{\partial}{\partial r}\left(r^2 \frac{\partial c_a}{\partial r}\right) \quad \text{(Eq. 2)}$$

$$\alpha_b\left(q_{bb}\frac{\partial c_b}{\partial t} + q_{ab}\frac{\partial c_a}{\partial t}\right) = \frac{1}{r^2}\frac{\partial}{\partial r}\left(r^2 \frac{\partial c_b}{\partial r}\right) \quad \text{(Eq. 3)}$$

where q_{ij} terms are derived from the multicomponent Langmuir isotherm:

$$q_{aa} = \frac{\partial q_a}{\partial c_a} = \frac{K_a + K_a K_b C_b}{\left(1 + K_a C_a + K_b C_b\right)^2} \qquad q_{bb} = \frac{\partial q_b}{\partial c_b} = \frac{K_b + K_b K_a C_a}{\left(1 + K_a C_a + K_b C_b\right)^2}$$

$$q_{ba} = \frac{\partial q_a}{\partial c_b} = \frac{-K_a K_b C_a}{\left(1 + K_a C_a + K_b C_b\right)^2} \qquad q_{ab} = \frac{\partial q_b}{\partial c_a} = \frac{-K_a K_b C_b}{\left(1 + K_a C_a + K_b C_b\right)^2}$$

Here we define K_i as a dimensionless "relative affinity" coefficient, given by $K_i = c_i^{in}/c_{i50}$. We can consider cytokine adsorption to be in a "low relative affinity" regime ($K_b << 1$) given $c_b^{in} \sim O(10^{-6}$ mg/ml) and C_{50} for protein adsorption in typical sorbent beads $\sim O(10^{-1}$mg/ml) [90]. Hence, cytokine concentrations in our application are much less than those necessary to reach ½ bead saturation (C_{50}). Assuming that competing serum components are at higher bulk concentrations than cytokine ($K_a >> K_b$), adsorption terms are simplified to:

$$q_{aa} = \frac{\partial q_a}{\partial c_a} = \frac{K_a}{\left(1 + K_a C_a\right)^2} \qquad q_{bb} = \frac{\partial q_b}{\partial c_b} = \frac{K_b}{1 + K_a C_a}$$

$$q_{ba} = \frac{\partial q_a}{\partial c_b} = \frac{-K_a K_b C_a}{\left(1 + K_a C_a\right)^2} \qquad q_{ab} = \frac{\partial q_b}{\partial c_a} = \frac{-K_a K_b C_b}{\left(1 + K_a C_a\right)^2}$$

From these relationships, we can see that q_{aa} is proportional to K_a, and q_{ba} is proportional to K_a and K_b. Since $K_b << K_a$, we can consider the q_{ba} term negligible in Eq. 2, i.e. adsorption of species *a* (serum) is independent of adsorption of species *b* (cytokine). The q_{ab} term in Eq. 3 gives rise to cytokine displacement by the higher relative affinity serum species. Our previously published single component model is a subset of the current model, where cytokine displacement is considered negligible ($q_{ab} \approx 0$).

4.1.4 Model Fitting to CLSM Data

Given the set of coupled equations describing mass transport of serum components and cytokine (Eq. 2 & 3, respectively), the unknown model parameters are:

$$\alpha_a = \frac{\rho q_a^{\max} R^2}{D_a c_a^{in} t_s} \qquad \alpha_b = \frac{\rho q_b^{\max} R^2}{D_b c_b^{in} t_s} \qquad K_a = \frac{c_a^{in}}{c_{50a}} \qquad K_b = \frac{c_b^{in}}{c_{50b}}$$

We can separate known constants from the α terms: $\rho = 1.02 g/cm^3$, $R = 266 \mu m$, $t_s = 21 hr$, $c_b^{in} = 1 \mu g/ml$. The remaining unknown parameters are:

$$\beta_a = \frac{q_a^{\max}}{D_a c_a^{in}} \qquad \beta_b = \frac{q_b^{\max}}{D_b} \qquad K_a = \frac{c_a^{in}}{c_{50a}} \qquad K_b = \frac{1}{c_{50b}}$$

The equation describing cytokine mass transport (Eq. 3) has three unknown parameters (K_a, K_b, β_b), but K_b and β_b only appear as a product, and therefore the two parameters cannot be fitted independently. A value of $\beta_b = 1x10^{12}\ mg_{bead} \cdot mg_{cytokine}^{-1} \cdot cm^{-2} \cdot s$ was used as a reasonable estimate based on previous work [99] in which the effective diffusion coefficient of IL-6 within CytoSorb beads was calculated, thereby permitting independent fitting of the remaining parameters.

The system of equations was solved for q_b (adsorbed cytokine) using the finite element method with Comsol Multiphysics™, and a parameter optimization technique was developed as

follows: numerical solutions from Comsol were imported into Matlab™, and the three unknown model parameters (β_a, K_a, K_b) were iteratively fit to IL-6 CLSM data by minimizing sum of squares error (SSE) between the numerical solutions and CLSM data using a Nelder-Mead simplex algorithm: $\min_{p=\{\beta_a,K_a,K_b\}} \sum_{j=1}^{Nt}\sum_{i=1}^{Nr}\left[d_j(i)-q_b(i,t,p)\right]^2$, where N_t is the number of incubation time points, N_r is the number of radii data points, and $d_j(i)$ is the normalized CLSM intensity value at incubation time j and radius segment i. Parameters were fit to 2.5hr and 5hr, or 2.5hr, 5hr and 21hr CLSM data sets, and SSE was calculated as the cumulative error for all time points. CLSM data were normalized by the maximum intraparticle intensity values, and model simulations were normalized by the maximum intraparticle q_b values. CLSM intensities are directly proportional to adsorbed cytokine within the particle, therefore normalized CLSM and simulation data can be compared in this manner. Normalized CLSM and simulation data were multiplied by ten within the parameter optimization routine to ensure that calculated SSE values were substantially greater than the tolerance of the error minimization algorithm.

4.1.5 Parametric Analysis

A parametric analysis was performed to determine (1) if multiple sets of parameter combinations existed that could fit the IL-6 CLSM data equally well, and (2) sensitivity of the model to parameter perturbations. Initial guesses for β_a, K_a, and K_b values were varied within a nominal range for each parameter, and best fit parameter values were estimated for all combinations using the iterative error minimization algorithm (Table 3). Parameter sensitivity was examined by running model simulations using a subset range of parameter values (Table 4), and then plotting

parameter values vs. SSE to quantify model sensitivity to parameter perturbations. All parametric analyses were run using solutions to the 2hr and 5.5hr time points.

4.2 RESULTS

4.2.1 Model Fits to Confocal Microscopy Data

Confocal laser scanning microscopy (CLSM) was used to quantify intraparticle adsorption profiles of fluorescently labeled IL-6 in horse serum. Baseline serum autofluorescence profiles for beads incubated only with horse serum for 2.5hr, 5hr, and 21hr are illustrated in Fig. 10. Various middle molecular weight serum solutes diffuse into the sorbent pores and adsorb to the polymer surface; certain adsorbed molecules autofluoresce in the wavelength range utilized during CLSM. Intraparticle intensity profiles for beads incubated with labeled IL-6 in horse serum are illustrated in Fig. 11. In contrast to adsorption behavior observed for baseline serum incubations, IL-6 profiles demonstrate peak intensities within the bead interior, suggesting competitive displacement phenomena [110]. Mean spatial intensities are shown from 4-5 beads imaged at each time point for both baseline and IL-6 incubations. Beads incubated in PBS were imaged to ascertain background signal from the bead itself, and intensities were negligible compared to those observed with serum or labeled IL-6 incubations (data not shown).

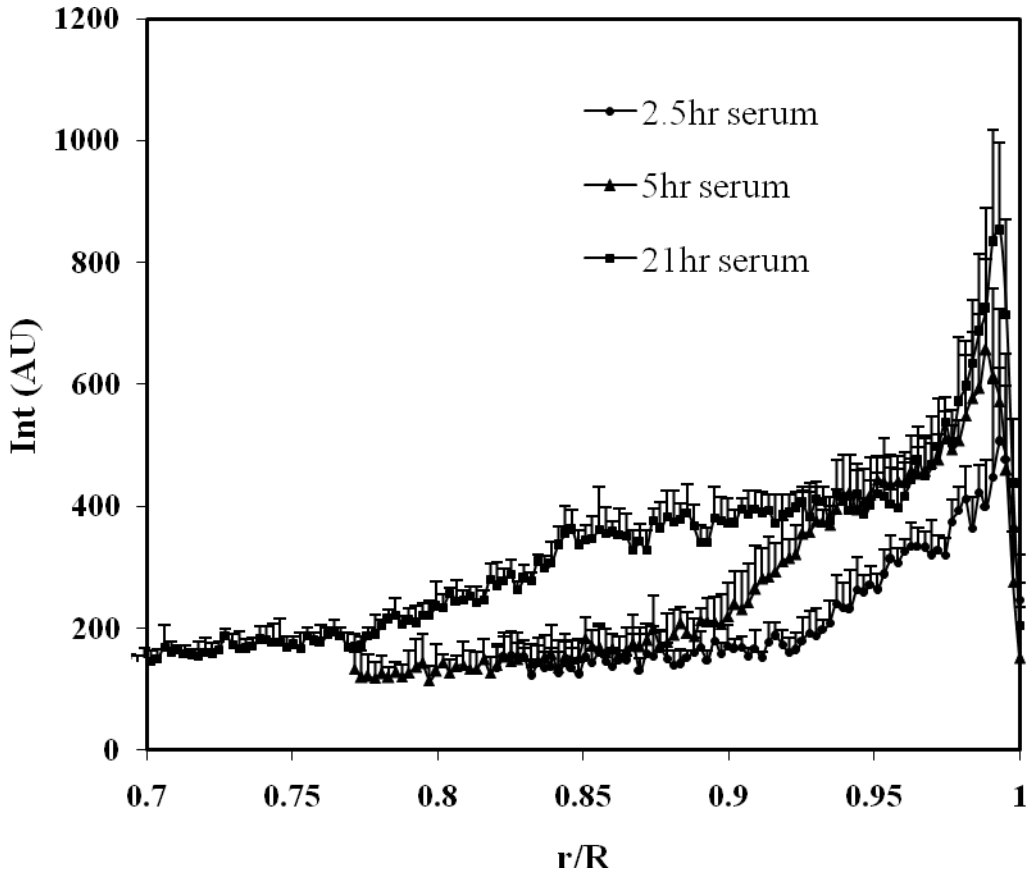

Figure 10: CLSM intraparticle intensity profiles for beads incubated with horse serum for 2.5hr, 5hr, and 21hr. Error bars indicate standard deviation from multiple beads imaged at each time point.

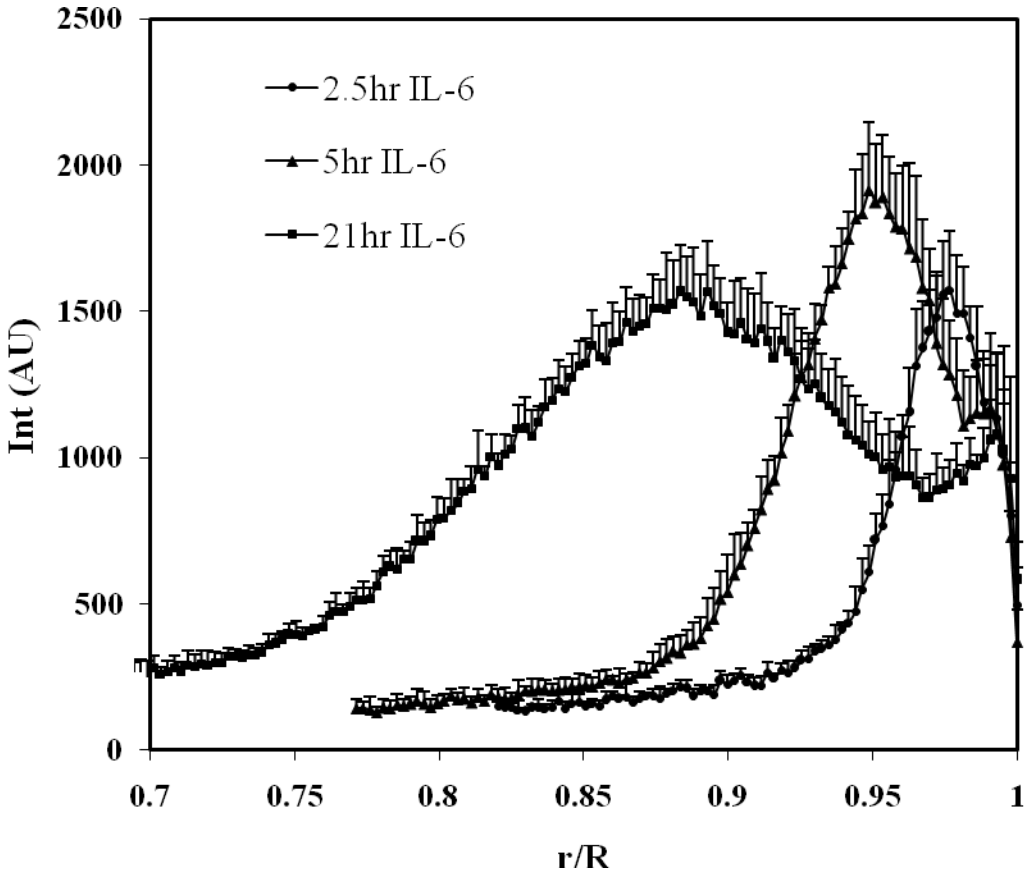

Figure 11: CLSM intraparticle intensity profiles for beads incubated with fluorescently labeled IL-6 in horse serum for 2.5hr, 5hr, and 21hr. Error bars indicate standard deviation from multiple beads imaged at each time point.

Baseline serum autofluorescence data (Fig. 10) were subtracted from CLSM profiles for labeled IL-6 in serum (Fig. 11), and resulting IL-6 profiles were used for model fitting. Model simulations were fit to normalized IL-6 CLSM data using an iterative parameter optimization technique. Model fits for 2.5hr and 5hr time points are illustrated in Fig. 12 and Fig. 13, respectively. The corresponding best fit parameter values are shown in Table 2. Model predictions agree with the observed CLSM intraparticle cytokine profiles, indicating competitive adsorption between IL-6 and serum components. As IL-6 and serum solutes concurrently diffuse

into the internal pore structure, high affinity serum components likely compete for binding sites with IL-6, leading to cytokine displacement within the particle. The model was also fit to IL-6 CLSM data for 2.5hr, 5hr, and 21hr incubation times (Fig. 14, Fig. 15, and Fig. 16, respectively). Addition of the 21hr time point did not have a substantial effect on the best fit parameter estimates compared to the 2.5/5hr simulation. Discrepancies between model predictions and CLSM data at the bead surface (r/R=1) are likely due to imaging artifacts, as obtaining consistent CLSM intensity values in this region is technically challenging.

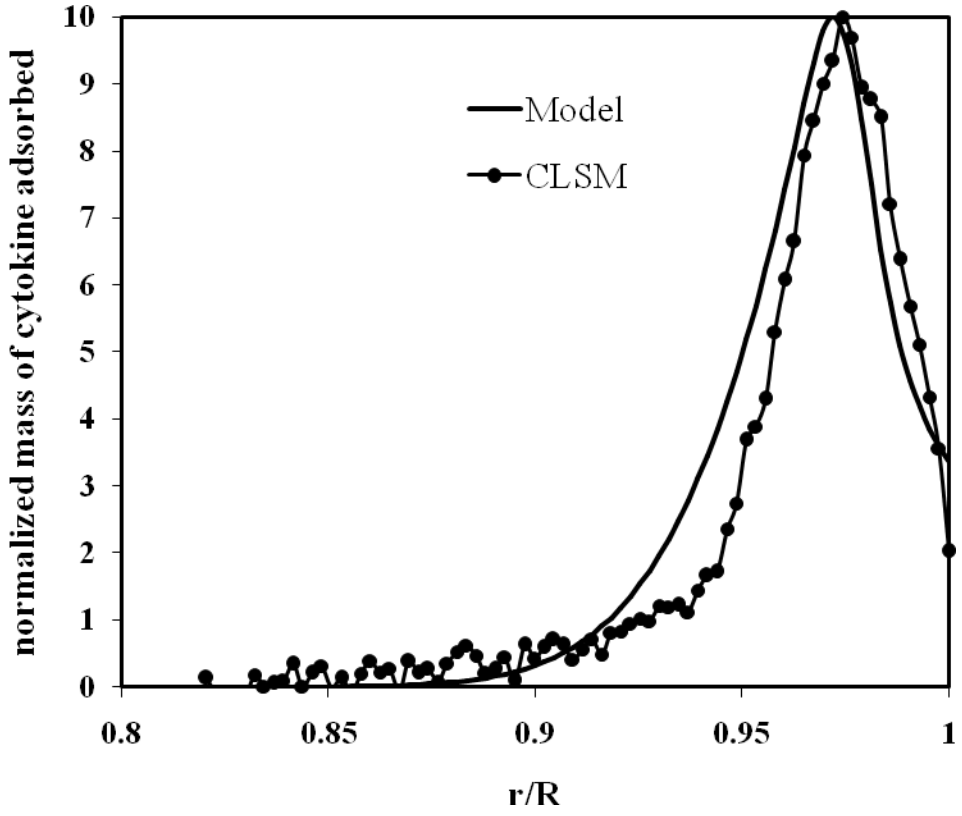

Figure 12: IL-6 CLSM profile for 2.5hr incubation and corresponding model fit. Model simulations were run using the 2.5/5hr CLSM data.

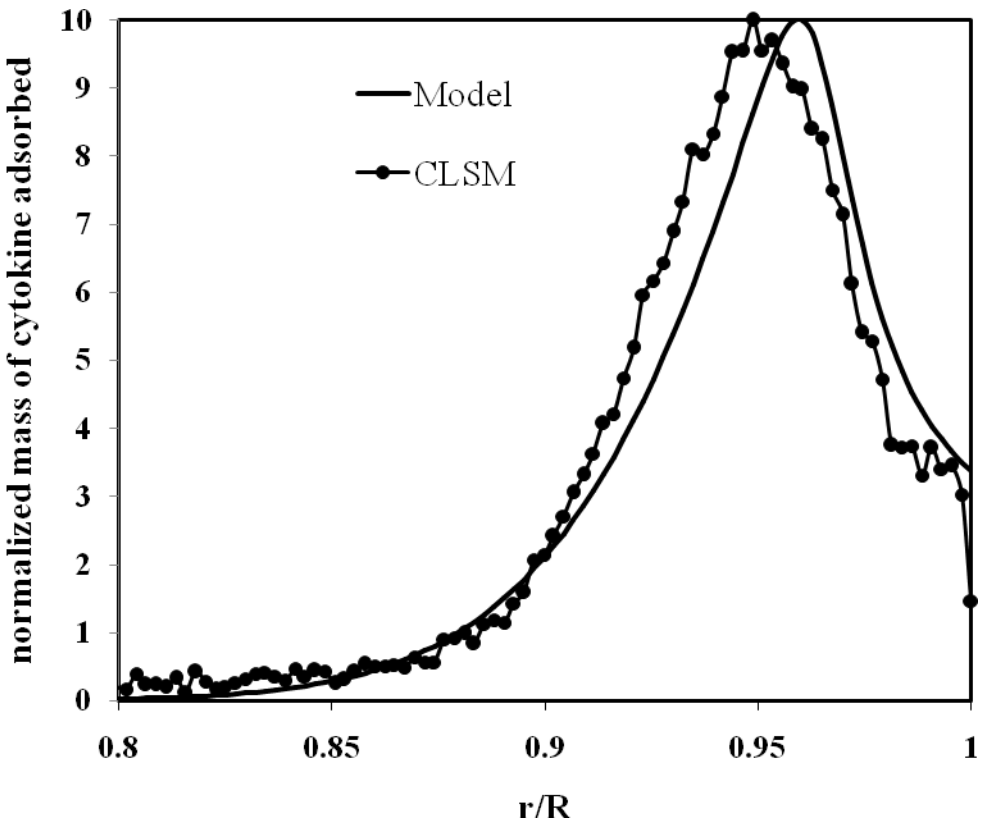

Figure 13: IL-6 CLSM profile for 5hr incubation and corresponding model fit. Model simulations were run using the 2.5/5hr CLSM data.

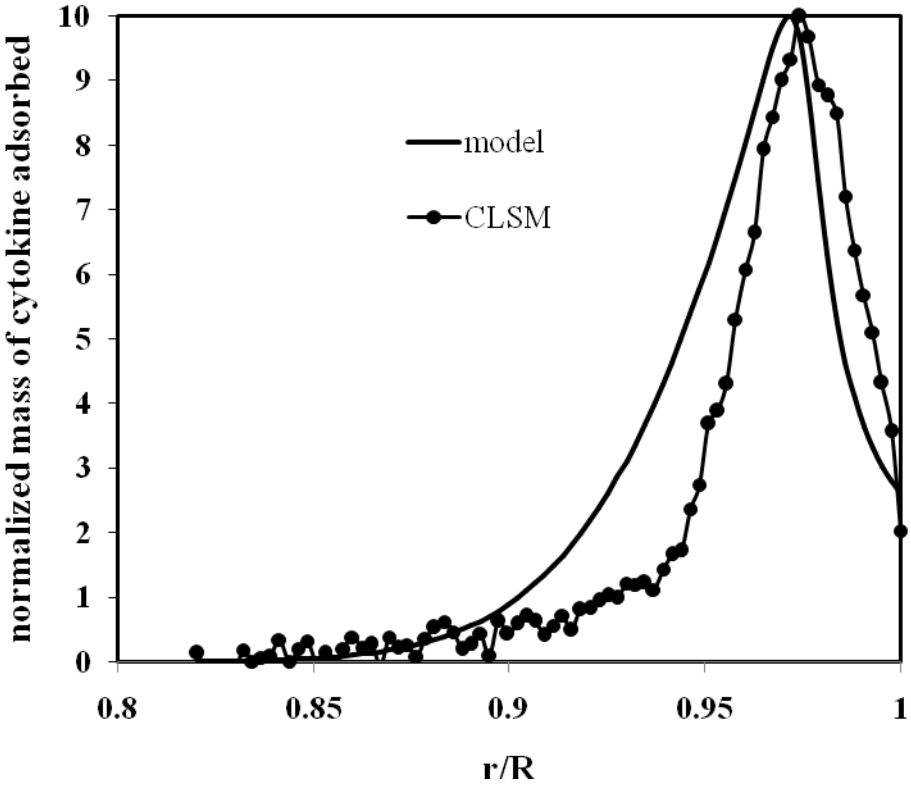

Figure 14: IL-6 CLSM profile for 2.5hr incubation and corresponding model fit. Model simulations were run using the 2.5/5/21hr CLSM data.

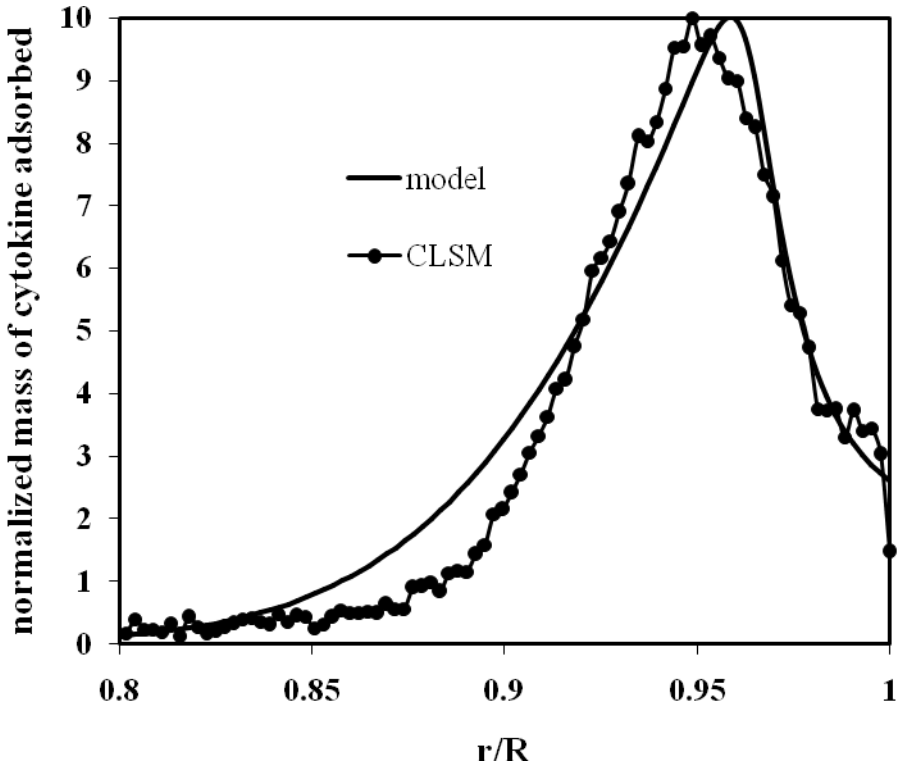

Figure 15: IL-6 CLSM profile for 5hr incubation and corresponding model fit. Model simulations were run using the 2.5/5/21hr CLSM data.

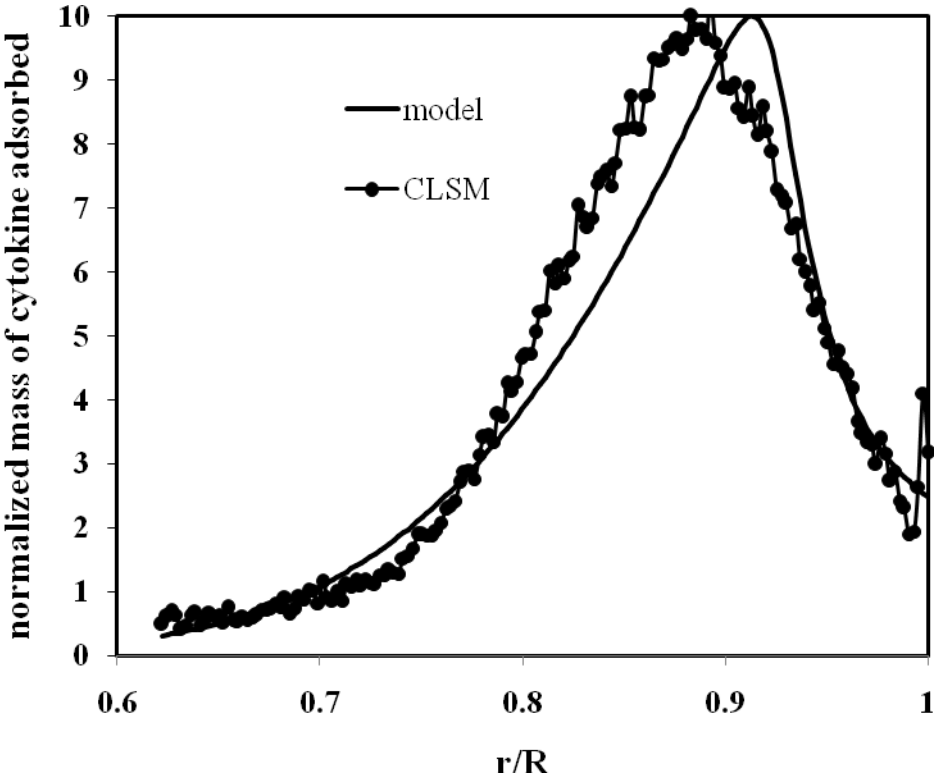

Figure 16: IL-6 CLSM profile for 21hr incubation and corresponding model fit. Model simulations were run using the 2.5/5/21hr CLSM data.

Table 2: Best fit model parameters based on sum of squares error (SSE) minimization between model simulations and IL-6 CLSM data.

	K_a	K_b	β_a ($s \cdot ml \cdot mg^{-1} \cdot cm^{-2}$)	SS Error
2.5hr, 5hr	4.43	1.43e-5	6.82e10	115.4
2.5hr, 5hr, 21hr	5.10	9.43e-6	6.89e10	341.8

4.2.2 Parametric Analysis

A parametric analysis was performed to determine if multiple combinations of the three model parameters fit the CLSM data equally well. The parameter optimization routine was run using a range of initial parameter guesses (Table 3), and small differences in best fit parameter estimates were observed compared to those reported in Table 2.

Table 3: Initial guess parameter values used within the parameter optimization routine, and resulting range of best fit parameter estimates.

	Initial parameter guesses		**Best fit parameter estimates**	
	low	**high**	**low**	**high**
K_a	**1**	**10**	**2.4**	**3.8**
K_b	**5e-6**	**1e-3**	**1.3e-5**	**1.52e-5**
β_a ($s \cdot ml \cdot mg^{-1} \cdot cm^{-2}$)	**3e10**	**50e10**	**7.27e10**	**9.56e10**

Variability of best fit parameter values was further examined to determine if these fluctuations were a result of multiple solutions to the model equations, or simply numerical tolerances of the error minimization algorithm. Parameter sensitivity was investigated by observing effects on model behavior (quantified by SSE) due to perturbations in parameter inputs (Table 4).

Table 4: Range of parameter inputs used to test parameter sensitivity of the model. Eleven equidistant parameter values were used within each specified parameter range.

	Parameter ranges	
	low	**high**
$\mathbf{K_a}$	**3.5**	**4.5**
$\mathbf{K_b}$	**0.5e-5**	**10e-5**
$\mathbf{\beta_a}$ $\mathbf{(s \cdot ml \cdot mg^{-1} \cdot cm^{-2})}$	**3e10**	**50e10**

Figures 17-19 illustrate model dependency on the three parameters (β_a, K_a, K_b). For each three dimensional graph, two parameters are plotted against SSE while the third parameter is held constant. A representative plot is shown for each parameter combination: K_a vs. K_b (Fig. 17), K_a vs. β_a (Fig. 18), K_b vs. β_a (Fig. 19). For each case, eleven separate graphs were generated using values for the third variable which was not plotted, but model behavior was comparable between each of the eleven graphs for all cases. In Figs. 17-18, changes in K_a have minimal effects on SSE, indicating negligible dependence of the model on K_a. Fig. 19 illustrates model dependence on both K_b and β_a. A smaller slice of the K_b vs. β_a graph was investigated to determine if multiple local minima existed that could result in variability of best fit parameter values obtained by the error minimization algorithm. Fig. 20 illustrates a 100-fold smaller range of parameter values for K_b and β_a. Small fluctuations in SSE are observed, which may cause the error minimization algorithm to terminate in any of the local SSE minima wells. Therefore,

small differences in best fit parameters based on initial parameter guess are most likely due to sensitivity of the SSE minimization algorithm, not multiple solutions to the model equations.

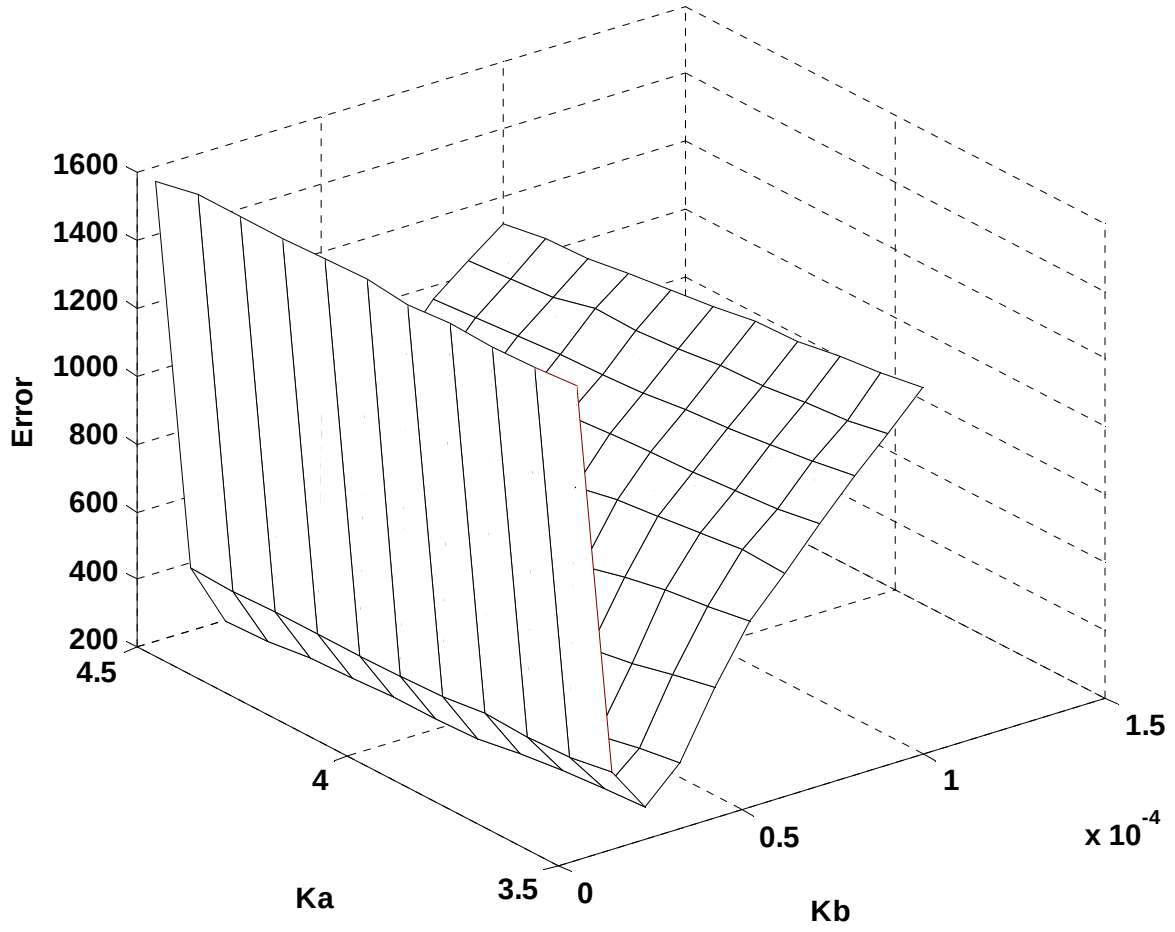

Figure 17: Effects on model behavior due to perturbations in parameter inputs. K_a and K_b are plotted against SSE, where β_a = 3e10 s·ml·mg^{-1}·cm^{-2}.

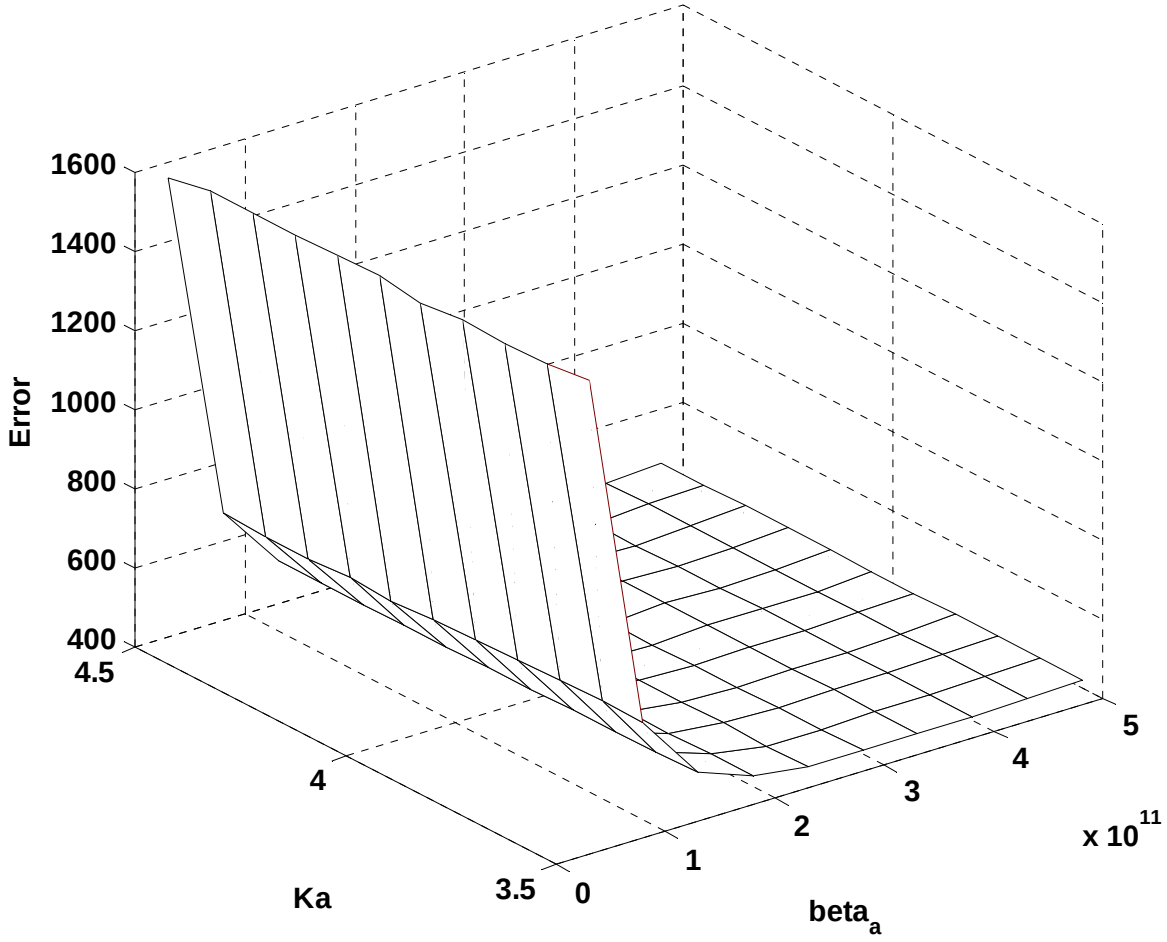

Figure 18: Effects on model behavior due to perturbations in parameter inputs. K_a and β_a are plotted against SSE, where K_b = 0.5e-5.

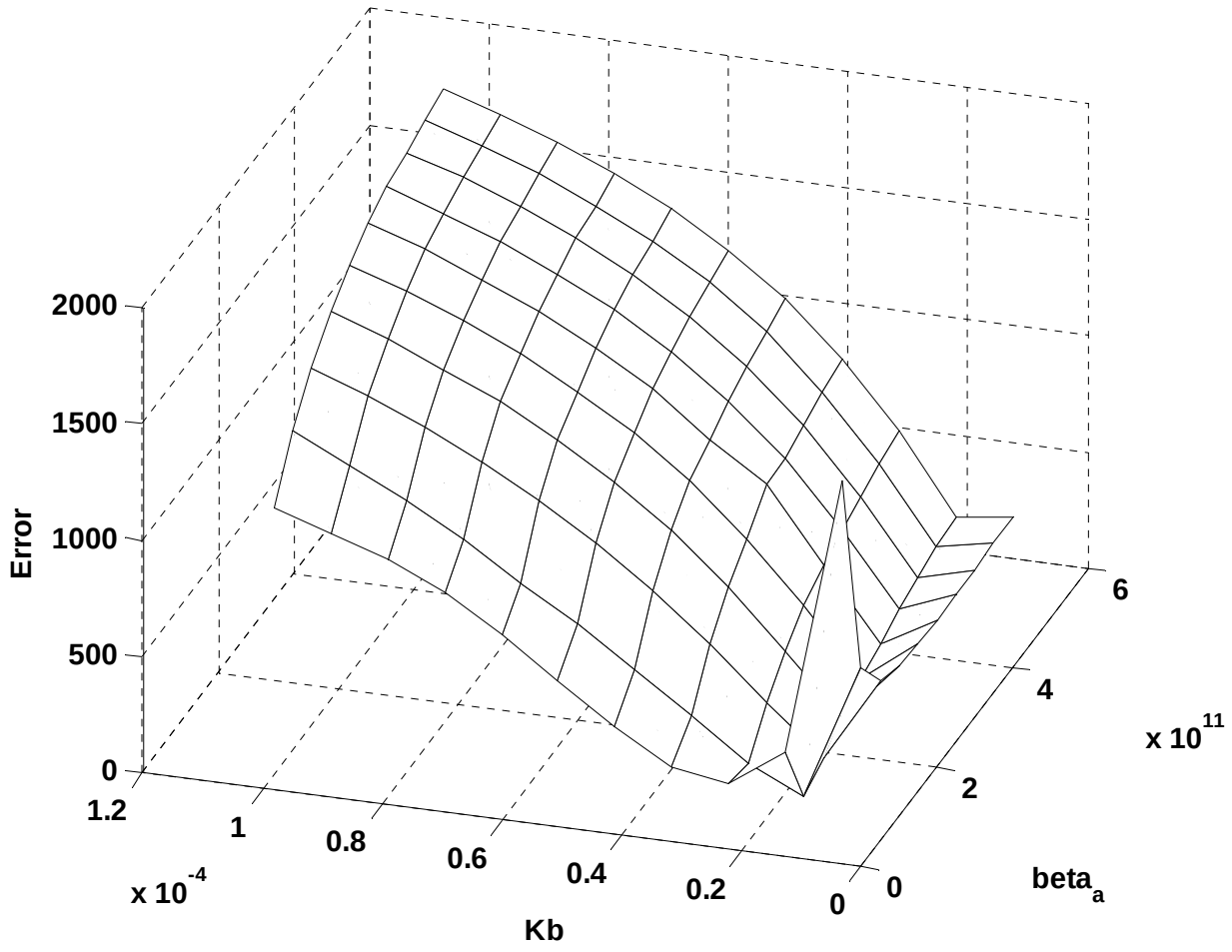

Figure 19: Effects on model behavior due to perturbations in parameter inputs. K_b and β_a are plotted against SSE, where $K_a = 3.5$.

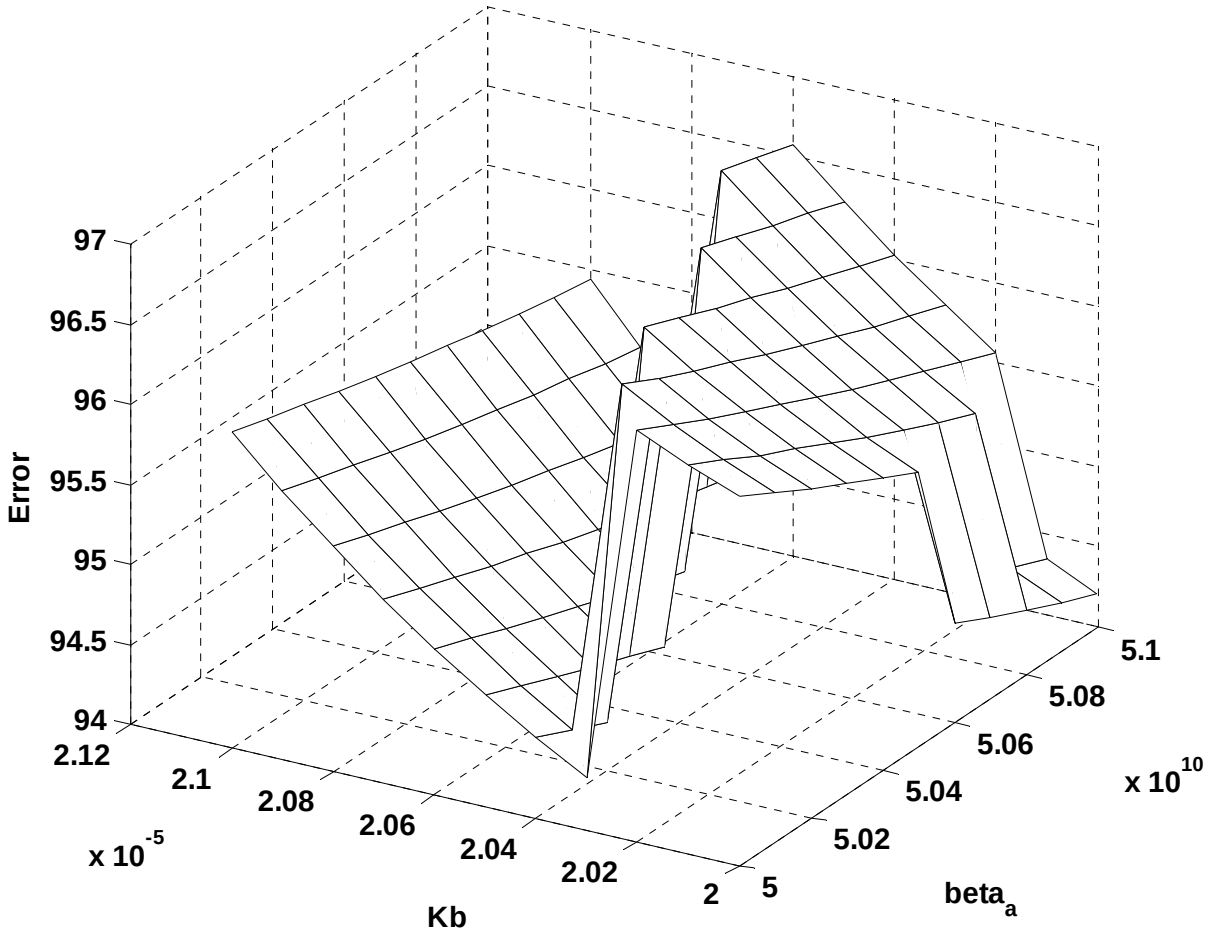

Figure 20: Model sensitivity to small changes in Kb and βa.

4.2.3 Physiologic Cytokine Concentration Simulation

The model was simulated for clinically relevant cytokine concentrations (c_b^{in} = 1ng/ml) that were below the detection limit for CLSM analysis, using the best fit model parameter values estimated from IL-6 CLSM data at 1μg/ml IL-6 concentrations (Table 2; 2.5hr & 5hr values). Fig. 21 illustrates model simulations for 2.5hr, 5hr and 21hr cytokine incubations at 1ng/ml IL-6 concentration. Predicted adsorption profiles demonstrate single component diffusion/adsorption

dynamics, in contrast to the displacement behavior observed for CLSM profiles at higher (~1μg/ml) IL-6 concentrations. β_a, K_a, and K_b were varied to determine if small changes in parameter inputs affected predicted adsorption behavior at low cytokine concentration, however, the same qualitative adsorption patterns were observed for all parameter values tested (data not shown). These results indicate that competitive adsorption effects between serum components and cytokine within the hemoadsorption beads are likely negligible at clinically relevant cytokine concentrations.

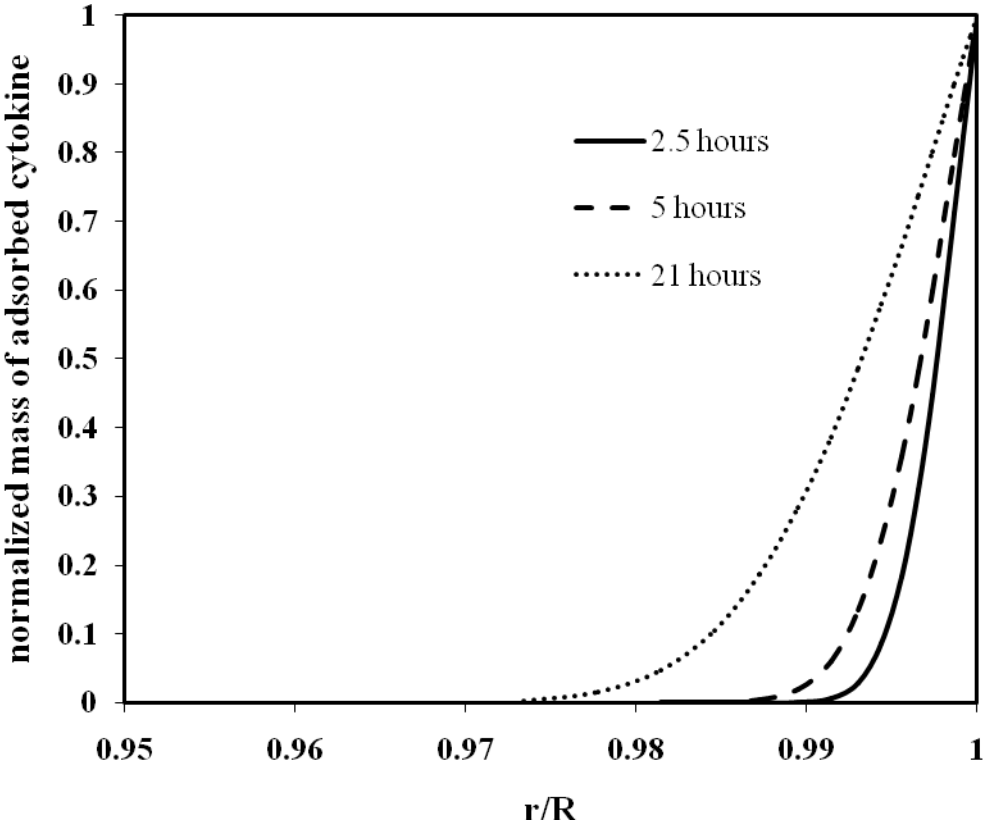

Figure 21: Model simulations for low cytokine concentration incubations (c^{in} = 1ng/ml).

4.3 DISCUSSION

The hemoadsorption device can be considered "semi-selective", by which middle molecular weight solutes (< ~50kD) such as cytokines are captured within the sorbent beads, while essential large molecules such as albumin and immunoglobulins are restricted from the interior sorbent structure via pore size exclusion. This approach enables broad spectrum removal of both pro- and anti- inflammatory cytokines, as well as other middle MW mediators that may play a role in the pathophysiology of sepsis [53]. Various serum solutes adsorb to the hydrophobic interior of the beads along with cytokines, and may affect cytokine removal dynamics within the device. The goal of this work was twofold: (1) to directly quantify competitive adsorption effects between cytokines and other adsorbing solutes within the sorbent beads, and (2) to utilize a multicomponent mathematical model to predict whether these effects are relevant at physiologic cytokine concentrations used with the device, which were below the CLSM detection limit.

In Chapter 3, we demonstrated that IL-6 intraparticle adsorption in the presence of PBS + 5% BSA was predicted by a single component diffusion/adsorption model [99]. In order to more closely mimic physiological conditions in this study, CLSM was performed with labeled IL-6 in horse serum, and resulting adsorption profiles indicated possible competitive adsorption behavior. We developed a two component model to describe concurrent diffusion and adsorption of cytokine and serum solutes, where all possible serum components were simplified into a single adsorbing species. We fit the model to CLSM data obtained at supraphysiologic cytokine concentrations necessary for adequate CLSM signal (~1μg/ml), and then used the fitted model to predict adsorption behavior at physiologically relevant cytokine concentrations (~1ng/ml) which were under the CLSM detection limit. The model was fit to 2.5/5hr and

2.5/5/21hr incubation data, and differences in best fit parameter estimates were negligible (Table 2). All parameter sensitivity and low concentration simulation results were obtained using best fit parameter values from the 2.5/5hr data, as this time scale is relevant to clinical use of the device.

Sorbent CLSM studies are typically performed using simple protein solutions, where a molecule of interest is labeled with a fluorophore, and visualized within the particle using laser excitation at a specific wavelength [88]. In this study, we were interested in examining adsorption behavior within a biological fluid, and found that accumulation of adsorbed serum solutes within the sorbent particle caused autofluorescence profiles over a wide range of excitation wavelengths. We chose an excitation/emission wavelength (543/572nm) that minimized serum autofluorescence and maintained adequate signal from the labeled IL-6. A simple signal processing technique was developed to subtract average serum autofluorescence signal from labeled IL-6 signal, and model simulations were fit to the post-processed IL-6 profiles. Although CLSM profiles of adsorbed serum components were quantified (Fig. 10), we chose to fit model simulations only to adsorbed IL-6 profiles. Intraparticle profiles from serum autofluorescence varied greatly depending on wavelength used during CLSM, likely due to differing diffusional rates and autofluorescence emissions of serum solutes. These data were not suitable for model fitting, therefore we used the IL-6 adsorption profiles to fit model parameters corresponding to diffusion/adsorption of both IL-6 (K_b) and serum solutes (β_a, K_a).

The set of model equations contained four unknown parameters (β_a, K_a, β_b, K_b), however, the β_b term existed only as a product with K_b, and therefore these two parameters could not be fitted independently. A value of $\beta_b = 1x10^{12}$ $mg_{bead} \cdot mg_{cytokine}^{-1} \cdot cm^{-2} \cdot s$ was used as a reasonable estimate based on previous results from Chapter 3 in which the effective diffusion coefficient of

IL-6 within CytoSorb beads was calculated. Model fitting results indicate that a single combination of the three fitted parameters fits the IL-6 CLSM data. Small differences in best fit parameter estimates based on initial parameter guesses (Table 3) are likely due to numerical tolerances within the error minimization algorithm, given the local SSE minima observed over small ranges of parameter values (Fig. 20). A range of best fit parameter inputs (Table 4) was tested using the low concentration simulation, and no qualitative changes in predicted IL-6 adsorption profiles were observed from those illustrated in Fig. 21. Additionally, varying β_b values did not have a meaningful effect on predicted low concentration IL-6 adsorption profiles (data not shown). Overall, our model fitting and parametric analysis results indicate that under clinically relevant cytokine concentrations (c^{in} = 1ng/ml), competitive adsorption effects within the hemoadsorption beads due to coadsorption of serum solutes are not likely.

The work presented in this chapter describes a technique to quantify competitive protein adsorption effects within hemoadsorption beads in whole serum. Most studies of mass transport within sorbent particles are applicable to well characterized feed stocks, whereas the complexity of biological fluids requires new methodologies to examine mass transport phenomena. Results confirm assumptions of our original model [12] that competitive adsorption effects do not significantly affect cytokine capture within the device under physiologic conditions.

5.0 DISSOCIATION OF OLIGOMERIC TNF AS A TOOL FOR ACCELERATED TNF REMOVAL

Tumor necrosis factor-α (TNF) is a potent, pleiotropic cytokine involved in the regulation of multiple physiological and pathophysiological signaling pathways [112-113]. TNF is an important initiator of the systemic inflammatory response [13, 114], and elevated levels of circulating TNF have been associated with increased mortality rates in sepsis [8]. Removal of TNF along with other inflammatory cytokines from the circulating blood may help attenuate systemic inflammation and promote immunologic homeostasis to patients treated for severe sepsis [9]. The goal of this work was to characterize TNF capture dynamics within the device to elucidate mechanisms for improved TNF removal using hemoadsorption.

TNF is secreted by numerous cell types as a 17kD monomer, which noncovalently associates to form a bioactive 51kD homotrimer [115]. Binding of TNF to its soluble and cell surface receptors is thought to be exclusive to the 51kD "bioactive" trimeric form [116-118], whereas monomeric TNF has demonstrated negligible bioactivity *in vitro* [119] and *in vivo* [120]. Trimeric TNF can spontaneously dissociate over time into its monomeric constituents [121], and chemical and biological compounds have been investigated for their ability to perturb TNF quaternary structure [122-124]. Various pharmacologic modalities have been developed to antagonize TNF activity, largely through sequestration of circulating TNF by soluble TNF receptor constructs [125-126] or anti-TNF antibodies [127]. While some of these strategies have

demonstrated efficacy in animal models [128], few have been successful in human clinical trials of sepsis [27]. Concurrent removal of TNF with other pro- and anti- inflammatory cytokines may provide a beneficial clinical effect by promoting down-regulation of systemic inflammation, versus blocking single cytokines within the complex network of interconnected humoral signaling pathways.

TNF is typically removed at slow rates in porous adsorbent devices [129-132], including our device, due to the large size of TNF (51kD) compared to other targeted cytokines such as IL-6 (21kD), IL-10 (19kD), and IL-8 (8kD). Monoclonal antibodies against TNF have been physically adsorbed [133] or covalently attached [134] to sorbent surfaces to facilitate enhanced capture of TNF from biological fluids. In our device, slow TNF removal is putatively due to hindered diffusion of the large trimeric molecule within the small sorbent pores (0.8-5nm). Trimeric TNF is on the cusp of molecular weight ranges excluded by the sorbent pore structure, thus resulting in ineffective removal. Small pores are required in the device to exclude essential large plasma proteins such as albumin, but allow smaller MW solutes such as cytokines to be removed from the blood. We hypothesized that TNF capture could be significantly accelerated by promoting dissociation of trimeric TNF into its smaller monomeric constituents, allowing faster diffusion of monomeric TNF into the sorbent pores, and increasing overall removal of bioactive TNF. The work presented in this chapter characterizes the dissociation behavior of TNF using DMSO to promote TNF deoligomerization. Gel filtration chromatography was utilized to confirm changes to TNF molecular size, and *in vitro* packed bed capture experiments were used to quantify TNF removal rates by the sorbent beads.

5.1 MATERIALS & METHODS

5.1.1 Materials

Recombinant human TNF (51kD, >95% purity) and IL-6 (21kD, >95% purity), Bis[2-(succinimidooxycarbonyloxy)ethyl]sulfone (BSOCOES) crosslinker, and dimethyl sulfoxide (DMSO) were purchased from Fisher Scientific (Waltham, MA). BSA (>96% purity) was purchased from Sigma Aldrich (St. Louis, MO). Horse serum and recombinant human soluble TNF receptor-I (sTNF-RI) were purchased from Invitrogen (Camarillo, CA). Human blood was obtained from healthy volunteers at the University of Pittsburgh Medical Center. All human blood protocols were approved by the University Institutional Review Board. Whole blood samples were collected in silica-coated clotting tubes (BD Bioscience, Franklin Lakes, NJ), and serum was collected after clotting and centrifugation, according to manufacturer instructions. CytoSorb sorbent beads were provided by CytoSorbents, Inc. (Monmouth, NJ). CytoSorb beads are polystyrene-divinylbenzene porous particles (450μm avg. particle diameter, 67% porosity, 1.02g/cm^3 density, ~0.8-5nm pore diameter, 850m^2/g surface area) with a biocompatible polyvinyl-pyrrolidone coating.

5.1.2 TNF Crosslinking

Intramolecular TNF crosslinking was performed using BSOCOES, a 435Da bifunctional crosslinking reagent consisting of a 13Å spacer arm with NHS-ester reactive groups on both ends. The NHS-ester binds to primary amine groups on the TNF molecule, covalently linking adjacent monomeric subunits to form a stable trimer. 2mg BSOCOES was dissolved in 200μl

DMSO, and 2.5µl of the dissolved reagent was added to 250µl of TNF or IL-6 (40µg/ml) in PBS. The products were incubated for 30min at ambient temperature, and excess crosslinker was removed using centrifugal desalting columns.

5.1.3 Gel Filtration Chromatography

Gel filtration chromatography was performed using a Superdex^{TM}75 column and AKTAexplorer^{TM} FPLC system (GE Healthcare, Piscataway, NJ). TNF was spiked in human serum, horse serum, or PBS + 10mg/ml BSA to achieve TNF concentrations of ~1ng/ml. Samples were incubated with 0% or 10% DMSO for 24hr at 4˚C, and 50µl aliquots were injected into the gel filtration column at a flow rate of 0.8ml/min. The column was equilibrated and eluted with 10mM PBS + 1mg/ml BSA, and 0% or 10% DMSO (corresponding to TNF samples incubated with 0% or 10% DMSO). Effluent fractions of 250µl were collected and assayed for TNF using ELISA. Chemically crosslinked TNF in PBS + 10mg/ml BSA was incubated with 0% or 10% DMSO for 24hr at 4˚C, and injected into the column in the same manner as described above. Soluble TNF receptor-I (sTNF-RI) (50ng/ml) was spiked with TNF into human serum or PBS+ 10mg/ml BSA, and injected into the column in the same manner as described above. BSA (67kD), ovalbumin (43kD), chymotripsinogen (25kD), and RNAase (13.7kD) in PBS or PBS + 10% DMSO were used as molecular weight standards to calibrate the column.

5.1.4 TNF Capture in a Sorbent Device

TNF or IL-6 was spiked in human serum or horse serum to achieve cytokine concentrations of ~1ng/ml. Samples were incubated with 0% or 10% DMSO for 24hr at 4˚C, and 8ml aliquots

were recirculated through a device filled with 1.5g CytoSorb beads, at a flow rate of 0.8ml/min using a peristaltic pump. The reservoir was sampled at specific time points during recirculation, and cytokine concentrations were quantified using ELISA. Chemically crosslinked TNF or IL-6 was spiked in PBS + 50mg/ml BSA +/- 10% DMSO for 24hr at 4˚C, and recirculated through a sorbent device in the same manner as described above. sTNF-RI (50ng/ml) was spiked with TNF or IL-6 in human serum or PBS + 50mg/ml BSA, and recirculated through a sorbent device in the same manner as described above. All cytokine capture trials were run in duplicate or triplicate, and cytokine concentration averages are shown with error bars indicating standard deviation between the trials.

Cytokine capture data were fit to a mathematical model previously developed by our group [12] using nonlinear least squares regression, where cytokine removal rate is dependent on convection through the column, and adsorption/diffusion within the porous beads. Removal rate was quantified for each capture experiment by fitting the data to the model, and then using the fitted model to interpolate time to reach 50% concentration in the reservoir ($t_{1/2}$). $t_{1/2}$ values were calculated for each cytokine capture trial, and average values are shown +/- standard deviation between the trials. Differences in removal rates between experimental conditions were evaluated by statistically comparing $t_{1/2}$ values using Student's t-test. p-values $< .05$ were considered statistically significant.

5.1.5 ELISA Controls

ELISA controls were performed to ensure that manipulation of TNF molecular structure did not affect detection within the ELISA assay. TNF concentrations were measured by ELISA for samples before and after 24hr incubation without DMSO, with 10% DMSO, and crosslinked

TNF. Student's t-test was used to statistically compare cytokine concentrations quantified by ELISA. Mass concentrations were not statistically different ($p > .05$) before and after 24hr incubation for each sample, indicating consistent TNF quantitation under the conditions tested (data not shown). TNF + DMSO samples were assayed using DMSO in the ELISA standards calibration, and no differences were observed between standard curves with or without DMSO.

5.2 RESULTS

5.2.1 Gel Filtration Chromatography

5.2.1.1 TNF in PBS/BSA Buffer

TNF was incubated with 10% DMSO to promote dissociation of TNF oligomeric structure. Fig. 22(a) illustrates TNF FPLC effluent after 24hr incubation with 0% and 10% DMSO in PBS + 10mg/ml BSA, quantified for TNF using ELISA. Under native conditions (0% DMSO), TNF eluted as a 38kD oligomer, consistent with apparent molecular weight observed by others [123, 135]. TNF eluted entirely in 10kD monomeric form after incubation with 10% DMSO. Chemically crosslinked TNF was incubated for 24hr with 0% and 10% DMSO in PBS + 10mg/ml BSA. Fig. 22(b) demonstrates that crosslinked TNF eluted as a 38kD oligomer after incubation with 0% or 10% DMSO. The slight shift in TNF peaks was due to column MW calibration differences between PBS and PBS + 10% DMSO mobile phases. This result indicates covalent linkage of TNF subunits via chemical crosslinking, which are subsequently resistant to dissociation by DMSO. Additionally, chemical crosslinking does not form high molecular weight aggregates of multiple TNF molecules, but promotes only intramolecular

binding [136]. Soluble TNF receptor-I (sTNF-RI) and TNF were spiked in PBS + 10mg/ml BSA to determine effects of TNF/receptor binding on TNF molecular size (Fig. 22(c)). As expected, addition of sTNF-RI promoted formation of a large molecular weight TNF complex (58kD), compared to the molecular size observed for TNF alone in PBS/BSA buffer (38kD).

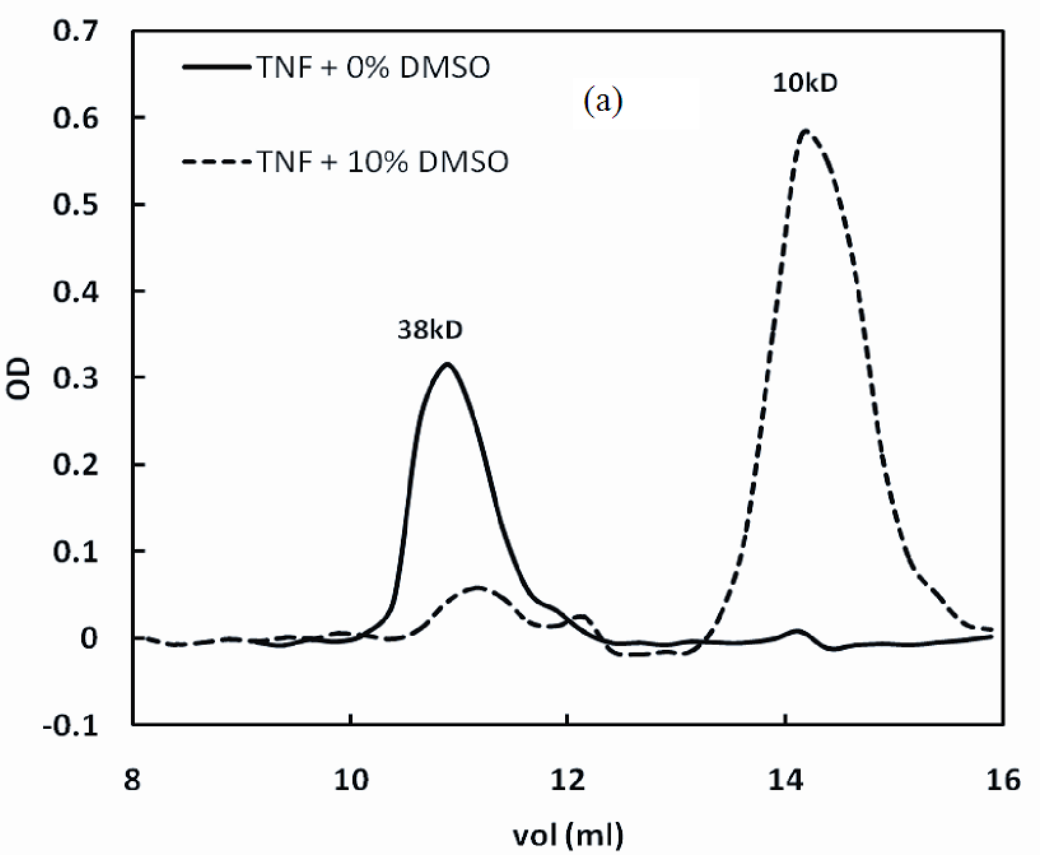

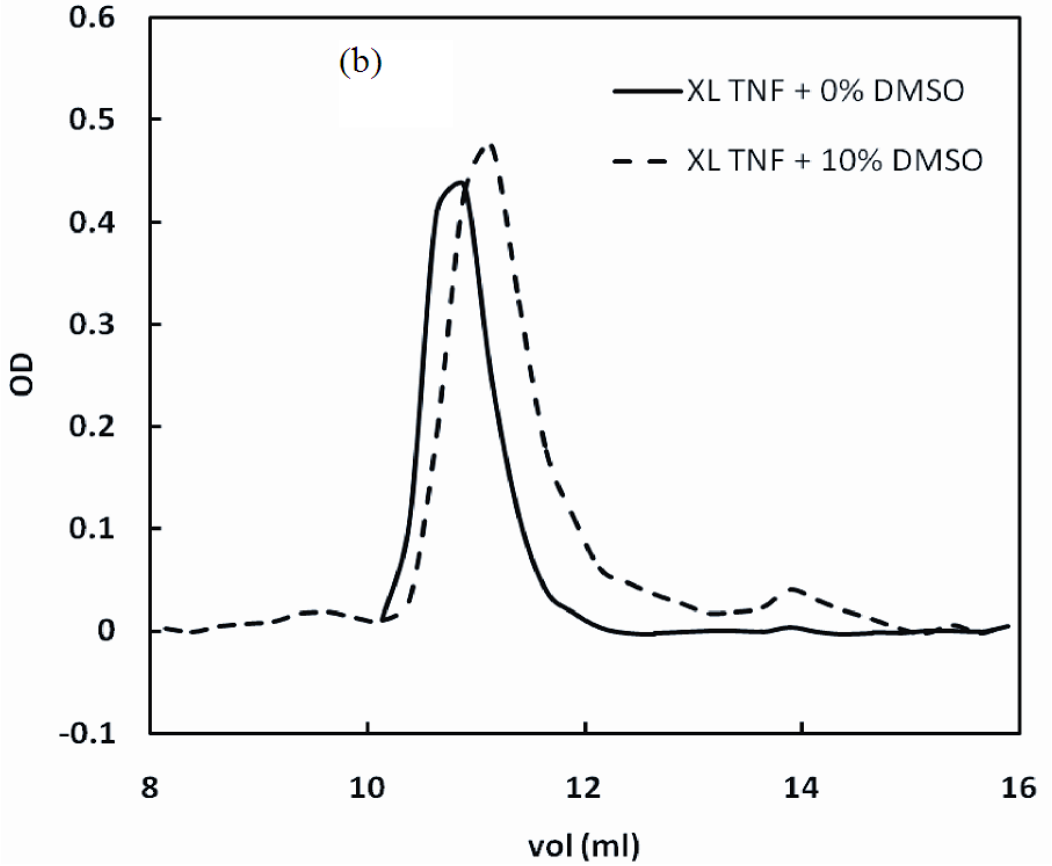
(b)
XL TNF + 0% DMSO
XL TNF + 10% DMSO
OD
0.6
0.5
0.4
0.3
0.2
0.1
0
-0.1
8
10
12
14
16
vol (ml)

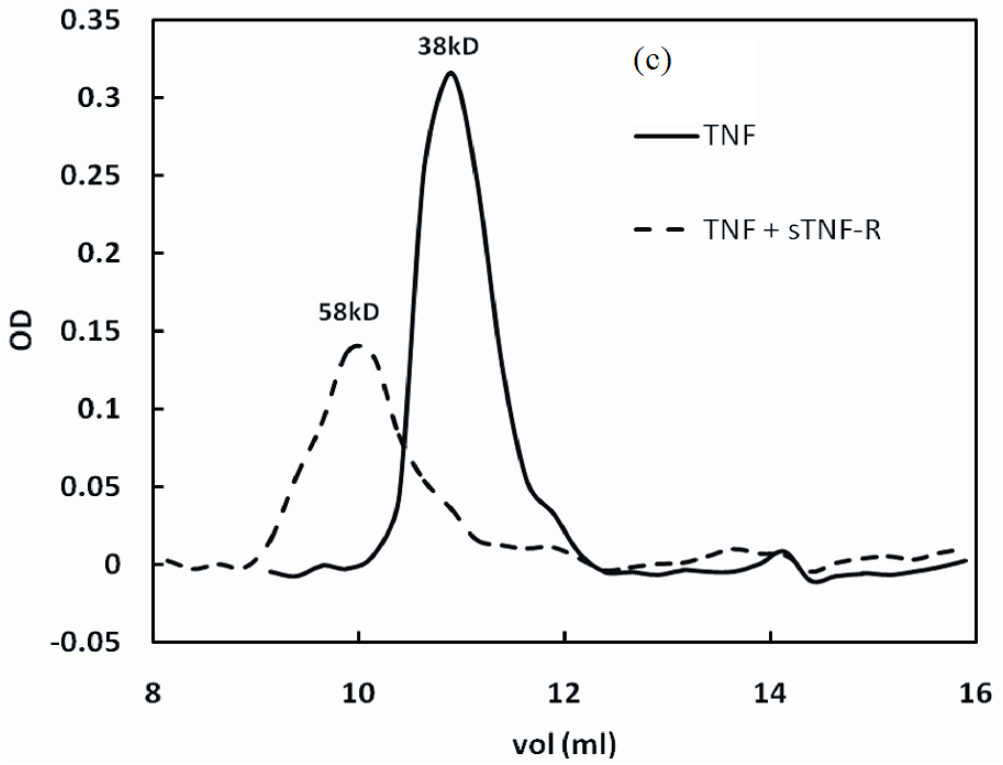

Figure 22: Gel filtration chromatography of TNF in PBS + 10mg/ml BSA. (a) TNF incubated with 0% or 10% DMSO (b) Crosslinked TNF incubated with 0% or 10% DMSO. (c) TNF spiked with sTNF-RI.

5.2.1.2 TNF in Serum

TNF was spiked in horse serum and human serum to investigate possible interactions between TNF and serum constituents. TNF incubated with 0% and 10% DMSO in horse serum eluted at 38kD and 10kD, respectively (Fig. 23(a)), consistent with the elution volumes observed for TNF in PBS/BSA buffer (Fig. 22(a)). TNF incubated in human serum eluted as two distinct peaks – one corresponding to a 35kD specie, and another corresponding to a 58kD specie (Fig. 23(b)). The latter result can be explained by TNF binding to endogenous sTNF-R, which promotes formation of a large molecular weight complex [135], similarly observed when recombinant sTNF-RI was added to TNF in PBS/BSA buffer (Fig. 22(c)). The absence of a significant

receptor-bound peak in horse serum is likely due to inefficient binding between spiked human TNF and endogenous horse sTNF-R, or negligible levels of sTNF-R in the horse serum. sTNF-RI was added to TNF in human serum, resulting in a single broad peak ~50kD. Human serum and horse serum without spiked TNF were run as controls, and endogenous TNF was not detected in the FPLC effluent.

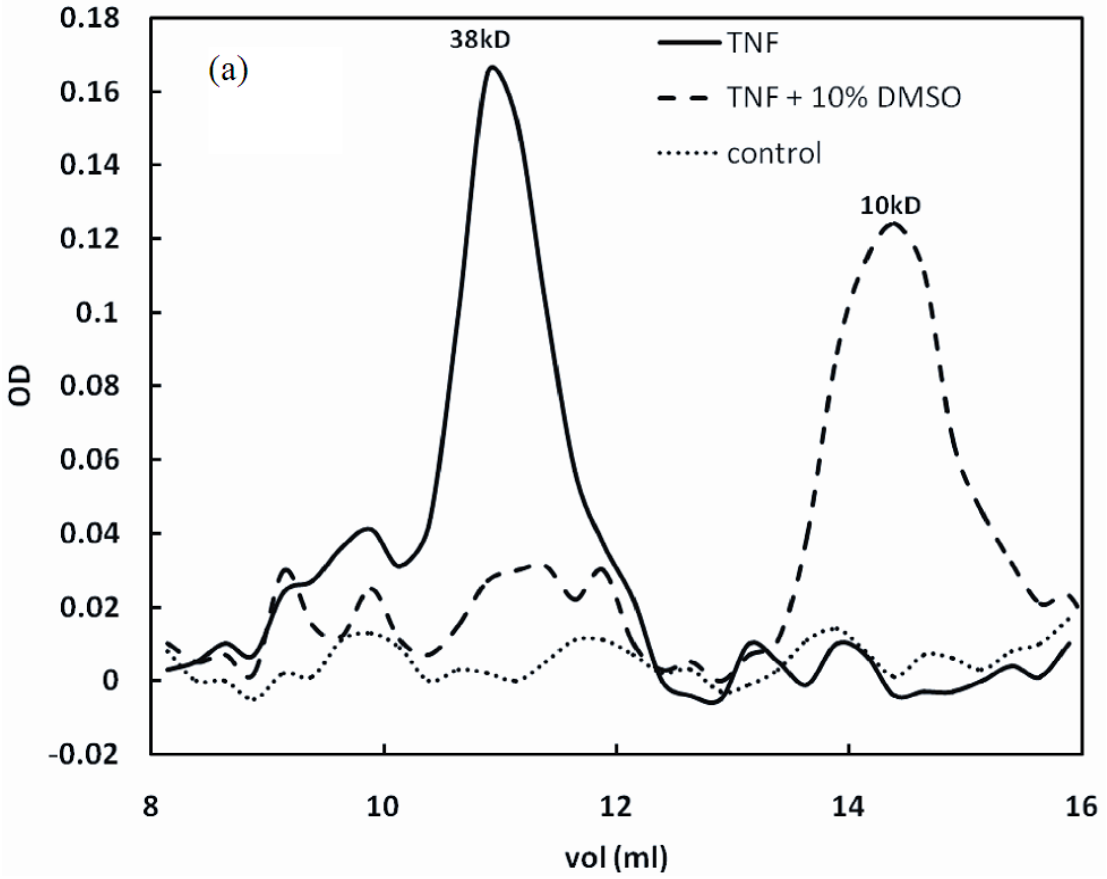

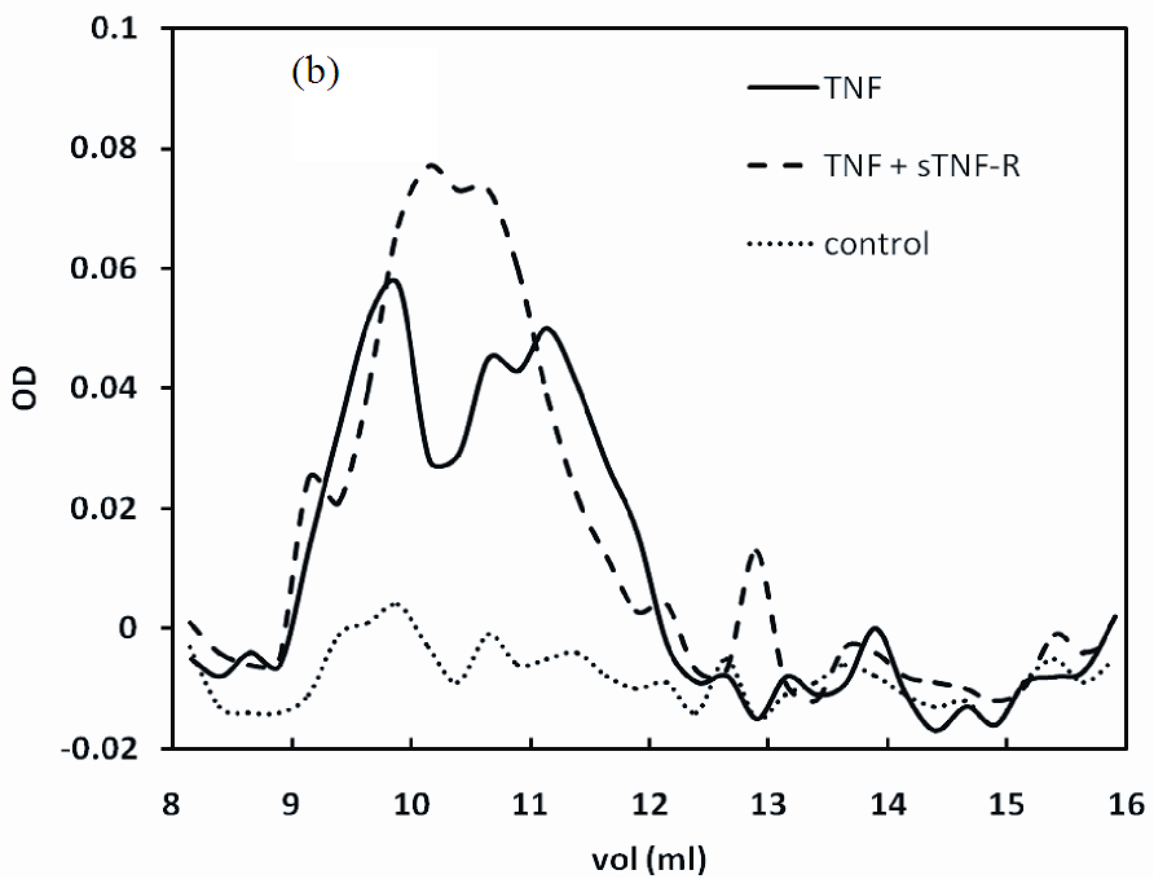

Figure 23: Gel filtration chromatography of TNF in horse and human serum. (a) TNF in horse serum incubated with 0% or 10% DMSO (b) TNF in human serum with sTNF-RI.

5.2.2 TNF Capture in a Sorbent Device

5.2.2.1 TNF Capture with DMSO

Effects of TNF deoligomerization on capture behavior in a sorbent device were tested using CytoSorb sorbent beads. TNF capture in horse serum after incubation with 0% and 10% DMSO for 24hr is illustrated in Fig. 24. TNF capture was substantially accelerated after incubation with 10% DMSO, compared to TNF incubated without DMSO ($t_{1/2}$ = 13.3 +/- 1.5min vs. 112.8 +/- 13.3min, respectively; $p < .05$). IL-6 capture after 24hr incubation with and without 10% DMSO

were equivalent ($t_{1/2}$ = 30.9 +/- 5.2min vs. 25.7 +/- 3.5min, respectively; $p > .05$), indicating that DMSO effects on capture rates are specific to TNF structural manipulation.

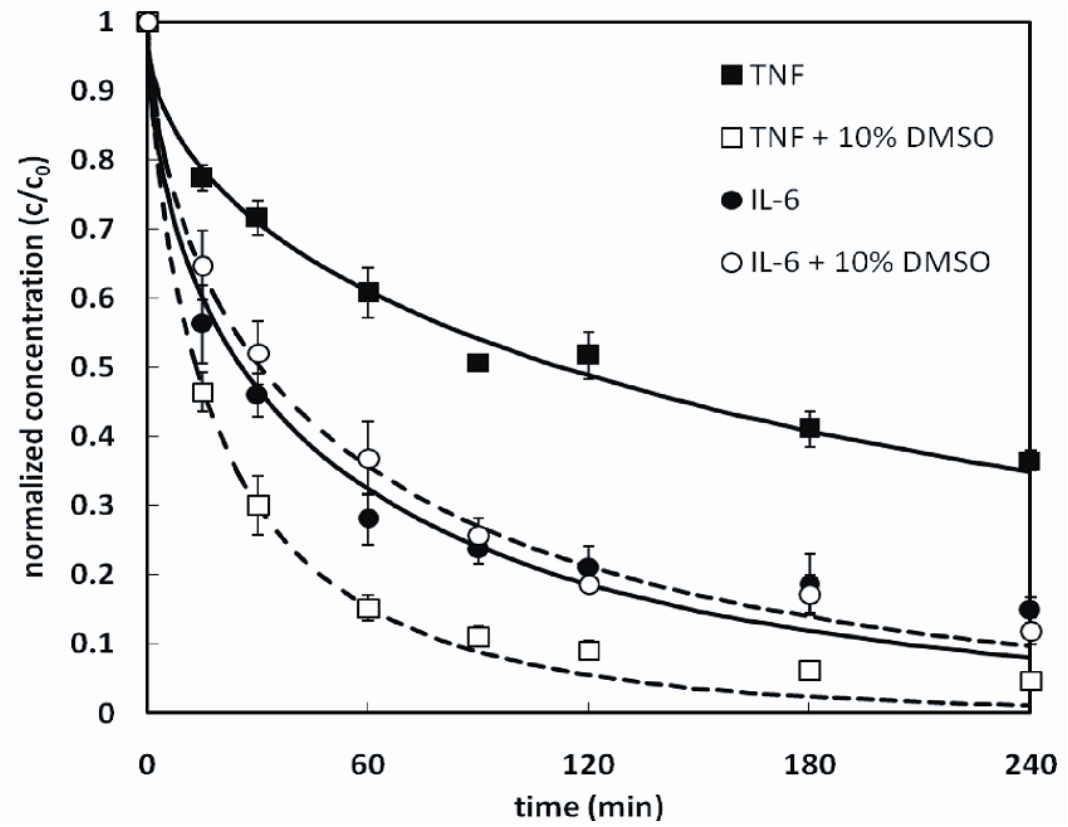

Figure 24: TNF and IL-6 capture from horse serum within a cytokine adsorption device. Model fits are shown for 0% DMSO (solid lines) and 10% DMSO (dashed lines) incubations.

5.2.2.2 Crosslinked TNF Capture

Crosslinked TNF was incubated with 0% and 10% DMSO for 24hr, and capture was performed in PBS + 50mg/ml BSA. Crosslinked TNF capture was the same after incubation with 0% and 10% DMSO ($t_{1/2}$ = 50.0 +/- 7.5min vs. 48.3 +/- 3.2min, respectively; $p > .05$) (Fig. 25), further substantiating FPLC results (Fig. 22(b)) that chemical crosslinking covalently stabilizes TNF trimeric structure and prevents DMSO induced monomerization. Crosslinked TNF capture was

slower than native TNF capture in PBS/BSA buffer ($t_{1/2}$ = 50.0 +/- 7.5min vs. 23.9 +/- 1.0min, respectively; $p < .05$). Crosslinked IL-6 capture was slower than native IL-6 capture ($t_{1/2}$ = 19.7 +/- 1.2min vs. 12.9 +/- 0.5min, respectively; $p < .05$), though percent IL-6 removed after 4 hours was the same.

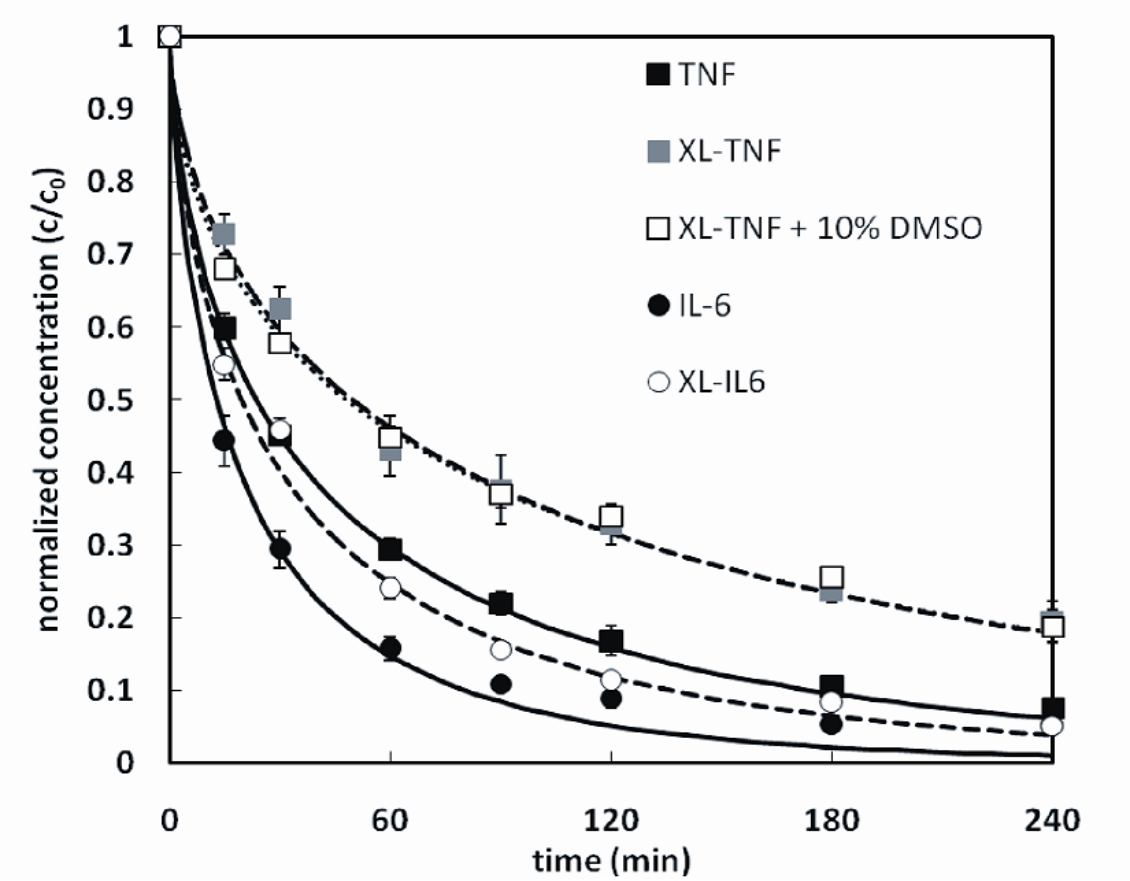

Figure 25: Crosslinked TNF and IL-6 capture from PBS + 50mg/ml BSA buffer in a cytokine adsorption device. Model fits are shown for native TNF and IL-6 (solid lines), XL-TNF and XL-IL6 (dashed lines), and XL-TNF + 10% DMSO (dotted line).

5.2.2.3 TNF + sTNF-RI Capture

TNF was incubated with soluble TNF receptor-I (sTNF-RI) to examine effects of receptor binding on TNF capture. Fig. 26 illustrates TNF capture from PBS + 50mg/ml BSA with and without sTNF-RI coincubation. TNF capture was slower after incubation with sTNF-RI compared to TNF alone ($t_{1/2}$ = 68.9 +/- 12.7min vs. 31.7 +/- 1.5min, respectively; $p < .05$). IL-6 was incubated with sTNF-RI, and capture was statistically faster compared to IL-6 alone ($t_{1/2}$ = 11.5 +/- 0.7min vs. 12.9 +/- 0.5min, respectively; $p < .05$), although the difference in removal rate magnitudes was negligible.

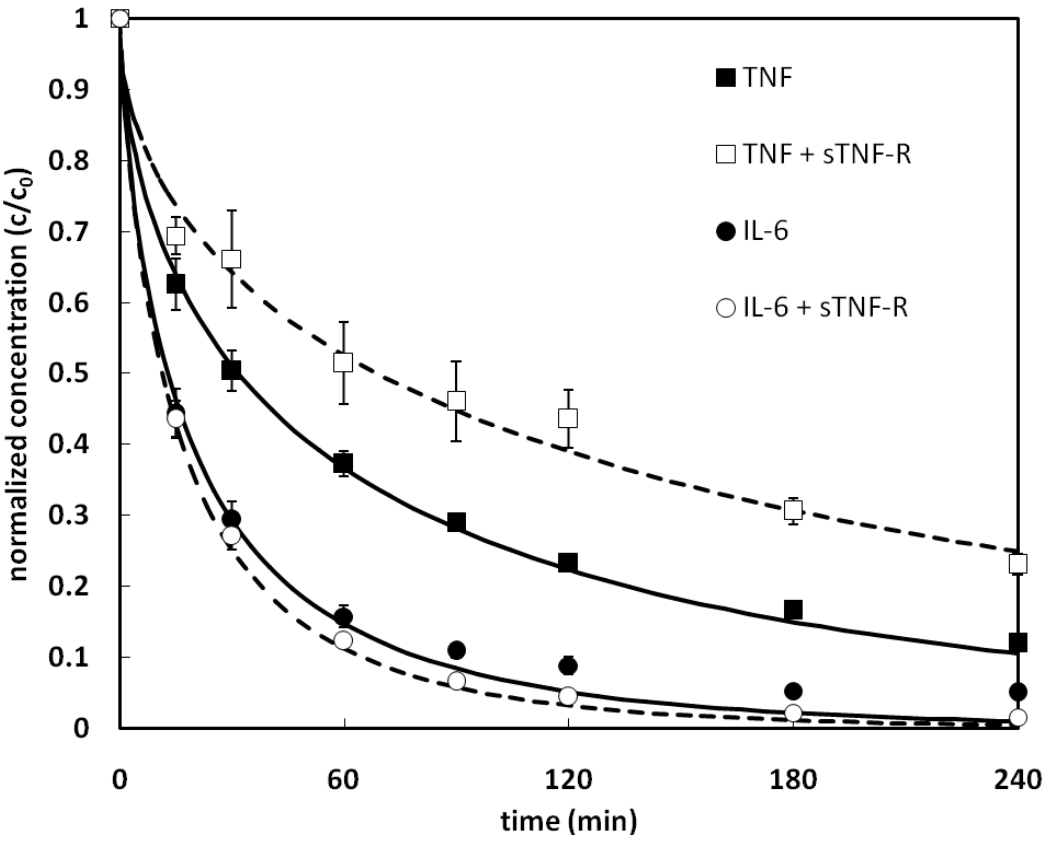

Figure 26: TNF and IL-6 capture from PBS + 50mg/ml BSA buffer with sTNF-RI in a cytokine adsorption device. Model fits are shown for TNF and IL-6 (solid lines), and TNF and IL-6 + sTNF-RI (dashed lines).

5.2.2.4 TNF Capture in Human Serum

TNF was spiked in human serum from healthy volunteers, and capture results are illustrated in Fig. 27. Capture rates were the same between TNF spiked in human serum with sTNF-RI and TNF alone ($t_{1/2}$ = 217.7 +/- 34.9min vs. 172.8 +/- 2.5min, respectively; $p > .05$). Capture of TNF incubated with 10% DMSO in human serum was accelerated compared to baseline TNF capture in human serum ($t_{1/2}$ = 217.7 +/- 34.9min vs. 18.1 +/- 2.3min, respectively; $p < .05$). Baseline TNF capture (no incubation period) was equivalent between horse and human serum – percent TNF removal at the 4hr end point was within 10% agreement (data not shown).

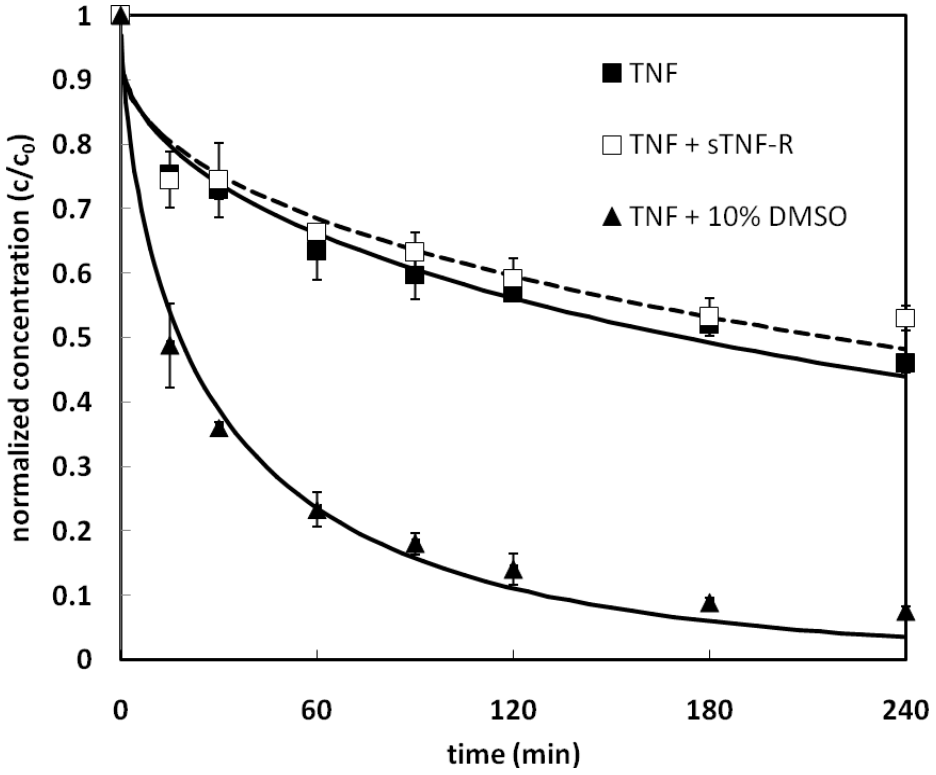

Figure 27: TNF capture from human serum with sTNF-RI, or incubated with 10% DMSO, in a cytokine adsorption device. Model fits are shown for TNF +/- DMSO (solid lines), and TNF + sTNF-RI (dashed lines).

5.3 DISCUSSION

Tumor necrosis factor (TNF), a 51kD pro-inflammatory cytokine, is removed at a slow rate within the device compared to smaller cytokines, putatively due to hindered diffusion of the large trimeric TNF molecule within the sorbent pores. Similar deficiencies in TNF capture have been reported using other cytokine-targeted sorbent materials [129-132]. Small sorbent pores are necessary to prevent essential large plasma proteins such as albumin from being removed by the device; hence, our goal was to develop strategies to accelerate TNF removal while maintaining an optimal pore size for whole blood filtration. The present work investigated the structural behavior of oligomeric TNF *in vitro*, and sought to quantify how specific perturbations of TNF quaternary structure would affect TNF capture within the hemoadsorption device.

TNF exists in solution primarily as a noncovalently associated homotrimer [115, 121, 136]. DMSO, a polar organic solvent, was used to disrupt subunit hydrophobic interactions and promote dissociation of the trimeric molecule, which was confirmed using gel filtration chromatography. Subsequent capture of monomerized TNF was substantially faster than native TNF capture in the device: removal halftime ($t_{1/2}$) in horse serum = 13.3 +/-1.5min vs. 112.8 +/-13.3min, respectively; $p < .05$. Cytokine capture is mediated by molecular diffusion into the internal pore structure, and adsorption to the polymeric surface through non-specific hydrophobic interactions. Trimeric TNF (51kD) is on the cusp of molecular weight ranges excluded by the CytoSorb pore structure, thus resulting in ineffective removal. We previously demonstrated that BSA (66kD) does not appreciably penetrate into the sorbent over time (Chapter 3, [99]), and would expect slower capture of large cytokines (e.g. TNF, 51kD) compared to smaller cytokines (e.g. IL-6, 21kD) within the adsorption device.

We covalently crosslinked TNF subunits to stabilize the trimeric structure, and confirmed that DMSO incubation had no effect on crosslinked TNF molecular size nor capture within the device. In PBS/BSA buffer, crosslinked TNF was removed at a slower rate than native TNF ($t_{1/2}$ = 50.0 +/- 7.5min vs. 23.9 +/- 1.0min, respectively; $p < .05$). We demonstrated using gel filtration chromatography that both native and crosslinked TNF exist predominantly in trimeric form under the experimental conditions presented. However, it is likely that a small population of monomeric TNF exists under native conditions, which can diffuse into the sorbent pores quickly and promote subsequent dissociation of bulk phase trimeric TNF to maintain equilibrium in the reservoir. This hypothesis can explain why crosslinked TNF is removed at a slower rate than native TNF.

Soluble TNF receptors (sTNF-R) are typically present in serum at ~ng/ml levels [137], and bind circulating TNF. They attenuate TNF signaling by blocking TNF activation of cell-surface receptors [138], and conversely, can prolong circulating TNF half-life by acting a slow release reservoir [135]. Expression of sTNF-R are elevated during sepsis [139], and their interactions with TNF may affect TNF removal dynamics within the device. When sTNF-RI was spiked with TNF in PBS/BSA, TNF capture was slower compared to TNF alone ($t_{1/2}$ = 68.9 +/- 12.7min vs. 31.7 +/- 1.5min, respectively; $p < .05$), due to the larger size of the TNF/receptor complex. In human serum, spiked TNF eluted in both free (38kD) and higher MW (58kD) forms, the latter likely due to interactions with endogenous TNF receptors. When recombinant sTNF-RI was spiked with TNF in human serum, FPLC effluent shifted towards a single broad peak, suggesting a higher ratio of receptor bound TNF, but the effects on TNF capture were minimal. TNF + 10% DMSO capture in horse and human serum were comparable ($t_{1/2}$= 13.3 +/- 1.5min vs. 18.1 +/- 2.3min, respectively; $p = .04$). TNF in horse serum eluted primarily in

trimeric form, while TNF in human serum eluted in trimeric and receptor-bound forms. Equivalent TNF capture rates in human and horse serum after DMSO incubation suggest that DMSO induced TNF monomerization prevents TNF/sTNF-R binding, which is consistent with findings in the literature indicating that TNF actively binds its soluble and cell receptors only in trimeric form [116-118].

Horse serum, human serum, and PBS/BSA buffer were used as test solutions to investigate different aspects of TNF adsorption dynamics. PBS/BSA buffer was the most simplistic, and allowed us to study native TNF without the influence of soluble TNF receptors or significant amounts of coadsorbing solutes. Horse serum provided a more realistic understanding of TNF capture within the device, although the absence of a substantial receptor-bound TNF peak in the FPLC effluent suggested minimal binding between spiked human TNF and endogenous horse soluble receptors. Finally, human serum was used to investigate TNF/sTNF-R interactions, although these results should not be extrapolated to predict *in vivo* dynamics, where the effects of mediator production by inflammatory cells and cytokine tissue/plasma transport are immensely complex. Overall, significantly slower TNF capture rates in horse serum compared to buffer ($t_{1/2}$ = 112.8 +/- 13.3min vs. 23.9 +/- 1.0min, respectively) are likely due to coadsorption of middle molecular weight solutes, which can cause pore occlusion and hindered TNF diffusional rates within the sorbent pores. Slower IL-6 capture was also observed in serum vs. buffer ($t_{1/2}$ = 25.7 +/- 3.5min vs. 12.9 +/- 0.5min, respectively), but the effects of coadsorption and pore occlusion on TNF capture are likely exacerbated due to the large size of TNF (51kD) compared to IL-6 (21kD). Furthermore, similarities between (1) baseline TNF capture in horse serum, (2) baseline TNF capture in human serum, and (3) TNF +

sTNF-R capture in human serum, suggest that soluble receptor binding is not the primary mechanism for slow TNF capture within the device.

Results from this study demonstrate that dissociation of oligomeric TNF is an effective strategy to significantly improve TNF capture within sorbent materials. TNF is an important initiator of systemic inflammation during sepsis, and removal of TNF from the circulating blood may help attenuate hyper-inflammatory signaling pathways and improve patient outcomes in the setting of severe sepsis. TNF deoligomerization promotes fast diffusion and adsorption of the small monomeric species within the sorbent beads. As monomeric TNF is continually removed, bulk phase trimeric TNF likely dissociates to maintain trimer/monomer equilibrium in the reservoir, although this phenomenon needs to be investigated *in vivo* where the equilibrium between monomeric, trimeric, and receptor-bound TNF are more complex.

The clinical efficacy of anti-TNF or anti-cytokine therapies for sepsis remains unclear [13, 27], but the TNF deoligomerization concept presented in this work may have broad applications in other disease states where TNF removal from the plasma is targeted, such as rheumatoid arthritis or Crohn's disease [126]. Additionally, this technique could be extended to improve capture of oligomeric cytokines such as IL-10, or other oligomeric biomolecules using size exclusion filtration materials. Although we utilized DMSO as a simple agent to induce TNF dissociation, a variety of small molecules have been shown to facilitate TNF deoligomerization [122-124]. Chapter 6 describes ongoing efforts to develop sorbent materials with immobilized dissociative agents, to locally deoligomerize TNF at the sorbent surface as a clinically viable hemoadsorption modality.

****The work in this chapter was published as:** Kimmel JD, Lacko CS, Delude RL, Federspiel WJ. Characterizing accelerated capture of deoligomerized TNF within hemoadsorption beads used to treat sepsis. *Journal of Biomedical Materials Research: Part B.* 2011, 98B(1); 47-53.

6.0 SMALL MOLECULE DISSOCIATION OF OLIGOMERIC TNF

Results presented in Chapter 5 demonstrate accelerated removal of deoligomerized TNF compared to native TNF removal within the sorbent device. DMSO incubation was used to dissociate trimeric TNF as proof of principle, however, incorporation of DMSO into the circulation is not a clinically feasible tool. Our ultimate goal is to develop surface modified sorbent beads capable of locally dissociating TNF within the device, eliminating the need for systemic administration of dissociating agents into the blood. This concept could have broad applications for dissociation of other large oligomeric molecules within a size exclusion filtration device. For example, one could envision dialysis fibers modified with small molecules capable of dissociating a variety of oligomeric molecules, facilitating removal of large solutes normally restricted by pore size exclusion. We have used TNF as a model to investigate feasibility of small molecule induced deoligomerization, and discuss potential applications outside the realm of cytokine capture for the treatment for sepsis.

6.1 SCREENING OF SMALL MOLECULE CANDIDATES

TNF is a homotrimer composed of three subunits stabilized by noncovalent hydrophobic interactions. As discussed previously, DMSO likely dissociates trimeric TNF through disruption of these subunit hydrophobic interactions. There has been great interest, particularly in the

pharmaceutical field, of identifying small molecule drugs that could dissociate TNF and consequently inactivate TNF biological activity *in vivo* [124]. Small molecules (< ~5kDa) are attractive candidates for conjugation to sorbent surfaces, due to their large size compared to solvents such as DMSO (78Da), and availability of functional groups that can be used for covalent linkage to a polymer surface. Using data available in the literature, a series of small molecules were tested to determine efficacy in promoting TNF deoligomerization (Table 5).

Table 5: Selection of small molecules tested for their ability to deoligomerize trimeric TNF.

Suramin MW = 1.4kDa	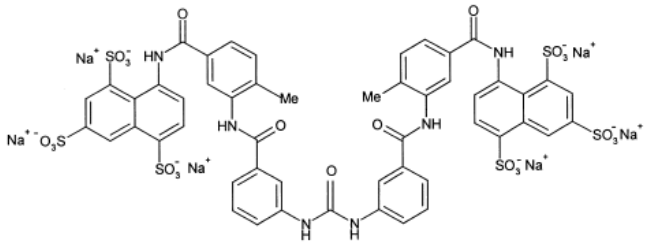
Trypan Blue MW = 873Da	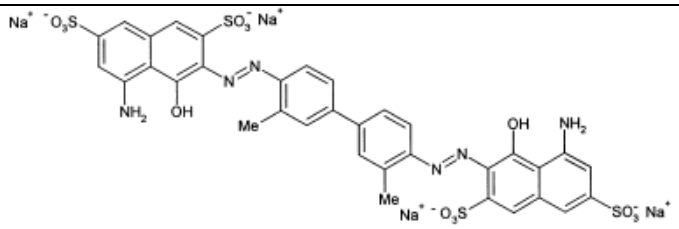
Evans Blue MW = 961Da	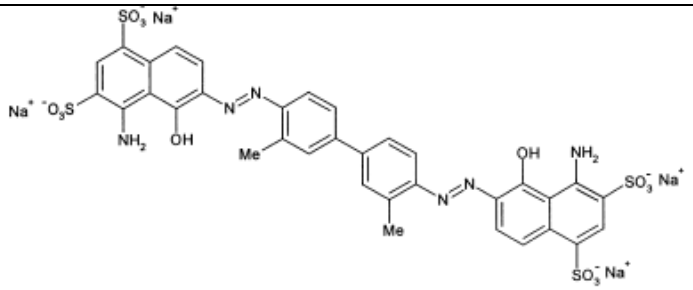

Table 5 (continued):

Erythrocin B MW = 880kDa	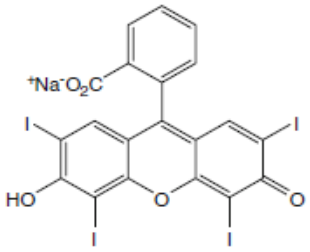
Triton X-100 MW = 647Da	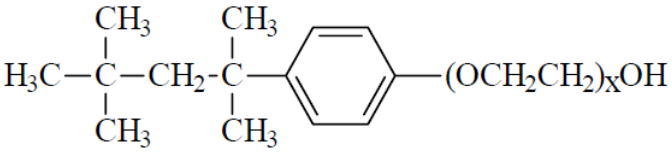

Suramin was chosen as a primary candidate based on its documented ability to dissociate TNF [123]. Suramin destabilizes the trimeric TNF quaternary structure, resulting in biologically inactive monomeric species [140]. Mancini, *et al.* performed molecular computational simulations, and concluded that electrostatic interactions and length/symmetry of the suramin molecule are responsible for interactions between suramin and the TNF trimer (Fig. 28) [122]. Trypan Blue and Evans Blue were identified as inexpensive structural analogues of suramin, and were therefore included in the screening process. Erythrocin B is an organic dye which has been shown to interact with TNF [141]. Triton X-100 is an amphiphilic surfactant which has been used to dissociate TNF [136]. Triton X-100 likely acts by interfering with TNF subunit interactions through its hydrophobic hydrocarbon group.

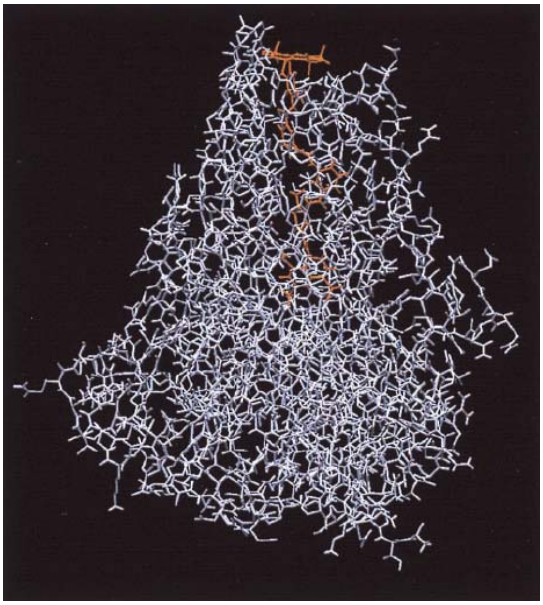

Figure 28: Computer simulation of suramin docked within the TNF trimeric core [122].

6.1.1 Methods

TNF was incubated in horse serum with each of the dissociating agents listed in Table 5, and standard *in vitro* recirculation capture experiments were performed to determine effects on TNF capture rates. Recirculation was performed as previously described in Chapter 5. Briefly, TNF was incubated with 1mM, 5mM, or 10mM of each dissociating agent for 24hr at 4˚C, and deoligomerization efficacy was evaluated by comparing TNF capture after incubation with baseline TNF capture. We assumed that accelerated TNF removal rates after incubation with dissociating agents were due to monomerization of trimeric TNF, as was observed using DMSO (Chapter 5). IL-6 capture controls were performed to ensure that effects from dissociating agent incubation on capture were specific to TNF.

6.1.2 Results

TNF capture in horse serum after incubation with suramin (1mM, 5mM, 10mM), Trypan Blue (1mM, 10mM), Evans Blue (1mM, 10mM), Erythrocin B (1mM, 10mM), and Triton X-100 (1.5mM) are illustrated in Figs. 29-33, respectively. Trypan Blue, Evans Blue, and Erythrocin B had negligible effects on TNF capture. These compounds have known affinities for albumin [142], therefore they may bind free albumin in horse serum, preventing potential interactions with TNF. Suramin accelerated TNF capture in a dose dependent manner, likely due to partial deoligomerization of trimeric TNF. Suramin incubation did not, however, accelerate TNF capture to the extent that was observed after 10% DMSO incubation. Triton X-100 incubation significantly accelerated TNF capture, resulting in similar capture rates compared to 10% DMSO incubation. This result suggests that Triton X-100 incubation is effective in completely dissociating TNF into monomeric form, as was shown previously using DMSO and gel filtration chromatography (Fig. 22).

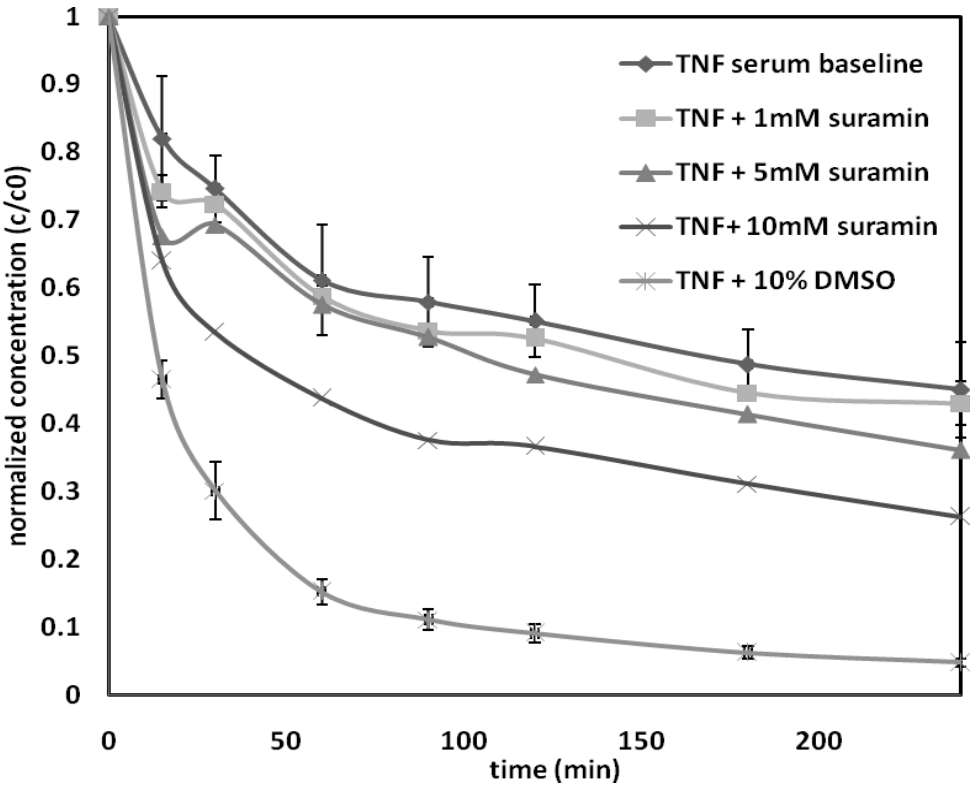

Figure 29: TNF capture in horse serum after 24hr incubation with suramin (1mM, 5mM, 10mM). Baseline TNF capture and TNF capture after 24hr incubation with 10% DMSO are shown as references.

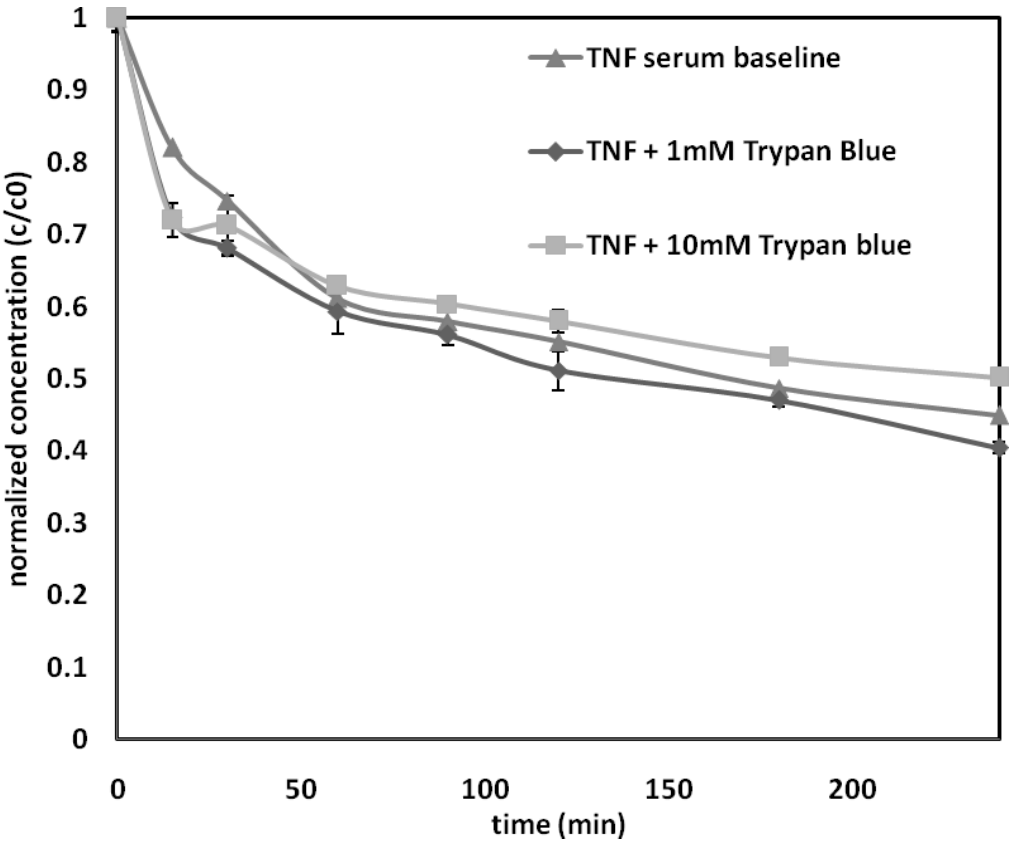

Figure 30: TNF capture in horse serum after 24hr incubation with Trypan Blue (1mM, 10mM). Baseline TNF capture is shown as a reference.

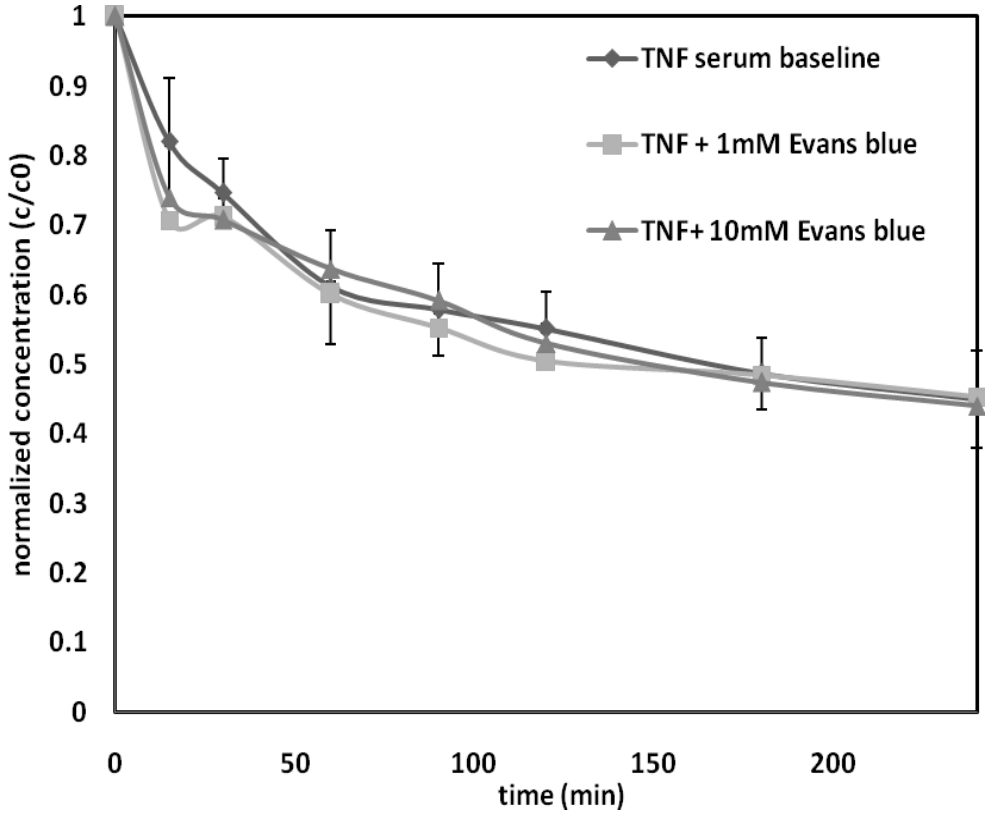

Figure 31: TNF capture in horse serum after 24hr incubation with Evans Blue (1mM, 10mM). Baseline TNF capture is shown as a reference.

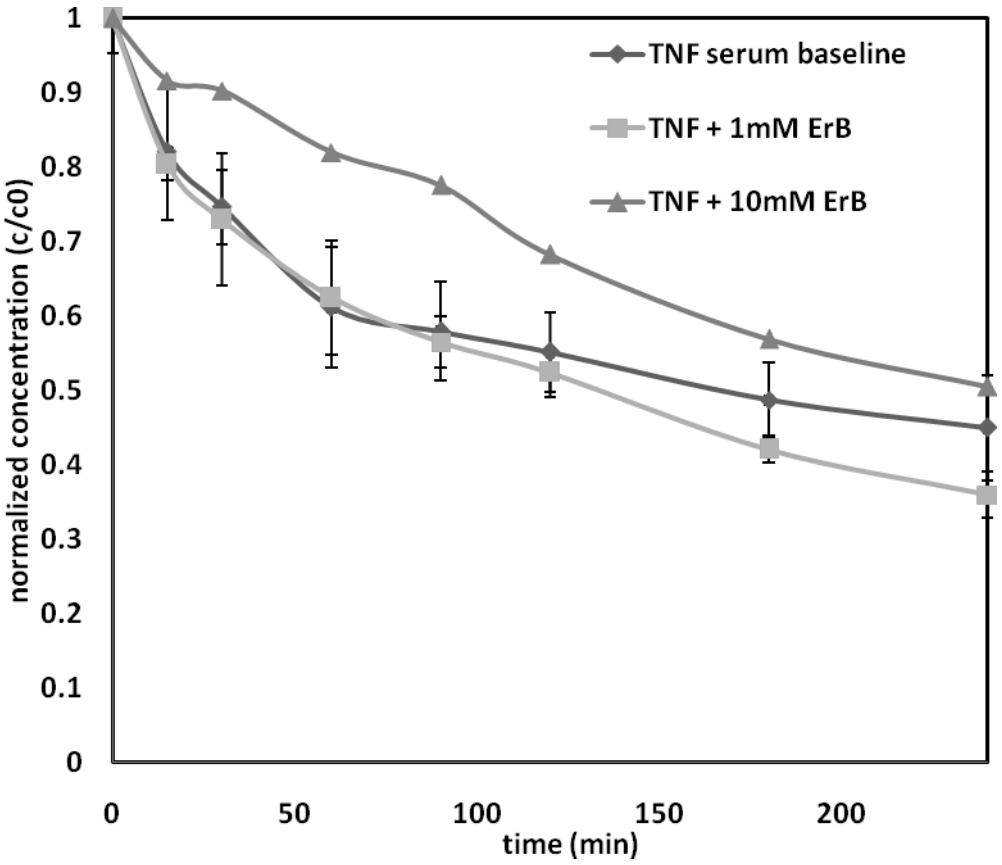

Figure 32: TNF capture in horse serum after 24hr incubation with Erythrocin B (ErB) (1mM, 10mM). Baseline TNF capture is shown as a reference.

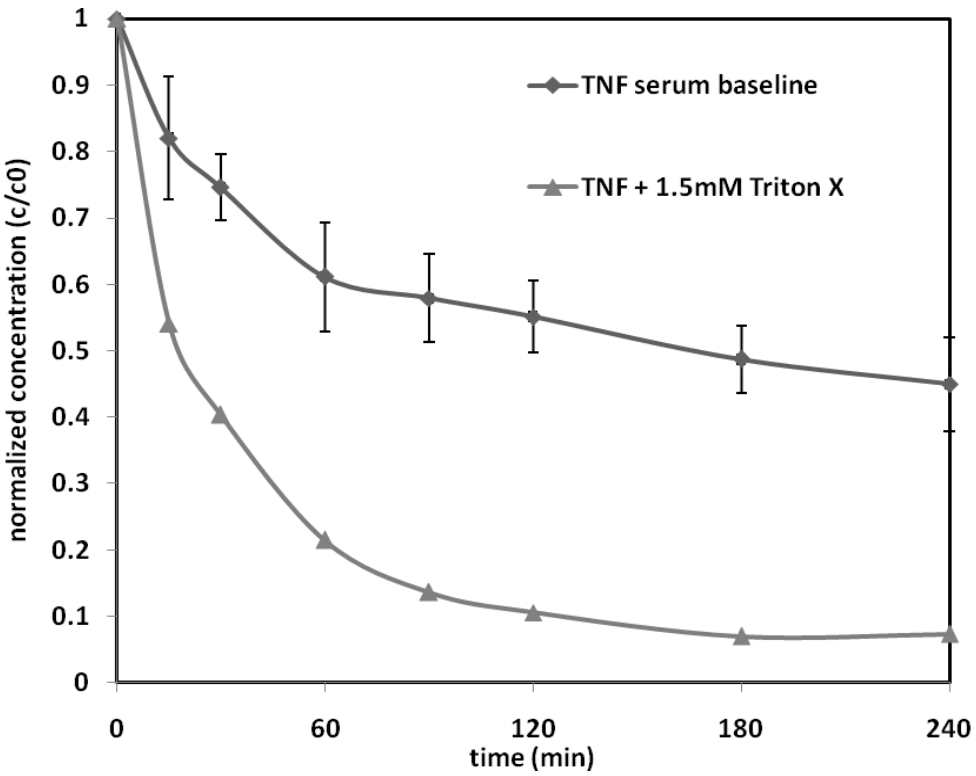

Figure 33: TNF capture in horse serum after 24hr incubation with Triton X-100 (1.5mM). Baseline TNF capture is shown as a reference.

IL-6 was incubated with 1mM suramin in PBS/BSA buffer for 24hr, and effects on IL-6 capture were negligible compared to baseline IL-6 capture (Fig. 34). Additionally, IL-6 was incubated with 1.5mM Triton X-100 in horse serum for 24hr, and effects on IL-6 capture were minimal (Fig. 35). These results suggest that effects from suramin and Triton X on cytokine capture are specific to TNF structural manipulation. Similar results were observed with IL-6 + 10% DMSO capture (Fig. 24).

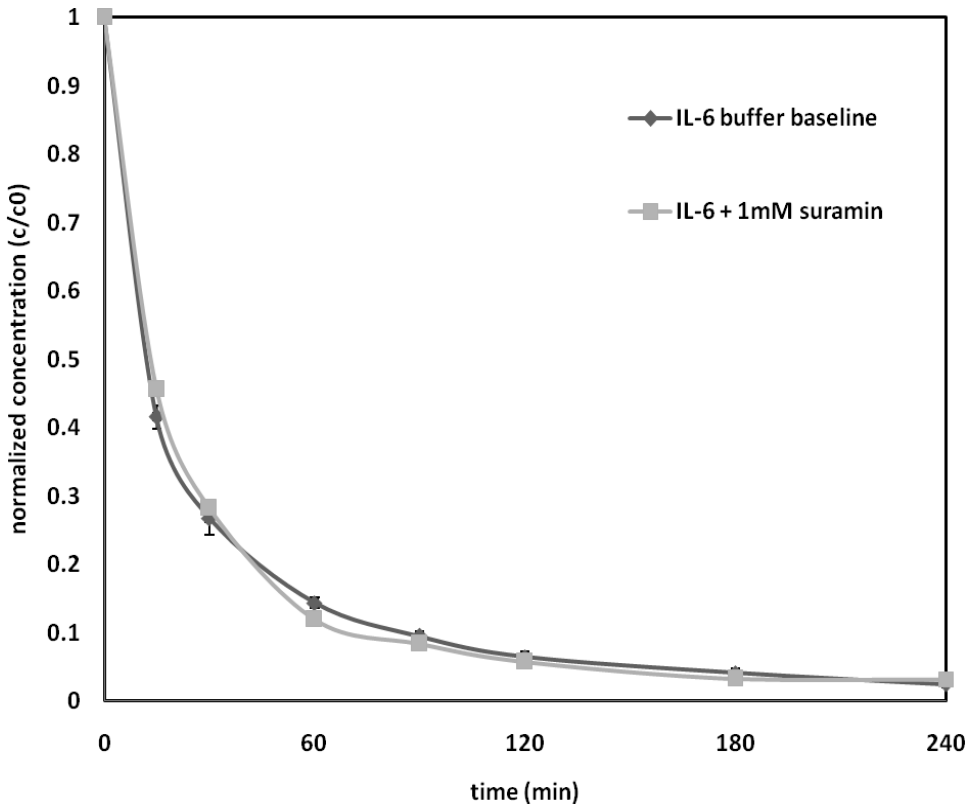

Figure 34: IL-6 capture in PBS/BSA buffer after incubation with 1mM suramin. Baseline IL-6 capture is shown as a reference.

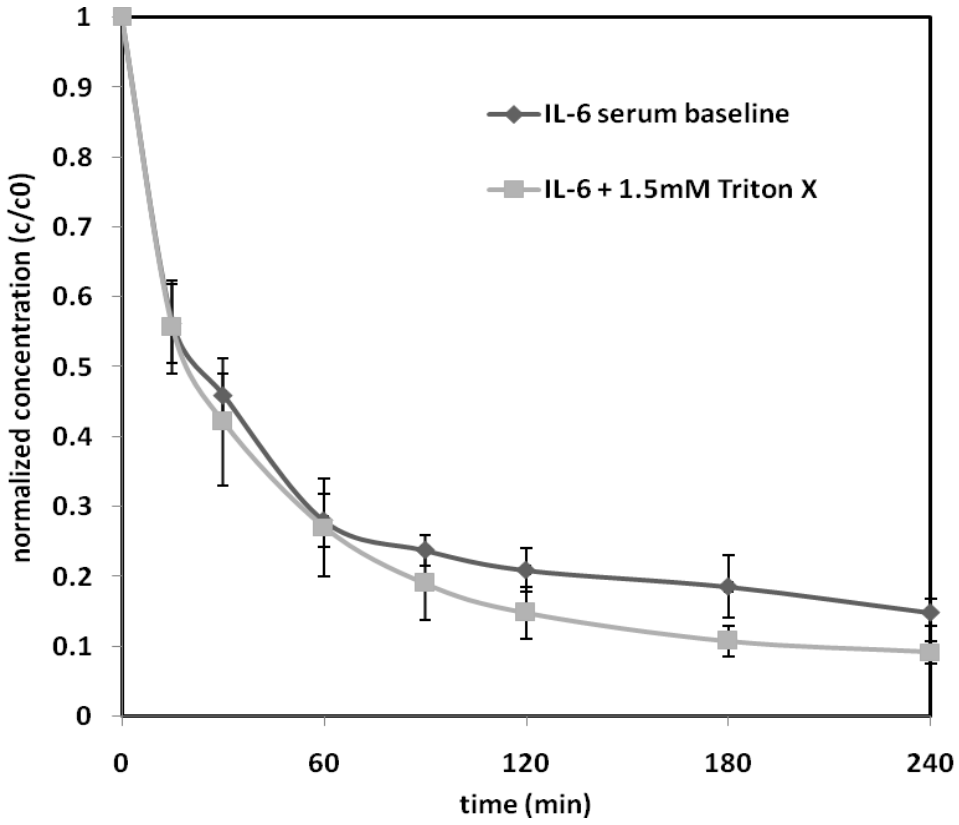

Figure 35: IL-6 capture in horse serum after incubation with 1.5mM Triton X-100. Baseline IL-6 capture is shown as a reference.

6.2 KINETICS OF TNF DEOLIGOMERIZATION

Based on results from screening of dissociating agent candidates, suramin and Triton X-100 demonstrated efficacy in accelerating TNF capture, putatively through deoligomerization of trimeric TNF. Although previous work with DMSO (Chapter 5) and the small molecule screening were performed using 24hr incubation with TNF, a clinically feasible device must have the ability to promote TNF deoligomerization within a time scale consistent with

therapeutic use of the device (~ 4-6hr). Therefore, kinetic studies were performed using DMSO, suramin, and Triton X-100 to quantify effects of incubation time on TNF capture rates.

6.2.1 Methods

6.2.1.1 Gel Filtration Chromatography

Gel filtration chromatography was performed using a Superdex^{TM}75 column and AKTAexplorer^{TM} FPLC system (GE Healthcare, Piscataway, NJ). TNF was spiked in PBS + 10mg/ml BSA to achieve TNF concentrations of ~1ng/ml. Samples were incubated with 10% DMSO for 15min, 4hr, and 24hr, and 50µl aliquots were injected into the gel filtration column at a flow rate of 0.8ml/min. The column was equilibrated and eluted with 10mM PBS + 1mg/ml BSA + 10% DMSO. Effluent fractions of 250µl were collected and assayed for TNF using ELISA.

6.2.1.2 Recirculation Capture

DMSO (10% v/v) was incubated with TNF in PBS/BSA buffer for 15min, 4hr, and 24hr prior to capture. Suramin (1mM) was incubated with TNF in PBS/BSA buffer for 0hr (immediate capture), 4hr, and 24hr prior to capture. Triton X (1.5mM) was incubated with TNF in horse serum for 4hr and 24hr prior to capture. As a control, TNF was incubated alone in serum for 24hr to determine effects from overnight incubation on baseline TNF capture. All recirculation capture experiments were performed as previously described in Chapter 5.

6.2.2 Results

Gel filtration chromatography results illustrate TNF deoligomerization kinetics in the presence of 10% DMSO (Fig. 36). After short incubation times (~15min), TNF primarily exists in trimeric form. By the 4hr incubation time point, a substantial monomer peak is observed, and at 24hr, TNF elutes primarily in monomeric form. These results indicate that TNF deoligomerization using DMSO is a relatively slow process, whereby TNF oligomeric structure is destabilized by DMSO, and slowly converts from trimeric to monomeric form over the experimental time course.

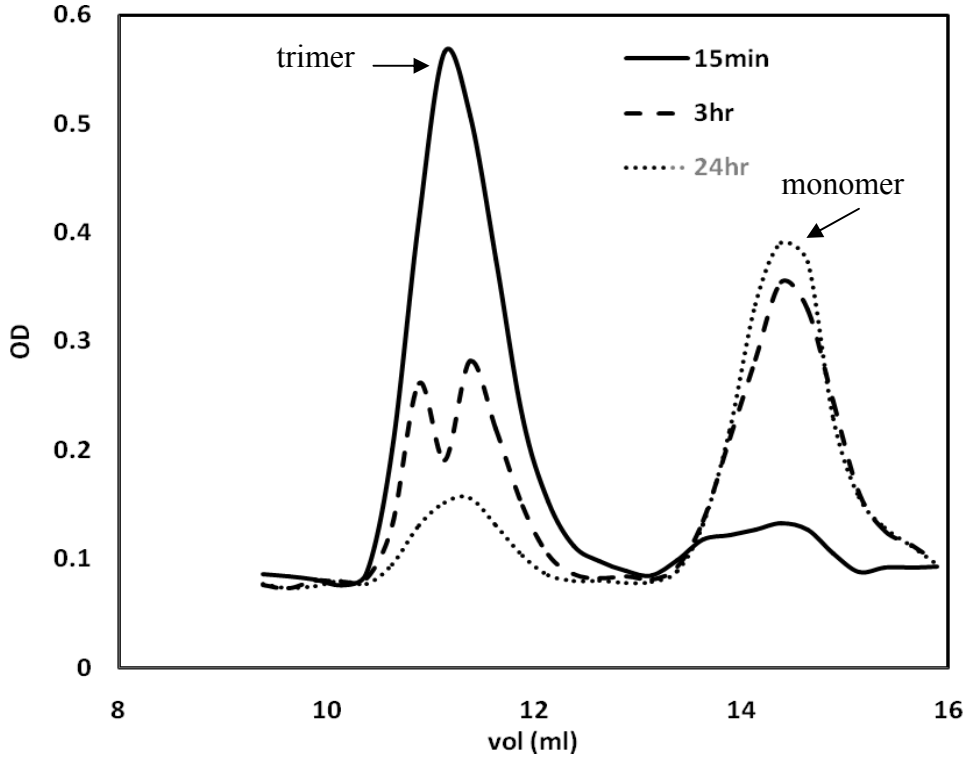

Figure 36: Gel filtration chromatography effluent of TNF after incubation with 10% DMSO for 15min, 3hr, and 24hr.

Kinetic capture studies with DMSO, suramin and Triton X were performed to quantify effects of incubation time on TNF capture behavior within the sorbent device. As illustrated in Figs. 37, 38 and 39, incubation time significantly affected TNF capture rates. Longer incubation times resulted in faster TNF removal, likely due to continued dissociation of oligomeric TNF into monomeric form, as was shown using DMSO and gel filtration chromatography (Fig. 36). Results from instant capture (addition of dissociating agent immediately prior to capture) using DMSO or suramin demonstrated slow capture within the first 15-30min, but resulted in overall increased capture by the 4hr end time point. This result is likely due to progression of TNF deoligomerization throughout the 4hr capture time frame. Baseline TNF capture rates were compared before and after 24hr incubation without addition of dissociating agents, and TNF capture after incubation was slightly faster than baseline capture (Fig. 40). This result is most likely due to spontaneous partial dissociation of TNF, which has been shown to occur over extended time frames at low (~ng/ml) TNF concentrations [143]. We did not perform gel filtration chromatography studies with suramin and Triton X, but would expect similar behavior as was observed with DMSO. We used TNF capture within the sorbent device as a measure of deoligomerization efficacy, since TNF removal rate is the primary outcome we are interested in manipulating. Furthermore, results from Chapter 5 demonstrated that TNF removal rate is a direct indicator of TNF oligomeric state.

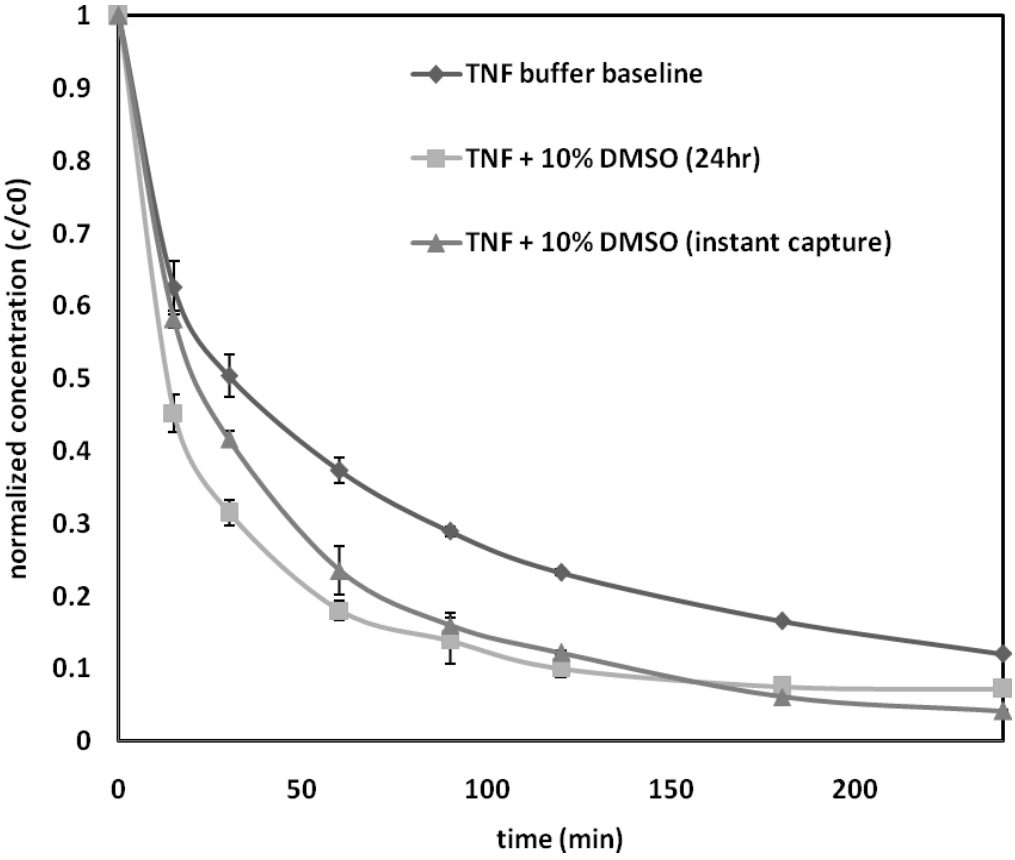

Figure 37: TNF capture in PBS/BSA buffer after 0hr (instant capture) or 24hr incubation with 10% DMSO. Baseline TNF capture is shown as a reference.

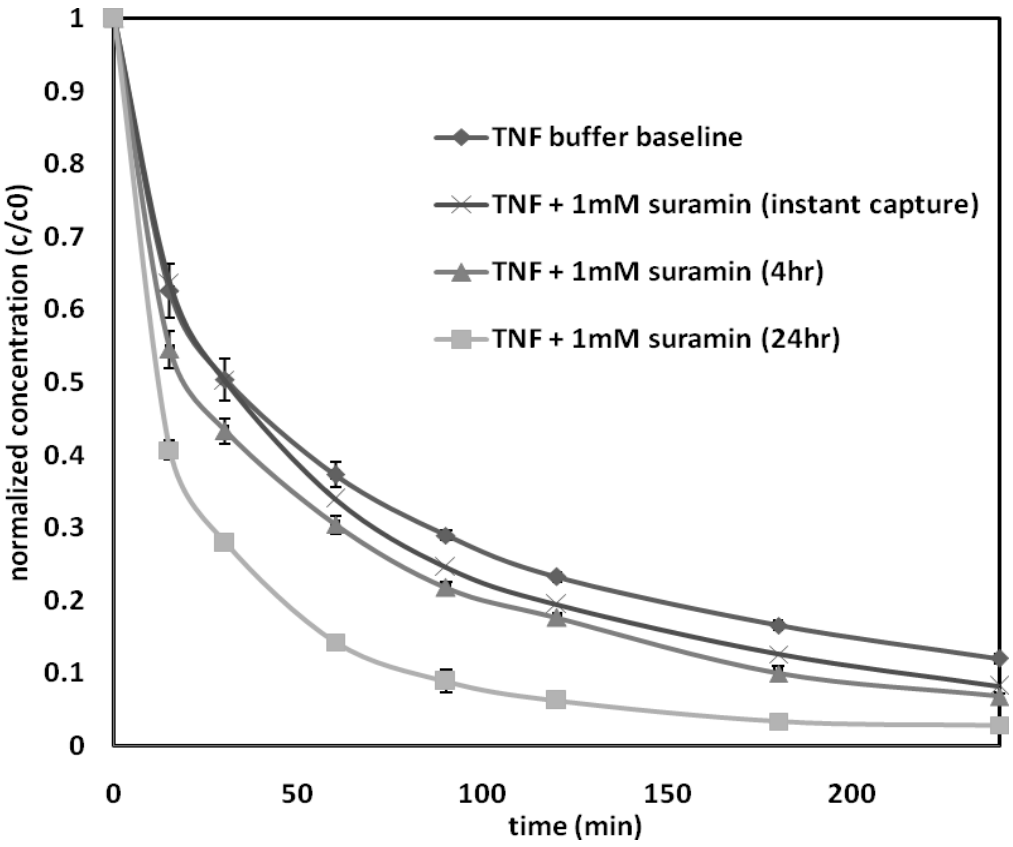

Figure 38: TNF capture in PBS/BSA buffer after 0hr (instant capture), 4hr or 24hr incubation with 1mM suramin. Baseline TNF capture is shown as a reference.

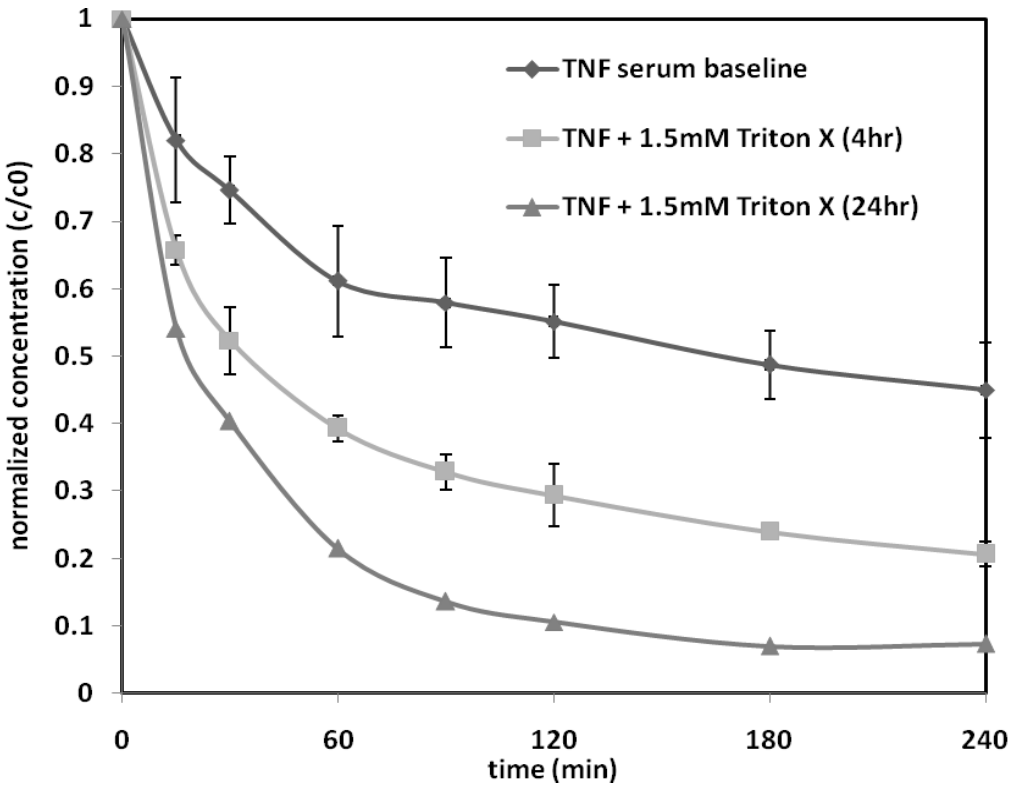

Figure 39: TNF capture in serum after 4hr or 24hr incubation with Triton X-100 (1.5mM). Baseline TNF capture is shown as a reference.

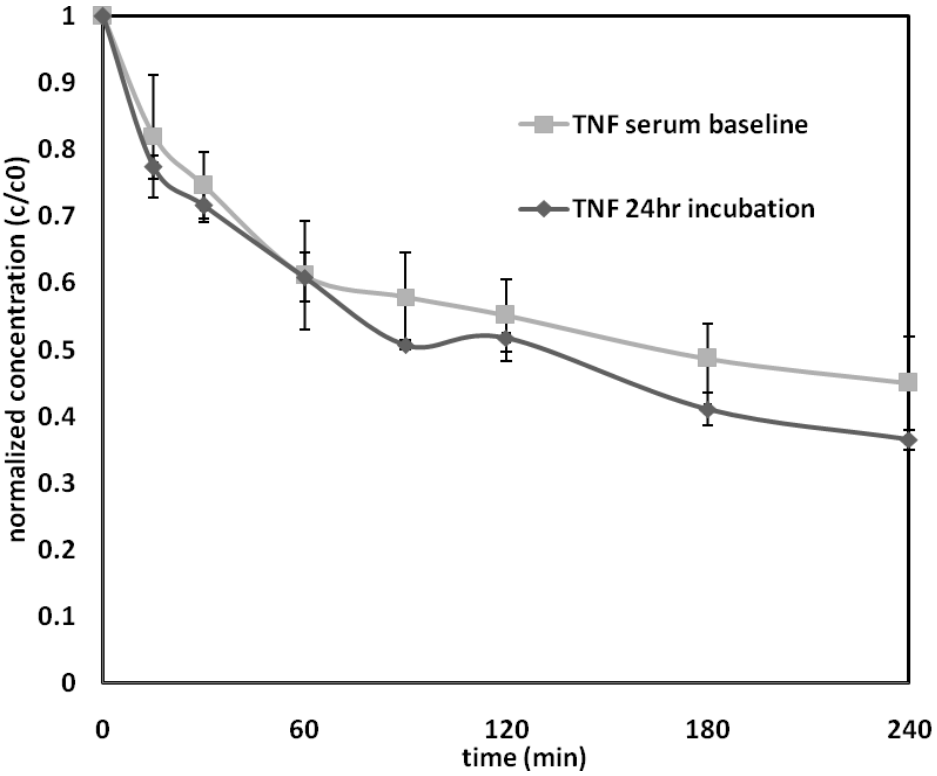

Figure 40: Baseline TNF capture in serum with and without 24hr incubation.

6.3 SURAMIN IMMOBILIZATION ON THE SORBENT SURFACE

Suramin and Triton X-100 demonstrated efficacy in accelerating TNF removal, putatively due to dissociation of oligomeric TNF structure, as shown by others [122-123, 136]. Our next step was to investigate methodologies for immobilization of these small molecules on the sorbent surface. A multitude of factors must be considered to successfully establish a functionalized sorbent surface, such as: available functional groups on the target molecule and polymer surface to initiate covalent linkage, sufficient size of the small molecule such that interaction with the sorbent is limited to the outer surface, functionality of the small molecule while in an

immobilized state, etc. Suramin was chosen as a test candidate to determine if (1) it could be covalently immobilized on the sorbent surface, and (2) it retained the ability to interact with TNF while immobilized.

6.3.1 Methods

Feasibility of suramin immobilization on a sorbent surface was tested using aminated CytoSorb beads. Aminated beads (Lot# TDG-077-166) were provided by CytoSorbents, Inc. (Monmouth Junction, NJ), and contained approximately 9% NH_2 groups per the manufacturer. Suramin was conjugated to the sorbent surface using formaldehyde-mediated condensation of active hydrogen groups on the suramin molecule with primary amine groups on the sorbent (Mannich reaction (Fig. 41)). This type of chemical reaction is useful for molecules that do not contain functional groups (OH, NH_2, COOH, etc.) typically utilized for conjugation chemistries. We hypothesized that the various hydrocarbon rings present on the suramin molecule (Table 5) would enable linkage to amine groups on the sorbent surface via the Mannich reaction, as shown by others [144].

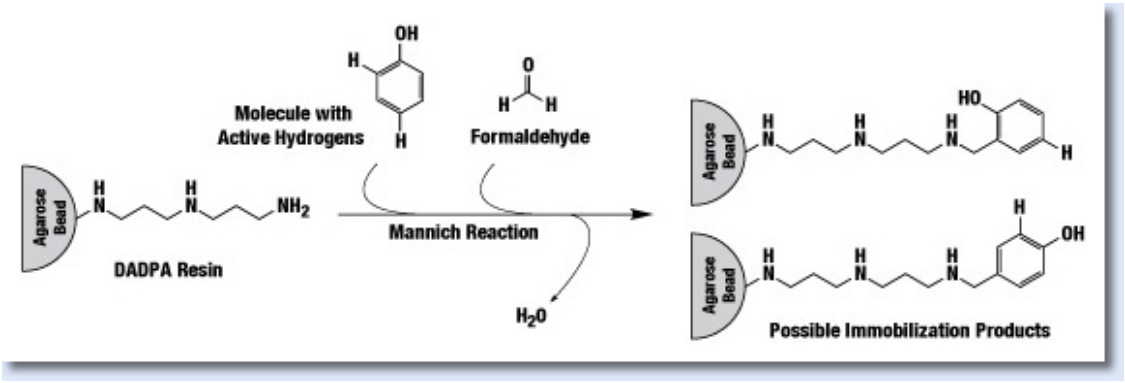

Figure 41: A generalized example of the Mannich reaction (Figure from Pierce Biotechnology, www.piercenet.com).

Since no direct assays can easily be utilized to quantify suramin concentrations in free solution or on the bead surface, radiolabeled (^{3}H) suramin (Moravek Biochemicals, Brea, CA) was used as a tracer to track the suramin conjugation reaction. 5µl ^{3}H suramin (33.7µg/ml, 1mCi/ml) was added to 10ml coupling buffer (0.1M MES, pH 4.7) and 40µl coupling reagent (37% formaldehyde) in two test tubes. 10µl samples were removed from each tube and added to 10ml liquid scintillation cocktail (Ultima Gold™, Perkin Elmer) for liquid scintillation counting (LSC) (LS1800 LSC, Beckman Coulter). Approximately 50mg dried beads (standard polymer or aminated, dried in a 37˚C oven overnight) were added to the test tubes and incubated on a rocker at 37˚C for 24hr. Dried beads were used to prevent diffusion of suramin into the internal pore structure. Aqueous solutions do not penetrate into the hydrophobic interior of the dried beads, therefore this technique can be used to restrict immobilization of small molecules to the outer sorbent surface. After incubation was complete, 10µl liquid samples were removed from each tube and processed for LSC as described above. Both tubes were then drained and flushed five times with wash buffer (0.1M Tris, pH 8.0). After the final wash step, 10µl liquid samples were removed from each tube and processed for LSC. Beads were removed from the tubes (not all could be retrieved), and directly added to 10ml LS cocktail for scintillation counting.

6.3.2 Results

Radioactivity levels were quantified using liquid scintillation counting (LSC), and resulting counts per minute (CPM) were directly proportional to concentration of radiolabeled (^{3}H) suramin in the test liquid (confirmed using a standard curve, data not shown). Fig. 42 illustrates CPM of ^{3}H suramin spiked in conjugation buffer before (pre inc) and after (post inc) 24hr incubation with standard and aminated dried sorbent beads. A significant decrease in CPM was

observed after incubation with both standard and aminated beads, possibly indicating physical adsorption of suramin to the sorbent surface, rather than covalent linkage. Since the standard beads do not have free NH_2 groups on the surface, it is unlikely that covalent linkage occurred between suramin and the standard polymer. Given the hydrophobic nature of the suramin molecule (multiple hydrocarbon rings), we hypothesized that hydrophobic interactions and/or hydrogen bonding were the main adsorptive forces between suramin and the sorbent beads, rather than covalent linkage to the sorbent surface. Fig. 43 illustrates CPM measurement of the wash effluent after incubation, and direct CPM measurement of the sorbent beads after washing. Substantial CPM in the wash effluent indicates desorption of suramin from both standard and aminated beads. Additionally, high CPM from the beads themselves indicates significant amounts of suramin retained either on the bead surface or within the bead pores. Collectively, results suggest that under the conditions tested, ^{3}H suramin physically adsorbs to the sorbent and partially desorbs after washing.

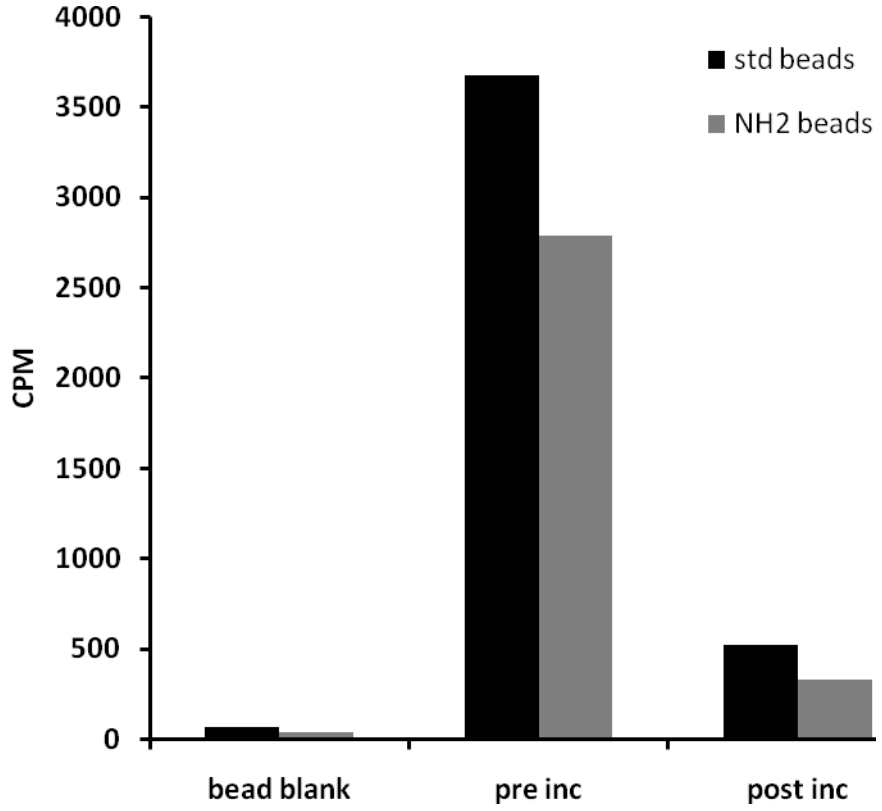

Figure 42: Liquid scintillation counts (CPM) for ^{3}H suramin incubated with standard and aminated CytoSorb beads.

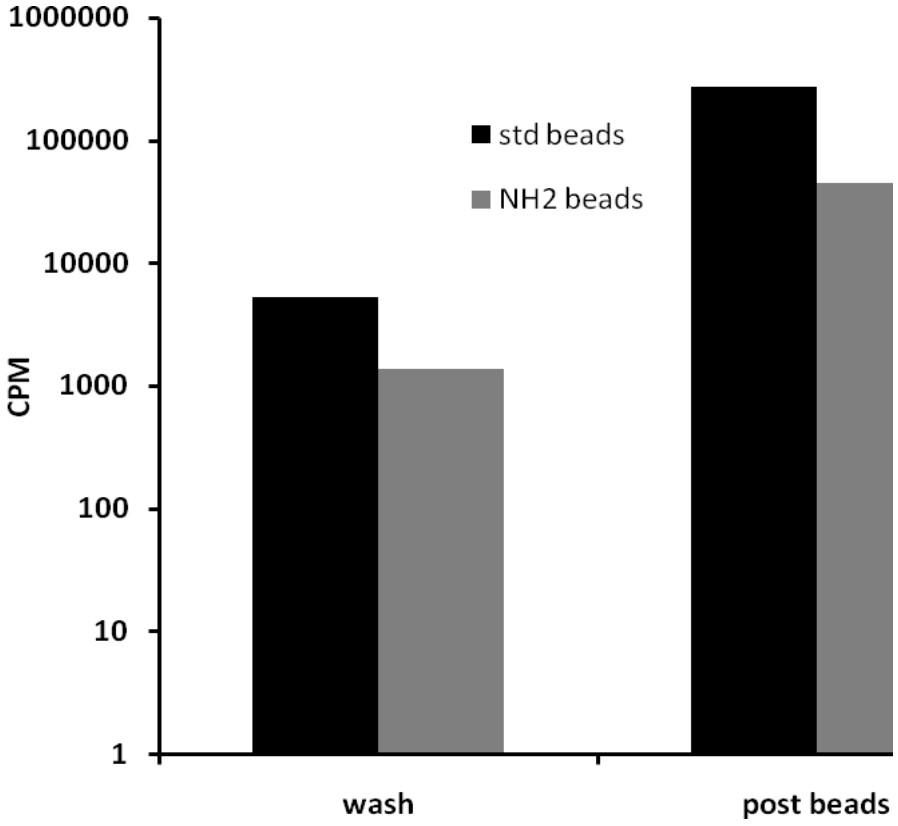

Figure 43: Liquid scintillation counts (CPM) for ^{3}H suramin wash effluent and beads post incubation.

6.4 SURAMIN LOADED SORBENT BEADS

Results from Section 6.3 indicate that covalent linkage of suramin to aminated beads was unsuccessful, however, suramin was found to physically adsorb to standard sorbent beads, and subsequently desorb during the wash phase. This result presented a potential technique for creating a localized microenvironment at the bead surface where suramin could be loaded onto the bead, desorb/diffuse out of the bead during cytokine capture, and locally interact with TNF to initiate TNF deoligomerization. To test this hypothesis, we investigated (1) the kinetics of suramin desorption from the beads and (2) effects of suramin preloading on TNF capture.

6.4.1 Methods

6.4.1.1 Suramin Loading

Radiolabeled suramin was spiked into a solution of 1mM native suramin to quantify desorption kinetics of suramin loaded beads. 10µl ^{3}H suramin (33.7µg/ml) was added to 8ml of 1mM suramin in 10mM PBS. A standard capture column was filled with 1.5g CytoSorb beads, flushed with PBS, and the 1mM suramin solution was recirculated through the column for 20hr at a flow rate of 0.8ml/min. Although initial suramin/sorbent interaction studies (Section 6.3) were performed with dried beads, we were unable to rewet dried beads for subsequent TNF capture experiments. Therefore, we pursued suramin loaded beads using standard wet sorbent to examine effects from suramin loading on TNF capture. We expected the small suramin molecule to diffuse/adsorb to the interior wet sorbent pore structure, however, we hypothesized that sufficient suramin would adsorb to the outer sorbent surface to promote interactions with bulk phase TNF.

6.4.1.2 TNF Capture with Suramin Loaded Beads

TNF (~1ng/ml) was spiked into a PBS + 5% BSA solution, and recirculated through the suramin loaded column for 4 hours, in the same manner as standard capture experiments previously described. A sample was taken from the reservoir immediately after the first pass of TNF solution through the column, and samples were periodically removed from the reservoir throughout capture to quantify both ^{3}H suramin levels (using liquid scintillation counting) and TNF concentration (using ELISA). In a separate experiment, beads were loaded with 1mM suramin as described above, and chemically crosslinked TNF capture in PBS/BSA buffer was performed as previously described in Section 5.2. IL-6 capture using suramin loaded beads was performed as a control to ensure that effects of suramin on cytokine capture were specific to TNF.

6.4.2 Results

Radiolabeled suramin was spiked into 1mM suramin to quantify desorption kinetics of suramin loaded beads. Fig. 44 illustrates radioactivity (CPM) in the reservoir during TNF capture using suramin loaded beads. Suramin desorbs/diffuses out of the bead over time into the reservoir, reaching equilibrium at approximately 120min. TNF and IL-6 capture using suramin loaded beads are shown in Figs. 45 and 46, respectively. TNF capture is accelerated compared to baseline TNF capture in PBS/BSA, although slower than TNF capture after 24hr incubation with 1mM free suramin. IL-6 capture was equivalent between suramin loaded beads, 24hr incubation with 1mM suramin, and baseline IL-6 capture.

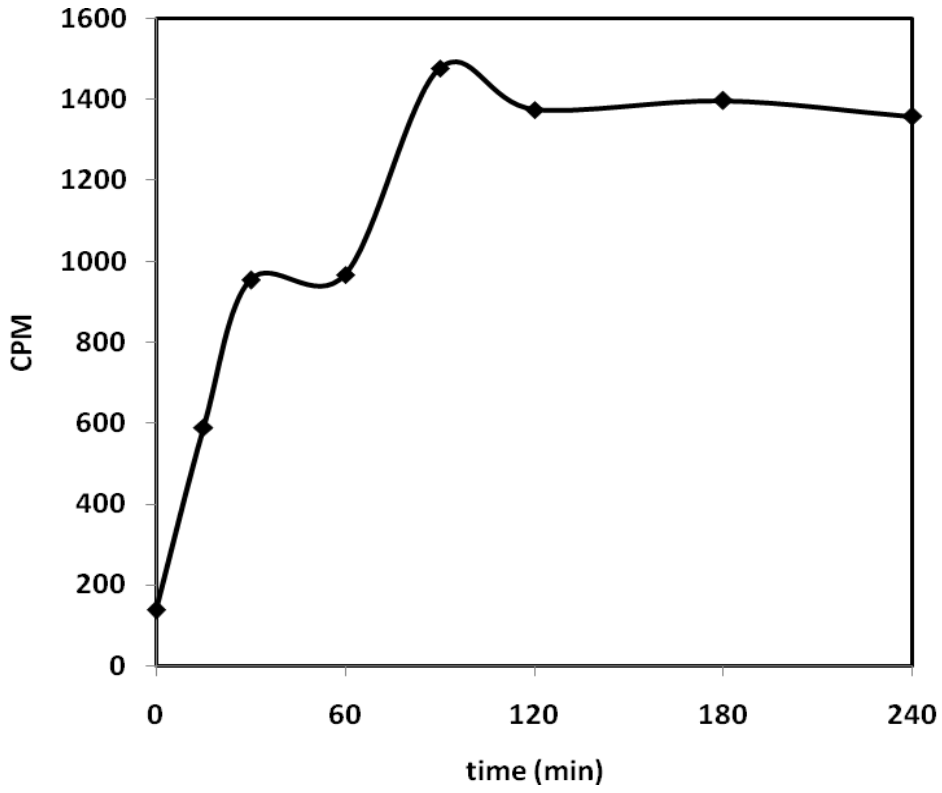

Figure 44: Radioactivity counts (CPM) of ^{3}H suramin desorbing from suramin loaded beads during TNF capture.

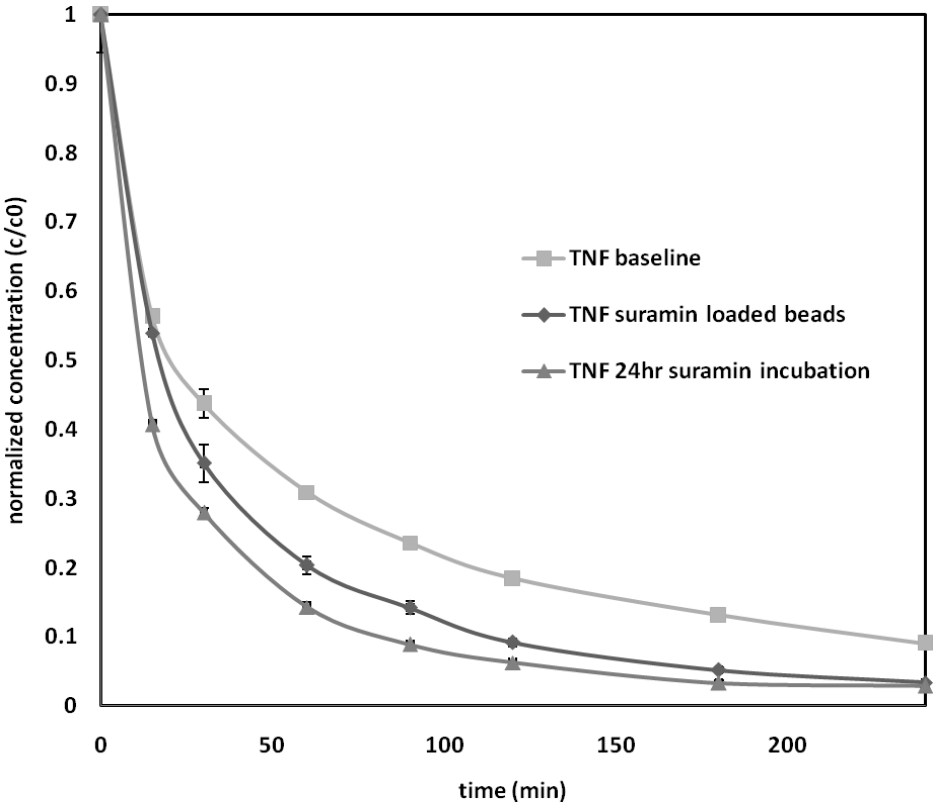

Figure 45: TNF capture using beads loaded with 1mM suramin.

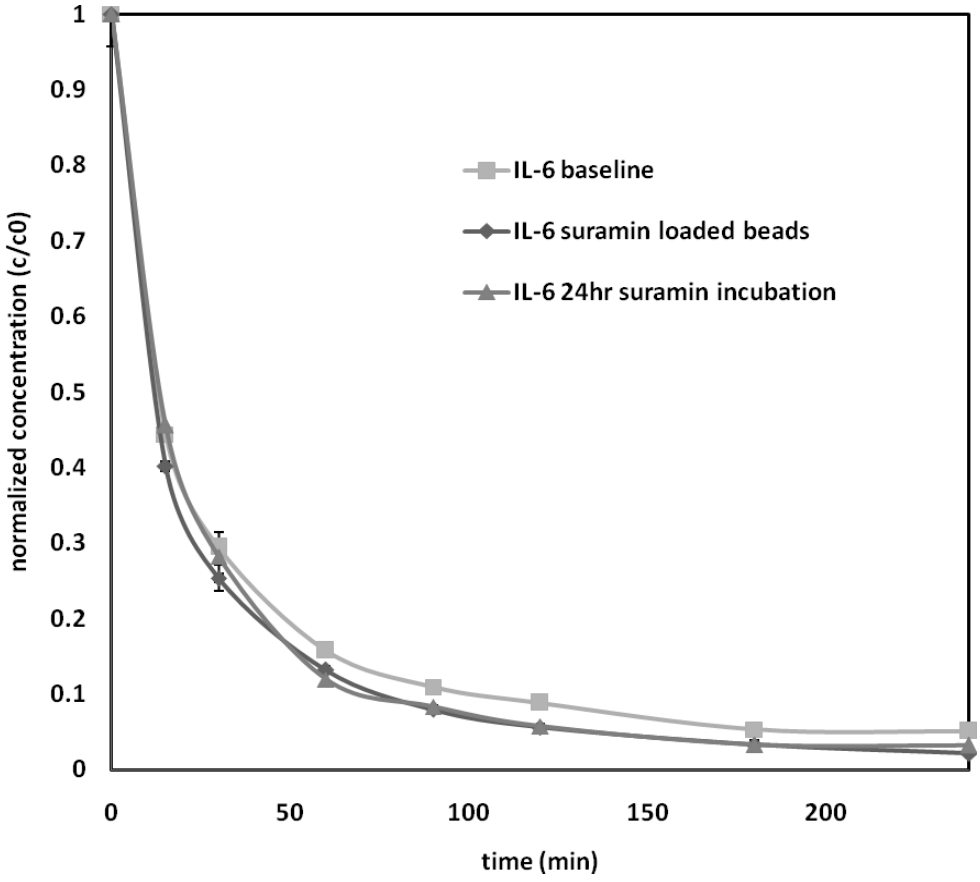

Figure 46: IL-6 capture using beads loaded with 1mM suramin.

TNF capture results using suramin loaded beads suggest that accelerated TNF capture could be a result of either (1) suramin desorbing/diffusing into the reservoir and dissociating TNF during recirculation, as originally hypothesized, or (2) adsorbed suramin acting as an affinity mechanism to bind TNF on the sorbent surface during capture. To test these hypotheses, capture with chemically crosslinked TNF and suramin loaded beads was performed. We previously demonstrated that crosslinked TNF is resistant to dissociation due to covalent linkage of individual subunits (Chapter 5). Therefore, suramin loaded beads should have no effect on crosslinked TNF capture if suramin is indeed desorbing from the bead and inducing TNF deoligomerization. Fig. 47 illustrates that capture of crosslinked TNF is accelerated using

suramin loaded beads, compared to baseline capture of crosslinked TNF. This result suggests that accelerated capture of TNF using suramin beads is due to binding of TNF to physically adsorbed suramin on the sorbent surface.

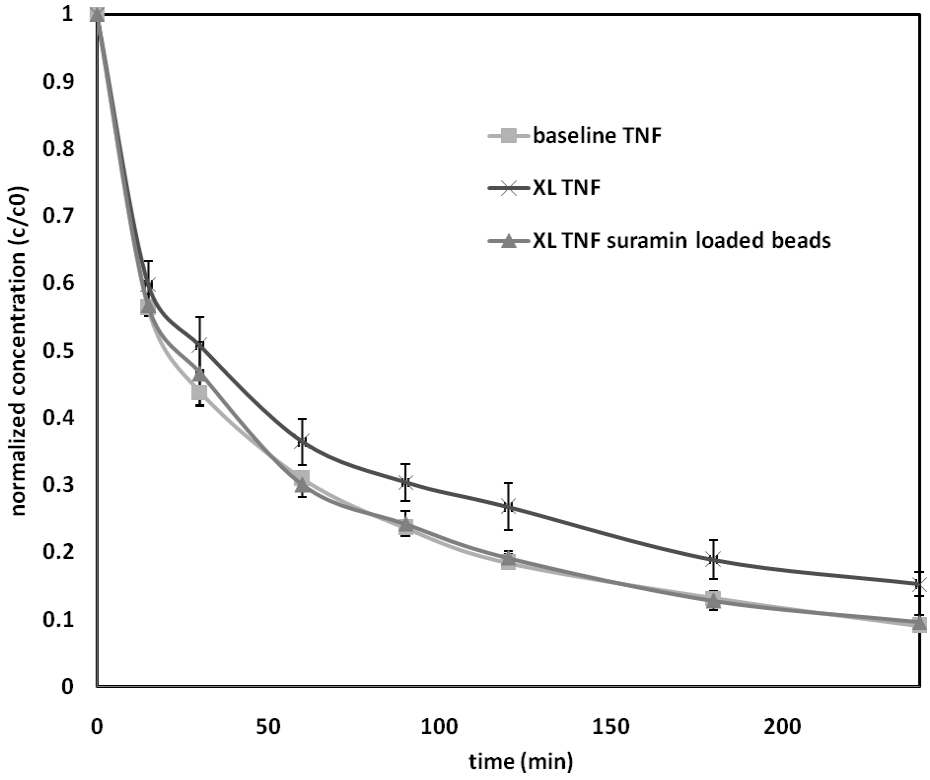

Figure 47: Crosslinked TNF capture using beads loaded with 1mM suramin.

6.5 TRITON X-100 LOADED BEADS

Results from small molecule screening indicated that Triton X-100 incubation was effective in accelerating TNF capture, to even a greater extent than suramin. Therefore, we repeated the same procedure used to load suramin onto sorbent beads, except with Triton X-100, and evaluated effects of Triton X-100 loaded beads on TNF capture.

6.5.1 Methods

1.5mM Triton X-100 was dissolved in 8ml of 10mM PBS. A standard capture column was filled with 1.5g CytoSorb beads, flushed with PBS, and the Triton X-100 solution was recirculated through the column for 20hr at a flow rate of 0.8ml/min. TNF (~1ng/ml) was spiked into horse serum, and recirculated through the Triton X-100 loaded column for 4 hours, in the same manner as standard capture experiments previously described.

6.5.2 Results

TNF capture using Triton X-100 loaded sorbent beads is illustrated in Fig. 48. Unexpectedly, capture was slower using the loaded sorbent beads compared to baseline TNF capture. Given the amphiphilic structure of Triton X-100, the hydrophobic portion of the molecule may physically adsorb to the hydrophobic interior of the bead, exposing the hydrophilic tail to the surrounding aqueous environment. Under these conditions, Triton X-100 most likely does not significantly interact with TNF at the bead surface, and may actually restrict TNF adsorption to the internal pore structure. Potential chemical immobilization strategies to conjugate the Triton X-100

hydrophilic tail to the sorbent surface, thereby exposing the hydrophobic portion, may facilitate interaction with TNF, although these experiments have not been performed.

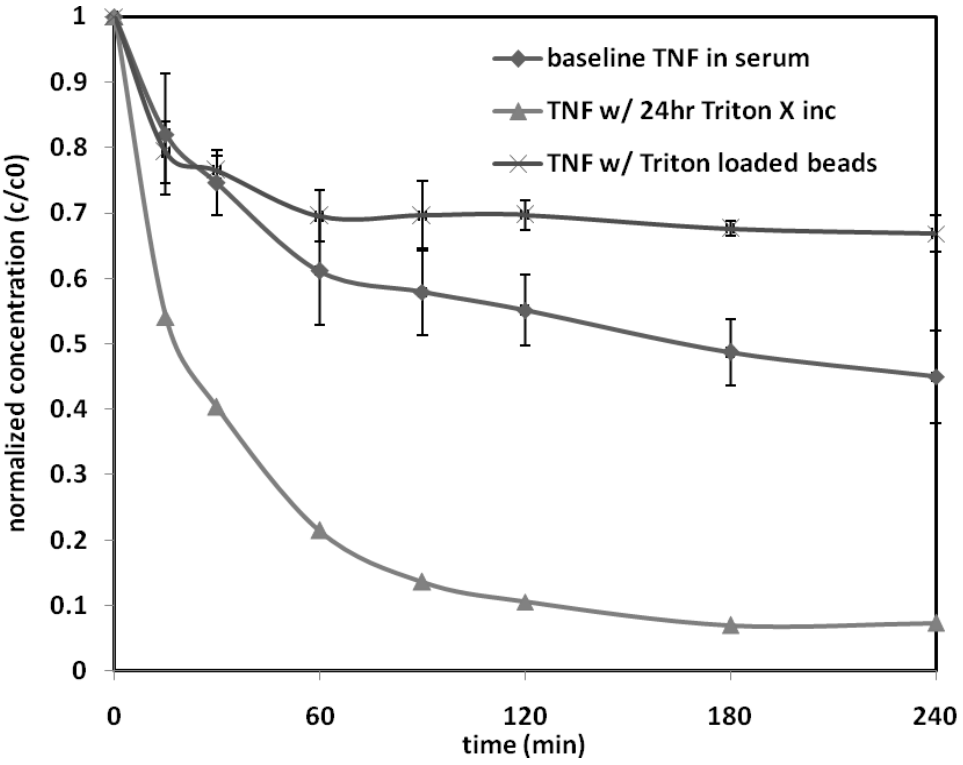

Figure 48: TNF capture using sorbent beads loaded with Triton X-100.

6.6 DISCUSSION

Results presented in Chapter 5 demonstrated significant acceleration of TNF capture within the sorbent device using DMSO preincubation. While this technique offered rationale for utilizing TNF deoligomerization to enhance TNF capture rates, DMSO is not a clinically feasible tool due to potential toxicity in the body. Our ultimate goal is to functionalize the surface of sorbent beads to induce localized deoligomerization of TNF within the device. To that end, we screened potential small molecule candidates for their efficacy in promoting TNF dissociation. Suramin was selected for further investigation based on its known ability to dissociate TNF [122-123], and potential for immobilization on the sorbent surface due to its chemical structure.

We attempted to covalently attach suramin to the surface of dried aminated sorbent beads, but observed similar levels of suramin loading on both aminated and standard beads, suggesting simple physical adsorption as the primary interaction mechanism between suramin and the bead. Covalent linkage of small molecules to surfaces is often difficult due to the dearth of available functional groups on the target molecule. Although further optimization of the conjugation reaction could lead to effective covalent linkage between suramin and the aminated sorbent surface, these experiments were outside the scope of the current work. Instead, we chose to investigate the ability of physically adsorbed suramin to locally interact with TNF and accelerate TNF capture within the device.

A central challenge for loading small molecules onto the surface of porous beads is the difficulty in restricting adsorption/immobilization only to the outer surface of the beads. Diffusion of small molecules into the interior sorbent pores would likely result in minimal interaction with TNF due to limited penetration of TNF expected within the bead (see Chapter 3), compared to rapid diffusion of small molecular weight solutes (suramin MW = 1.4kDa, TNF

MW = 51kD). Hence, we investigated whether physically adsorbed suramin could interact with TNF either by binding TNF at the sorbent surface, or through desorption into the reservoir and subsequent deoligomerization of TNF. Although initial suramin/sorbent interaction studies (Section 6.3) were performed with dried beads, we were unable to rewet dried beads for subsequent TNF capture experiments. Therefore, we pursued suramin loaded beads using standard wet sorbent to examine effects from suramin loading on TNF capture. We expected the small suramin molecule to diffuse/adsorb to the interior wet sorbent pore structure, however, we hypothesized that sufficient suramin would adsorb to the outer sorbent surface to promote interactions with bulk phase TNF.

Cytokine capture results using suramin loaded beads demonstrated accelerated removal of TNF from PBS/BSA buffer, and minimal effects on IL-6 capture. However, crosslinked TNF capture using suramin loaded beads was also accelerated, indicating that suramin induced TNF deoligomerization was not responsible for the observed TNF capture behavior. Instead, results suggest that physically adsorbed suramin acts as an affinity mechanism to bind TNF and enhance TNF capture rates. The exact mechanism of suramin interaction with TNF is unknown, however, the same interactions which cause TNF dissociation in free solution could lead to transient binding of TNF to physically adsorbed suramin on the sorbent surface. Alternatively, desorption of suramin into the reservoir could potentially accelerate TNF capture via trimeric dissociation under optimized suramin loading conditions, although further work is needed to verify this hypothesis.

The concepts presented in this chapter describe the framework for surface functionalization of sorbent beads with small molecules capable of locally dissociating TNF within the adsorption device. In the ideal case, the target molecule would be covalently tethered

to the sorbent surface, possibly through utilization of a large MW spacer arm such as polyethylene glycol (PEG). Use of a spacer arm would have three potential functions: (1) presenting the small molecule away from the sorbent surface such that localized interactions with the bead surface are minimized, (2) preventing diffusion of the small molecule into the interior sorbent pores by using a spacer arm larger than the MW cut off of the pores, and (3) enabling a broad range of potential conjugation chemistries through functionalized terminal ends of the spacer arm. In addition to tethering the dissociating agent to the sorbent surface, the kinetics of induced TNF deoligomerization must be rapid, such that deoligomerization can proceed within a time scale corresponding to clinical use of the device. Under the experimental conditions presented, physically adsorbed suramin acts as an affinity mechanism to bind TNF at the sorbent surface. This result suggests that suramin could be used as an inexpensive ligand to bind TNF, compared to using recombinant anti-TNF antibodies [133], which have high affinities for TNF, but are prohibitively expensive for use in a clinical device.

Although suramin was used a test candidate to explore the concept of surface functionalized beads, preliminary results suggest that amphiphilic surfactants such as Triton-X could also be promising dissociative agents. Further work is needed to explore mechanisms of small molecule induced TNF deoligomerization, and feasibility of conjugating such molecules to the surface of sorbent beads. We foresee the concept of oligomeric molecule dissociation as a broad framework for facilitating removal of large solutes using size exclusion filtration materials. Small sorbent pores are necessary in direct blood filtration devices to prevent removal of cells and essential large molecular weight molecules (e.g. albumin, immunoglobulins). However, structural manipulation of molecules within the device could enable targeted removal of large solutes while retaining a small pore size. The concept of functionalized size exclusion

sorbent materials could potentially be expanded to accelerate removal of various oligomeric solutes, such as cytokines, enzymes, and bacterial products in a variety of disease states.

7.0 SUMMARY & CONCLUSIONS

Despite significant advances in our understanding of the biological mechanisms during sepsis, little progress has been made in the development of effective clinical therapies. Over the past decades, experimental therapies have often targeted individual mediators within the dysfunctional immunologic, coagulatory, or hemodynamic systems. The failures of these therapies indicate that new approaches are necessary to combat the interdependent cellular and molecular pathways that result in poor clinical outcomes. Recent evidence has suggested that a complex interplay between pro-inflammatory and compensatory anti-inflammatory events leads to systemic dysfunction of multiple physiological systems during sepsis. A new paradigm based on broad-spectrum mediator removal from the blood has emerged as a promising therapeutic modality. Non-specific removal of endogenous mediators may help down-regulate systemic inflammation and modulate the dysfunctional innate immune response towards homeostasis. The work presented in this dissertation summarizes efforts to characterize the behavior of sorbent beads used within a cytokine adsorption device, and to explore novel sorbent materials for enhanced cytokine capture.

The first goal of this dissertation was to investigate cytokine transport dynamics within sorbent beads, and compare the results to predictions of a mathematical model (Chapters 3 & 4). We utilized confocal laser scanning microscopy (CLSM) to quantify penetration profiles of fluorescently tagged IL-6 in PBS/BSA buffer, and found that intraparticle adsorption dynamics

agreed with predictions of a single component adsorption/diffusion model. Results indicated that only a small portion (< 20%) of available sorbent surface area participates in cytokine adsorption, suggesting significant enhancements in cytokine removal could be realized by utilizing smaller sorbent beads. Further work by our group confirmed this hypothesis, demonstrating accelerated cytokine capture using small diameter sorbent beads compared to standard sorbent beads (50μm vs. 260μm avg. radius, respectively) in a redesigned device [145]. IL-6 CLSM was also performed in serum to simulate physiologically relevant conditions, and resulting intraparticle profiles demonstrated peak intensities within the bead interior, deviating from results obtained using PBS/BSA buffer. We developed a two component competitive adsorption model, and demonstrated that CLSM behavior in serum was likely due to competitive adsorption between cytokine and coadsorbing serum solutes. We utilized a numerical simulation/parameter optimization technique, and concluded that competitive adsorption effects were likely negligible under physiologic cytokine concentrations. This work was the first study to investigate protein adsorption dynamics within sorbent beads in whole serum, and may serve as a novel technique for investigating solute transport within sorbent blood filtration materials.

The second goal of this dissertation was to investigate techniques to accelerate TNF capture within the device (Chapters 5 & 6). Although various studies have illustrated the unstable oligomeric behavior of TNF *in vitro*, we are the first group to use deoligomerization as a method for enhanced removal of TNF within a size exclusion filtration device. We utilized DMSO to dissociate trimeric TNF into monomeric form, and demonstrated significantly accelerated capture of monomeric TNF compared to native TNF within the device. DMSO was used as a simple dissociating agent, however, systemic injection of DMSO into a patient is not a clinically feasible tool. We screened a series of small molecules for their ability to destabilize

TNF subunit interactions, and found that preincubation with suramin or Triton X-100 were effective in accelerating TNF capture, putatively due to TNF deoligomerization.

Strategies were discussed for tethering small molecules to the sorbent surface, with the goal of developing functionalized sorbent materials capable of locally dissociating TNF within the device. Suramin loaded sorbent beads demonstrated accelerated TNF capture in PBS/BSA buffer, although results suggest that this effect was due to binding of TNF to suramin on the sorbent surface, rather than suramin-induced TNF deoligomerization. Further research in this area should focus on: kinetics of TNF deoligomerization relative to therapeutic duration of the device, efficacy of TNF dissociating agents while in an immobilized state, and potential effects from functionalized sorbent beads on removal of other solutes. The concept of dissociating large oligomeric molecules within a size exclusion filtration device may have broad applications outside the realm of TNF removal for sepsis. TNF removal from the circulating blood may be a novel adjuvant therapy for other diseases such as rheumatoid arthritis or Crohns' disease, where pharmacologic anti-TNF therapies have been used. Additionally, the technology could be expanded to facilitate dissociation of other oligomeric molecules using functionalized size exclusion sorbent materials for a variety of disease states.

In conclusion, blood purification may be a promising strategy to improve patient outcomes in the setting of severe sepsis and septic shock. The work presented in this dissertation summarizes efforts to characterize cytokine capture within sorbent beads, and to elucidate novel mechanisms for enhanced capture of a large oligomeric cytokine. Sorbent blood purification for the treatment of sepsis is a nascent field, and limited studies have investigated solute transport within hemoadsorption beads. We believe that a robust, mechanistic understanding of cytokine capture within the device will facilitate development of clinically useful technologies. Our

future goals are to integrate models of cytokine capture with large-scale systems models of inflammation, in an attempt to understand downstream immunologic effects from hemoadsorption therapy. Additionally, we plan on developing new sorbent materials with enhanced adsorptive capabilities, capable of modulating capture of specific solutes through disruption of molecular structure. We hope these concepts will lead to new developments in the field of blood purification for the critically ill.

APPENDIX A

BSA EFFECTS ON CYTOKINE TRANSPORT

In Chapter 3, IL-6 CLSM studies were performed in PBS + 1% BSA. BSA was used as a carrier protein to help stabilize low concentration IL-6 and prevent nonspecific adsorption to tubing, pipette tips, etc. However, *in vitro* recirculation capture experiments in buffer (Chapters 5 & 6) were performed using PBS + 5% BSA, as this concentration of BSA is comparable to total albumin levels found in the blood. We previously assumed that BSA concentration would have negligible effects on cytokine removal within the device, since BSA (66kD) does appreciably adsorb within the sorbent pores due to pore size exclusion. In this experiment, we directly tested effects of BSA concentration on (1) CLSM intraparticle transport behavior, and (2) *in vitro* cytokine capture rates within the sorbent device.

A.1 BSA EFFECTS ON INTRAPARTICLE TRANSPORT

We previously demonstrated that BSA does not penetrate into the sorbent pores over time (Chapter 3, Fig. 5b), putatively due to size exclusion of the large albumin molecule (66kD). In that experiment, gel permeation chromatography was utilized to remove small MW impurities in

the BSA stock prior to BSA labeling. In preliminary work, we observed significant penetration of unknown solutes into the sorbent interior when fluorescently labeled BSA stock (no chromatographic purification) was incubated with sorbent beads. We attributed this behavior to small MW impurities in the BSA, which can rapidly diffuse into the bead over time.

A.1.1 Methods

CLSM was performed as described in Chapter 3. Briefly, IL-6 or TNF was fluorescently labeled, and incubated with CytoSorb beads in PBS + BSA (0%, 0.1%, 1%, 2.5% or 5%) for 2hr, 5hr, and 24hr. Beads were removed at the specific time points, sliced, and imaged using CLSM. Images were quantified for signal intensity across the diameter of the bead, and 4-5 beads were imaged at each time point.

A.1.2 Results

CLSM intraparticle intensity profiles for TNF incubated with varying BSA concentrations for 5hr are shown in Fig. 49. As BSA concentration increases, resulting intensity profiles exhibit reduced peak intensities, and greater penetration distance into the bead. The experiment was also performed using labeled IL-6 in varying concentrations of BSA, and intraparticle intensity curves exhibited the same qualitative behavior as observed with TNF (data not shown).

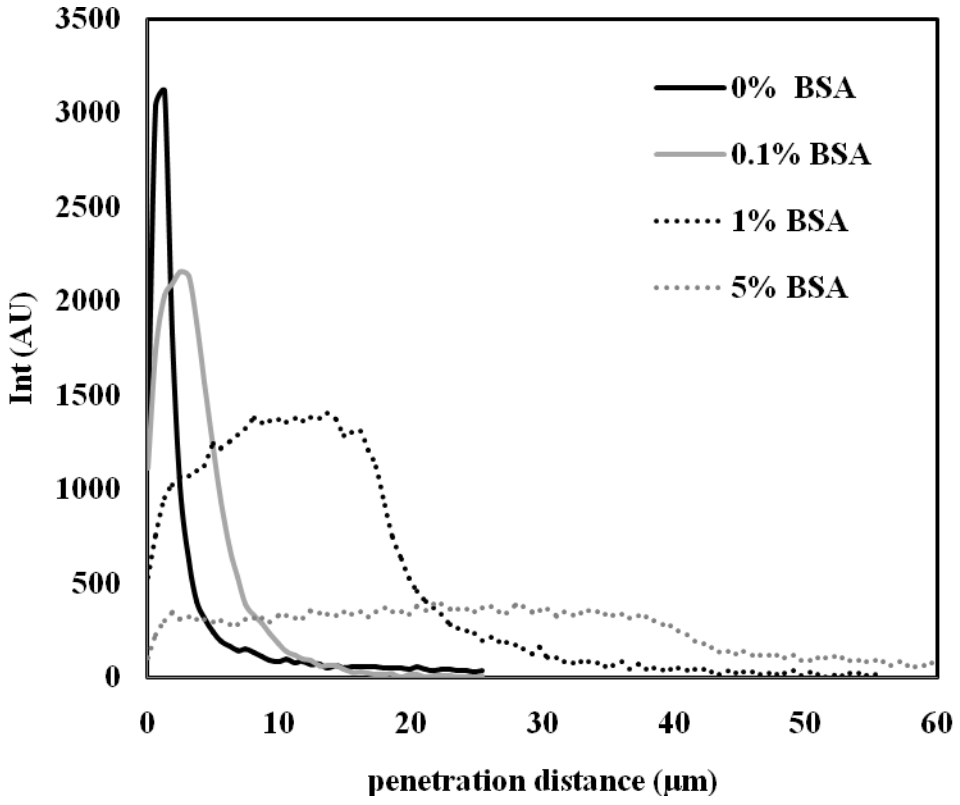

Figure 49: CLSM intraparticle intensity profiles of fluorescently labeled TNF incubated with CytoSorb beads for 5hr. Beads were incubated in PBS and varying concentrations of BSA.

A.2 BSA EFFECTS ON RECIRCULATION CAPTURE

Results from CLSM studies demonstrated significant effects from BSA concentration on intraparticle cytokine penetration behavior. We evaluated BSA concentration effects on recirculation capture to determine whether the CLSM behavior translated to appreciable effects on cytokine removal rates within the sorbent device.

A.2.1 Methods

In vitro recirculation capture was performed as described in Chapter 5. Briefly, columns were packed with 1.5g CytoSorb beads, and primed with 10mM PBS. IL-6 was spiked in PBS + BSA (1%, 2.5%, 5%, 10%), and recirculated through the column at a flow rate of 0.8ml/min. IL-6 concentration in the reservoir throughout capture was quantified by ELISA.

A.2.2 Results

IL-6 removal rates using a sorbent device under varying BSA concentrations are illustrated in Fig. 50. BSA concentration has a significant effect on IL-6 capture, where higher BSA concentrations resulted in slower IL-6 removal.

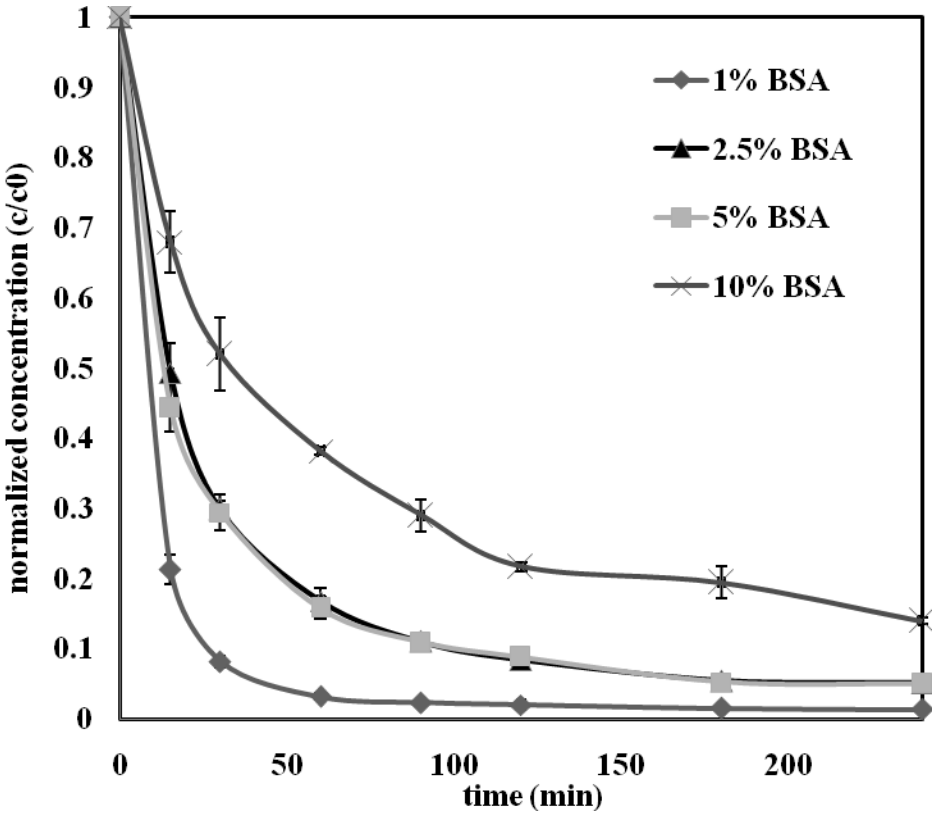

Figure 50: IL-6 removal within a sorbent device using variable BSA concentrations in the reservoir.

A.3 DISCUSSION

The goal of this study was to examine effects from BSA on cytokine adsorption/diffusion dynamics within the sorbent beads. We previously demonstrated that BSA (66kD) does not appreciably penetrate into the sorbent pore structure (Chapter 3), putatively due to the large size of the BSA molecule relative to the small pore diameter. This data was generated by first running stock BSA (>96% purity) through a gel permeation column to remove impurities, followed by fluorescent labeling of the BSA molecule. However, preliminary CLSM work using unpurified BSA suggested that small molecular weight impurities in the BSA stock could affect

cytokine removal dynamics within the sorbent beads. We therefore directly tested effects of BSA on intraparticle cytokine transport using CLSM, and on cytokine removal within a sorbent device using *in vitro* recirculation capture.

CLSM results demonstrated significant effects from BSA concentration on intraparticle cytokine transport (Fig. 49). As BSA concentration increases, resulting intensity profiles exhibit reduced peak intensities, and greater penetration distance into the bead. We hypothesize that as BSA concentration in the bulk liquid increases, small MW impurities diffuse faster into the bead interior, due to increased concentration gradient. As these solutes diffuse into the bead, they likely adsorb to the polymer surface and minimize subsequent cytokine adsorption by reducing available binding sites. Therefore, cytokine must diffuse farther into the bead before accessing a binding site, as observed in the CLSM data. Recirculation capture experiments also demonstrated significant effects from BSA concentration on cytokine capture. IL-6 removal rate decreased with increasing BSA concentration in the reservoir, likely due to similar mechanisms observed with the CLSM data. In addition to effects from diffusion/adsorption of small MW impurities within the bead interior, adsorption of BSA on the sorbent surface likely affects cytokine capture. Increased BSA concentration in the reservoir would facilitate greater BSA adsorption on the bead surface, likely resulting in pore occlusion and hindered transport of cytokine into the bead interior. Results from this study demonstrate significant effects from BSA on cytokine transport within the hemoadsorption beads. Although BSA was initially utilized as a simple protein solution to examine cytokine adsorption dynamics, results indicate that realistic media (serum, plasma) should be utilized to generate physiologically relevant conditions for examining cytokine transport within the hemoadsorption device.

APPENDIX B

CYTOKINE DESORPTION FROM SORBENT BEADS

CytoSorb hemoadsorption beads are comprised of a polystyrene-divinylbenzene copolymer, with a biocompatible polyvinyl-pyrrolidone coating. Protein adsorption to the internal polymer surface is assumed to be a result of hydrophobic interactions. Other molecular interactions such as electrostatic, hydrogen bonding, and van der Waals forces may also contribute to cytokine retention by the sorbent beads. In our intraparticle modeling work (Chapters 3 & 4), we utilized the Langmuir adsorption isotherm to describe simple physical adsorption equilibrium between cytokine and the polymer surface. However, we were further interested in determining whether the adsorption process could be considered irreversible, where adsorbed cytokine would not desorb from the bead once the concentration gradient was reversed (i.e. adsorbed cytokine within the bead, no cytokine in the bulk reservoir). The current experiment directly tested this hypothesis by performing a standard *in vitro* cytokine capture, followed by elution using serum without spiked cytokine, and measurement of desorbed cytokine in the reservoir over time.

B.1 METHODS

A standard *in vitro* IL-6 capture experiment was performed as previously described. Briefly, a column was packed with 1.5g CytoSorb beads, and flushed with PBS. IL-6 was spiked in horse serum, and recirculated through the column for 4hr at a flow rate of 0.8ml/min. Aliquots were removed from the reservoir periodically and quantified for IL-6 concentration using ELISA. After the last time point, the reservoir was switched to horse serum without any spiked IL-6, and the serum solution was recirculated for an additional 4hr. Reservoir aliquots were sampled after the first pass of serum through the IL-6 loaded column, and then periodically throughout the 4hr experiment.

B.2 RESULTS

Capture/desorption results are illustrated in Fig. 51. IL-6 is removed from the reservoir throughout the first 4hr of the experiment, as expected. However, once the reservoir was switched to serum without IL-6, negligible amounts of IL-6 were detected in the reservoir for the remainder of the experiment. This result suggests minimal desorption of IL-6 from the sorbent beads after the IL-6 concentration gradient was reversed.

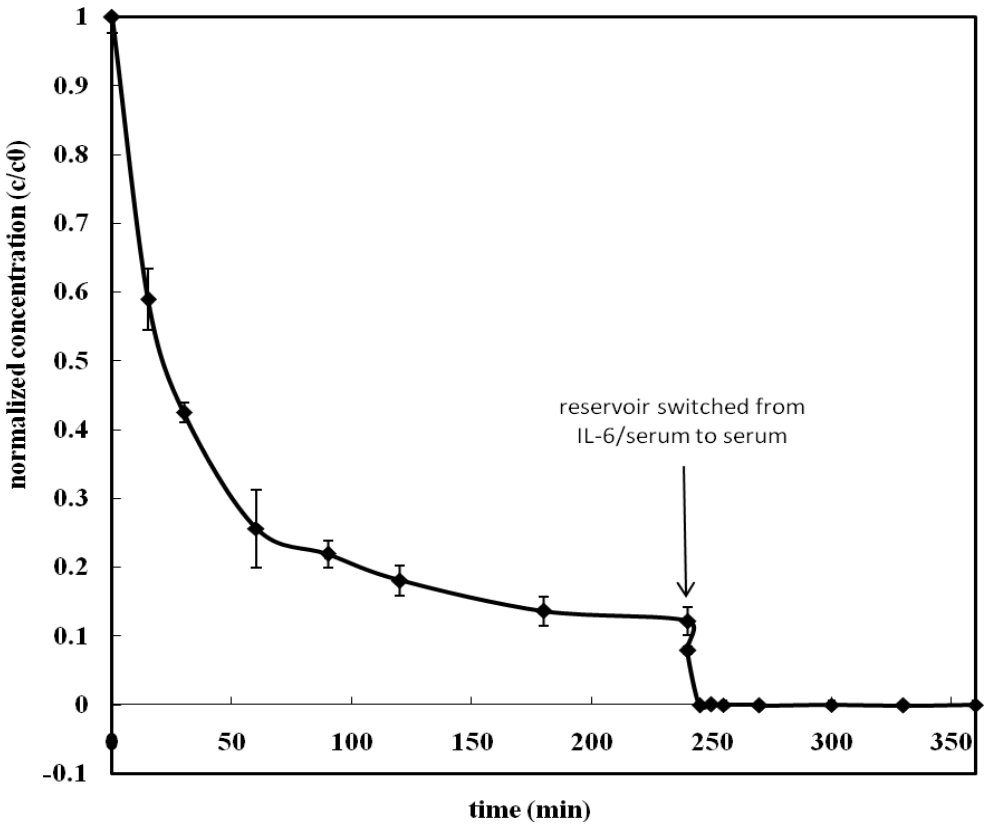

Figure 51: Standard IL-6 recirculation capture in horse serum, followed by elution with horse serum (no IL-6).

B.3 DISCUSSION

Results from this study demonstrate that IL-6 adsorption within the sorbent beads can be considered an irreversible process under the experimental conditions presented. Physical adsorption is an equilibrium state whereby solute adsorption/desorption is dictated by the concentration gradient between adsorbed and free species, and affinity between the solute and surface. However, hydrophobic interactions between proteins and a highly hydrophobic surface

(polystyrene-divinylbenzene) include complexities not assumed under a general Langmuir-type adsorption isotherm. Protein adsorption on hydrophobic surfaces is often accompanied by protein unfolding and spreading along the surface to form a minimal energetic state. The required energy to subsequently desorb the unfolded protein is likely much greater than available by simply reversing the solute concentration gradient. Results from this study suggest that cytokines adsorb to the hydrophobic polymer surface, and remain bound under clinically relevant conditions. Although this phenomenon was not tested *in vivo*, results using whole blood would likely not differ from those observed here.

BIBLIOGRAPHY

1. Angus, D., et al., *Epidemiology of severe sepsis in the United States: Analysis of incidence, outcome, and associated costs of care.* Crit Care Med, 2001. **29**(7): p. 1303-1310.

2. Baillie, J.K., *Activated protein C: Controversy and hope in the treatment of sepsis.* Current Opinion in Investigational Drugs, 2007. **8**(11): p. 933-938.

3. Abraham, E., et al., *Efficacy and safety of monoclonal antibody to human necrosis factor α in patients with sepsis syndrome. A randomized, controlled, double-blind, multicenter clinical trial. TNF-α mAb sepsis study group.* J Am Med Assoc, 1995. **273**(12): p. 934-941.

4. Fisher, C., et al., *Recombinant human interleukin 1 receptor antagonist in the treatment of patients with sepsis syndrome. Results from a randomized, double-blind, placebo-controlled trial. Phase III rhIL-1ra sepsis syndrome study group.* J Am Med Assoc, 1994. **271**(23): p. 1836-1843.

5. Ziegler, E., et al., *Treatment of Gram-negative bacteremia and septic shock with HA-1A human monoclonal antibody against endotoxin. A randomized, double-blind, placebo-controlled trial. The HA-1A sepsis study group.* N Engl J Med, 1991. **324**(7): p. 429-436.

6. Kellum, J.A., M. Song, and R. Venkataraman, *Hemoadsorption removes tumor necrosis factor, interleukin-6, and interleukin-10, reduces nuclear factor-KB DNA binding, and improves short-term survival in lethal endotoxemia.* Crit Care Med, 2004. **32**(3): p. 801-805.

7. Casey, L.C., *Immunologic response to infection and its role in septic shock.* Critical Care Clinics, 2000. **16**(2): p. 193-213.

8. Kellum, J.A., et al., *Understanding the inflammatory cytokine response in pneumonia and sepsis: results of the Genetic and Inflammatory Markers of Sepsis (GenIMS) Study.* Archives of Internal Medicine, 2007. **167**(15): p. 1655-1663.

9. Venkataraman, R., S. Subramanian, and J.A. Kellum, *Clinical review: Extracorporeal blood purification in severe sepsis.* Critical Care, 2003. **7**: p. 139-145.

10. Peng, Z., M. Carter, and J.A. Kellum, *Effects of hemoadsorption on cytokine removal and short-term survival in septic rats.* Crit Care Med, 2008. **36**(5): p. 1573-1577.

11. Peng, Z., et al., *Hemoadsorption improves long-term survival after sepsis in the rat.* Crit Care Med, 2008. **36**(12): p. A1.

12. DiLeo, M.V., J.A. Kellum, and W.J. Federspiel, *A simple mathematical model of cytokine capture using a hemoadsorption device.* Annals of Biomedical Engineering, 2009. **37**(1): p. 222-229.

13. Lorente, J.A. and J.C. Marshall, *Neutralization of tumor necrosis factor in preclinical models of sepsis.* Shock, 2005. **24**(Suppl. 1): p. 107-119.

14. Ronco, C., R. Bellomo, and G. La Grecca, *Blood purification in intensive care*. Contributions to nephrology, ed. G. Berlyne and C. Ronco. Vol. 132. 2001, Basel: Karger.

15. Vincent, J., et al., *Sepsis in European intensive care untis: Results of the SOAP study.* Crit Care Med, 2006. **34**(2): p. 344-353.

16. Thomas, L., *Germs.* N Engl J Med, 1972. **287**: p. 553-5.

17. Pugin, J., *Toll-like receptors*, in *Evolving concepts in sepsis and septic shock*, P. Eichacker and J. Pugin, Editors. 2001, Kluwer Academic Publishers: Norwell.

18. Cinel, I. and S. Opal, *Molecular biology of inflammation and sepsis: A primer.* Crit Care Med, 2009. **37**: p. 291-304.

19. Kotsovolis, G. and K. Kallaras, *The role of endothelium and endogenous vasoactive substances in sepsis.* Hippokratia, 2010. **14**: p. 88-93.

20. Biss, T. and J. Wallace-Jonathan, *Hematological and coagulation changes in sepsis*, in *Sepsis: Competency-Based Critical Care*, S. Baudouin, Editor. 2008, Springer: London.

21. Yang, K., Q.-H. Shi, and Y. Sun, *Modeling and simulation of protein uptake in cation exchanger visualized by confocal laser scanning microscopy.* Journal of Chromatography A, 2006. **1136**: p. 19-28.

22. Levy, M., et al., *2001 SCCM/ESICM/ACCP/ATS/SIS International Sepsis Definitions conference.* Intensive Care Med, 2003. **29**: p. 530-538.

23. Remick, D., *Pathophysiology of sepsis.* Am J Pathol, 2007. **170**: p. 1435-44.

24. Opal, S. and V. DePalo, *Anti-inflammatory cytokines.* Chest, 2000. **117**: p. 1162-72.

25. Wang, H. and S. Ma, *The cytokine storm and factors determining the sequence and severity of organ dysfunction in multiple organ dysfunction syndrome.* Am J Emerg Med, 2008. **26**: p. 711-5.

26. Bone, R., C. Fisher, and T. Clemmer, *A controlled clinical trial of high-dose methylprednisolone in the treatment of sever sepsis and septic shock.* N Engl J Med, 1987. **317**: p. 653-658.

27. Marshall, J.C., *Such stuff as dreams are made on: mediator-targeted therapy in sepsis.* Nat Rev Drug Discov, 2003. **2**: p. 391-405.

28. Bone, R., *Why sepsis trials fail.* J Am Med Assoc, 1996. **276**: p. 565-566.

29. Hotchkiss, R. and I. Karl, *The pathophysiology and treatment of sepsis.* N Engl J Med, 2003. **348**: p. 138-150.

30. Hotchkiss, R. and S. Opal, *Immunotherapy for sepsis - a new approach against an ancient foe.* N Engl J Med, 2010. **363**: p. 87-89.

31. Oberholzer, A., C. Oberholzer, and L. Moldawer, *Sepsis syndromes: understanding the role of innate and acquired immunity.* Shock, 2001. **16**: p. 83-96.

32. Limaye, A., et al., *Cytomegalovirus reactivation in critically ill immunocompetent patients.* J Am Med Assoc, 2008. **300**(413-22).

33. Hollenberg, S., et al., *Practice parameters for hemodynamic support of sepsis in adult patients: 2004 update.* Crit Care Med, 2004. **32**: p. 1928-48.

34. Dellinger, R., et al., *Surviving Sepsis Campaign: international guidelines for management of severe sepsis and septic shock: 2008.* Intensive Care Med, 2008. **34**: p. 17-60.

35. Rivers, E., B. Nguyen, and S. Havstad, *Early goal-directed therapy in the treatment of sepsis and septic shock.* N Engl J Med, 2001. **345**: p. 1368-77.

36. Beal, A. and F. Cerra, *Multiple organ failure syndrome in the 1990s: systemic inflammatory response and organ dysfunction.* J Am Med Assoc, 1994. **271**: p. 226-233.

37. Sevransky, J. and C. Natanson, *Anti-inflammatory therapy in sepsi*, in *Evolving concepts in sepsis and septic shock*, P. Eichacker and J. Pugin, Editors. 2001, Kluwer Academic Publishers: Norwell.

38. Volk, H., et al., *Immunostimulation in sepsis*, in *Evolving concepts in sepsis and septic shock*, P. Eichacker and J. Pugin, Editors. 2001, Kluwer Academic Publishers: Norwell.

39. Docke, W., F. Randow, and U. Syrbe, *Monocyte deactivation in septic patients: restoration by IFN-gamma treatment.* Nat Med, 1997. **3**: p. 678-81.

40. Root, R., et al., *Multicenter, double-blind, placebo-controlled study of the use of filgrastim in patients hospitalized with pneumonia and sever sepsis.* Crit Care Med, 2003. **31**: p. 367-73.

41. Nelson, S., et al., *A randomized controlled trial of filgrastim as an adjunct to antibiotics for treatment of hospitalized patients with community-acquired pneumonia. CAP study group.* J Infect Dis, 1998. **178**: p. 1075-80.

42. Warren, B., et al., *Caring for the critically ill patient. High-dose antithrombin III in sever sepsis: A randomized controlled trial.* J Am Med Assoc, 2001. **286**: p. 1869-78.

43. Abraham, E., et al., *Efficacy and safety of tifacogin (recombinant tissue factor pathway inhibitor) in sever sepsis: A randomized controlled trial.* J Am Med Assoc, 2003. **290**: p. 238-47.

44. Bernard, G., et al., *Efficacy and safety of recombinant human activated protein C for sever sepsis.* N Engl J Med, 2001. **344**: p. 669-709.

45. Mackenzie, A., *Activated protein C: Do more survive?* Intensive Care Med, 2005. **31**: p. 1624-26.

46. Abraham, E., et al., *Drotrecogin alfa (activated) for adults with sever sepsis and a low risk of death.* N Engl J Med, 2005. **353**: p. 1332-41.

47. Rimmele, T. and J.A. Kellum, *Clinical review: Blood purification for sepsis.* Critical Care, 2011. **15**: p. 205-15.

48. Suzuki, H. and H. Hirasawa, *Acute blood purification*. Contributions to nephrology, ed. C. Ronco. Vol. 166. 2010, Basel: Karger.

49. Kaizu, K., et al., *Current status of blood purification in critical care in Japan*, in *Acute Blood Purification*, H. Suzuki and H. Hirasawa, Editors. 2010, Karger: Basel.

50. Kellum, J.A. and S. Uchino, *International differences in the treatment of sepsis: Are they justified?* J Am Med Assoc, 2009. **301**: p. 2496-7.

51. Honore, P. and J. Matson, *Extracorporeal removal for sepsis: acting at the tissue level - the beginning of a new era for this treatment modality in septic shock.* Crit Care Med, 2004. **32**: p. 896-7.

52. Ronco, C., et al., *Interpreting the mechanisms of continuous renal replacement therapy in sepsis: the peak concentration hypothesis.* Artif Organs, 2003. **27**: p. 792-801.

53. Peng, Z., et al., *Blood purification in sepsis: a new paradigm.* Contrib. Nephrol., 2010. **165**: p. 322-328.

54. Marshall, J.C., D. Foster, and J. Vincent, *Diagnostic and prognostic implications of endotoxaemia in critical illness. Results of the MEDIC trial.* J Infect Dis, 2004. **190**: p. 527-34.

55. van Deventer, S., et al., *Experimental endotoxemia in humans: analysis of cytokine release and coagulation, fibrinolytic, and complement pathways.* Blood, 1990. **76**: p. 2520-26.

56. Davies, B. and J. Cohen, *Endotoxin removal devices for the treatment of sepsis and septic shock.* Lancet Infect Dis, 2011. **11**: p. 65-71.

57. Li, J., R. Nation, and J. Turnidge, *Colistin: the re-emerging antibiotic for multidrug-resistant gram-negative bacterial infections.* Lancet Infect Dis, 2006. **6**: p. 589-601.

58. Cohen, J., M. Aslam, and C.R. Pusey, CJ, *Protection from endotoxemia: a rat model of plasmapheresis and specific adsorption with polymyxin B.* J Infect Dis, 1987. **155**: p. 690-95.

59. Vincent, J., P. Laterre, and J. Cohen, *A pilot-controlled study of a polymyxin-B immobilized hemoperfusion cartridge in patients with sever sepsis secondary to intra-abominal infection.* Shock, 2005. **23**: p. 400-05.

60. Cruz, D., M. Antonelli, and R. Fumagalli, *Early use of polymyxin B hemoperfusion in abdominal septic shock: the EUPHAS randomized controlled trial.* J Am Med Assoc, 2009. **301**: p. 2445-52.

61. Vincent, J., *Polymyxin B hemoperfusion and mortality in abdominal septic shock.* J Am Med Assoc, 2009. **302**: p. 1968.

62. Rachoin, J., D. Foster, and R. Dellinger, *Endotoxin removal: how far from the evidence? From EUPHAS to EUPHRATES.* Contrib. Nephrol., 2010. **167**: p. 111-8.

63. Martin, E., et al., *Endotoxin removal: how far from the evidence? The EUPHAS 2 Project.* Contrib. Nephrol., 2010. **167**: p. 119-25.

64. Cole, L., et al., *A phase II randomized, controlled trial of continuous hemofiltration in sepsis.* Crit Care Med, 2002. **30**: p. 100-106.

65. Payen, D., et al., *Impact of continuous venovenous hemofiltration on organ failure during the early phase of sever sepsis: a randomized controlled trial.* Crit Care Med, 2009. **37**(803-10).

66. Bellomo, R., I. Baldwin, and C. Ronco, *High-volume hemofiltration*, in *Blood Purification in Intensive Care*, C. Ronco, R. Bellomo, and G. La Grecca, Editors. 2001, Karger: Basel.

67. Cole, L., et al., *High-volume haemofiltration in human septic shock.* Intensive Care Med, 2001. **27**: p. 978-86.

68. Boussekey, N., et al., *A pilot randomized study comparing high and low volume hemofiltration on vasopressor use in septic shock.* Intensive Care Med, 2008. **34**: p. 1646-53.

69. Honore, P., et al., *Prospective evaluation of short-term, high-volume isovolemic hemofiltration on the hemodynamic course and outcome in patients with intractable circulatory failure resulting from septic shock.* Crit Care Med, 2000. **28**: p. 3581-7.

70. Joannes-Boyau, O., et al., *Impact of high volume hemofiltration on hemodynamic disturbance and outcome during septic shock.* ASAIO, 2004. **50**: p. 102-9.

71. Rimmele, T., et al., *Hemofiltration with the Cascade system in an experimental porcine model of septic shock.* Therapeutic Apheresis and Dialysis, 2009. **13**: p. 63-70.

72. Cole, L., et al., *The effect of coupled haemofiltration and adsorption on inflammatory cytokines in an ex vivo model.* Nephrol Dial Transplant, 2002. **17**: p. 1950-56.

73. Haase, M., et al., *High cut-off point membranes in septic acute renal failure: a systematic review.* Int J Artif Organs, 2007. **30**: p. 1031-41.

74. Rimmele, T., et al., *High-volume haemofiltration with a new hemofiltration membrane having enhanced adsorption properties in septic pigs.* Nephrol Dial Transplant, 2009. **24**: p. 421-27.

75. Joannes-Boyau, O., et al., *Are the synergistic effects of high-volume haemofiltration and enhanced adsorption the missing key in sepsis modulation?* Nephrol Dial Transplant, 2009. **24**: p. 354-7.

76. Winchester, J., et al., *Sorbents in acute renal failure and the systemic inflammatory response syndrome.* Blood Purification, 2003. **21**: p. 79-84.

77. Kellum, J.A. and M. Dishart, *Effect of hemofiltration filter adsorption on circulating IL-6 levels in septic rats.* Crit Care, 2000. **6**: p. 429-33.

78. De Vriese, A., et al., *Cytokine removal during continuous hemofiltration in septic patients.* J Am Soc Nephrol, 1999. **10**: p. 846-53.

79. Taniguchi, T., et al., *A novel adsorbent of circulating bacterial toxins and cytokines: the effect of direct hemoperfusion with CTR column for the treatment of experimental endotoxemia.* Crit Care Med, 2006. **34**: p. 800-6.

80. Ljunglof, A. and R. Hjorth, *Confocal microscopy as a tool for studying protein adsorption to chromatographic matrices.* Journal of Chromatography A, 1996. **743**(1): p. 75-83.

81. Hubbuch, J., et al., *Mechanism and kinetics of protein transport in chromatographic media studied by confocal laser scanning microscopy, Part 1. The interplay of sorbent structure and fluid phase conditions.* Journal of Chromatography A, 2003. **1021**: p. 93-104.

82. Ljunglof, A., et al., *Direct visualisation of plasmid DNA in individual chromatography adsorbent particles by confocal scanning laser microscopy.* Journal of Chromatography A, 1999. **844**(1-2): p. 129-135.

83. Zhou, X.-P., et al., *Analysis of mass transport models for protein adsorption to cation exchanger by visualization with confocal laser scanning microscopy.* Journal of Chromatography A, 2006. **1103**: p. 110-117.

84. Ljunglof, A. and J. Thommes, *Visualising intraparticle protein transport in porous adsorbents by confocal microscopy.* Journal of Chromatography A, 1998. **813**: p. 387-395.

85. Harinarayan, C., et al., *An exclusion mechanism in ion exchange chromatography.* Biotechnology and Bioengineering, 2006. **95**(5): p. 775-787.

86. Kasche, V., et al., *Direct observation of intraparticle equilibration and the rate-limiting step in adsorption of proteins in chromatographic adsorbents with confocal laser scanning microscopy.* Journal of Chromatography B, 2003. **790**: p. 115-129.

87. Hubbuch, J., et al., *Dynamics of protein uptake within the adsorbent particle during packed bed chromatography.* Biotechnology and Bioengineering, 2002. **80**(4): p. 359-368.

88. Hubbuch, J. and M.R. Kula, *Confocal laser scanning microscopy as an analytical tool in chromatographic research.* Bioprocess Biosyst Eng, 2008. **31**: p. 241-259.

89. Lundberg, E., et al., *A novel method for reproducible fluorescent labeling of small amounts of antibodies on solid phase.* Journal of Immunological Methods, 2007. **322**: p. 40-49.

90. Song, M., et al., *Cytokine removal with a novel adsorbent polymer.* Blood Purification, 2004. **22**(5): p. 428-434.

91. DiLeo, M.V., J.D. Fisher, and W.J. Federspiel, *Experimental validation of a theoretical model of cytokine capture using a hemoadsorption device.* Annals of Biomedical Engineering, 2009. **37**(11): p. 2310-6.

92. Schroder, M., E. von Lieres, and J. Hubbuch, *Direct quantification of intraparticle protein diffusion in chromatographic media.* J. Phys. Chem. B, 2006. **110**: p. 1429-1436.

93. Sharma, U. and J.D. Carbeck, *Hydrodynamic radius ladders of proteins.* Electrophoresis, 2005. **26**(11): p. 2086-2091.

94. Bassingthwaighte, J.B., *A practical extension of hydrodynamic theory of porous transport for hydrophilic solutes.* Microcirculation, 2006. **13**: p. 111-118.

95. Beck, R. and J. Schultz, *Hindered diffusion in microporous membranes with known pore geometry.* Science, 1970. **170**(3964): p. 1302-1305.

96. Renkin, E.M., *Filtration, diffusion, and molecular sieving through porous cellulose membranes.* J. Gen. Physiology, 1954. **38**: p. 225-243.

97. Susanto, A., T. Herrmann, and J. Hubbuch, *Short-cut method for the correction of light attenuation influences in the experimental data obtained from confocal laser scanning microscopy.* Journal of Chromatography A, 2006. **1136**: p. 29-36.

98. Linden, T., et al., *Visualizing patterns of protein uptake to porous media using confocal laser scanning microscopy.* Separation Science and Technology, 2002. **37**(1): p. 1-32.

99. Kimmel, J.D., et al., *IL-6 adsorption dynamics in hemoadsorption beads studied using confocal laser scanning microscopy.* J Biomed Mater Res B Appl Biomater, 2010. **92**(2): p. 390-396.

100. Noriega, J.A., et al., *Modeling column regeneration effects on dye-ligand affinity chromatography.* Biotechnol. Prog., 1997. **13**: p. 296-300.

101. Horstmann, B.J. and H.A. Chase, *Rate-limiting mass transfer in immunosorbents: characterisation of the adsorption of paraquat-protein conjugates to anti-paraquat Sepharose 4B.* Bioseparation, 1998. **7**: p. 145-157.

102. Bak, H., O.R.T. Thomas, and J. Abildskov, *Lumped parameter model for prediction of initial breakthrough profiles for the chromatographic capture of antibodies from a complex feedstock.* Journal of Chromatography B, 2007. **848**: p. 131-141.

103. House, A.H. and C. Ronco, *Extracorporeal blood purification in sepsis and sepsis-related acute kidney injury.* Blood Purification, 2008. **26**: p. 30-35.

104. Li, L., J. Pan, and Y. Yu, *Development of sorbent therapy for multiple organ dysfunction syndrome (MODS).* Biomed. Mater., 2007. **2**: p. R12-R16.

105. Gallant, S.R., *Modeling ion-exchange adsorption of proteins in a spherical particle.* Journal of Chromatography A, 2004. **1028**: p. 189-195.

106. Linden, T., et al., *Visualizing two-component protein diffusion in porous adsorbents by confocal scanning laser microscopy.* Biotechnology and Bioengineering, 1999. **65**(6): p. 622-630.

107. Finette, G.M., et al., *Adsorption behavior of multicomponent protein mixtures containing r1-proteinase inhibitor with the anion exchanger, 2-(diethylamino)ethyl-Spherodex.* Biotechnol. Prog., 1997. **13**: p. 265-275.

108. Skidmore, G.L. and H.A. Chase, *Two-component protein adsorption to the cation exchanger S Sepharose FF.* Journal of Chromatography A, 1990. **505**: p. 329-347.

109. Lewus, R.K. and G. Carta, *Binary protein adsorption on gel-composite ion-exchange media.* AIChE Journal, 1999. **45**(3): p. 512-522.

110. Martin, C., et al., *Two-component protein adsorption kinetics in porous ion exchange media.* Journal of Chromatography A, 2005. **1079**: p. 105-115.

111. Brooks, C.A. and S.M. Cramer, *Steric mass-action ion exchange: displacement profiles and induced salt gradients.* AIChE Journal, 1992. **38**: p. 1969-1978.

112. Aggarwal, B., *Signalling pathways of the TNF superfamily: a doubleedged sword.* Nat Rev Immunology, 2003. **3**: p. 745-756.

113. Bazzoni, F. and B. Beutler, *The tumor necrosis factor ligand and receptor families.* N Engl J Med., 1996. **334**(26): p. 1717-25.

114. Michie, H., et al., *Detection of circulating tumor necrosis factor after endotoxin administration.* N Engl J Med, 1988. **318**: p. 1481-1486.

115. Eck, M.J. and S.R. Sprang, *The structure of tumor necrosis factor-alpha at 2.6A resolution: implications for receptor binding.* J. Biological Chemistry, 1989. **264**(29): p. 17595-17605.

116. Naismith, J.A., et al., *Structures of the extracellular domain of the type I tumor necrosis factor receptor.* Structure, 1996. **4**: p. 1251-1262.

117. Banner, D.W., et al., *Crystal structure of the soluble human 55 kd TNF receptor-human TNFB complex: Implications for TNF receptor activation.* Cell, 1993. **73**: p. 431-445.

118. Idriss, H. and J.A. Naismith, *TNFα and the TNF receptor superfamily: Structure-function relationship(s).* Microscopy Research and Technique, 2000. **50**: p. 184-195.

119. Petersen, C.M., et al., *Bioactive human recombinant tumor necrosis factor-α: an unstable dimer?* Eur. J. of Immunology, 1989. **19**(10): p. 1887-1894.

120. Moller, B., et al., *Bioactive and inactive forms of tumor necrosis factor-α in spinal fluid from patients with meningitis.* J. Infectious Diseases, 1991. **163**: p. 886-889.

121. Corti, A., et al., *Oligomeric tumour necrosis factor a slowly converts into inactive forms at bioactive levels.* Biochem. J., 1992. **284**: p. 905-910.

122. Mancini, F., et al., *Inhibition of tumor necrosis factor-α (TNF-α)/TNF-α receptor binding by structural analogues of suramin.* Biochemical Pharmacology, 1999. **58**: p. 851-859.

123. Alzani, R., et al., *Suramin induces deoligomerization of human tumor necrosis factor-α.* J. Biological Chemistry, 1993. **268**(17): p. 12526-29.

124. He, M.M., et al., *Small-molecule inhibition of TNF-α.* Science, 2005. **310**(5750): p. 1022-1025.

125. Tracey, D., et al., *Tumor necrosis factor antagonist mechanisms of action: A comprehensive review.* Pharmacology & Therapeutics, 2008. **117**: p. 244-279.

126. Scallon, B., et al., *Binding and functional comparisons of two types of tumor necrosis factor antagonists.* J Pharmacol Exp Ther., 2002. **301**(2): p. 418-426.

127. Clark, M.A., et al., *Effect of a chimeric antibody to tumor necrosis factor-alpha on cytokine and physiologic responses in patients with severe sepsis-A randomized, clinical trial.* Crit Care Med, 1998. **26**: p. 1650-1659.

128. Opal, S., et al., *Efficacy of a monoclonal antibody directed against tumor necrosis factor in protecting neutropenic rats from lethal infection with Pseudomonas aeruginosa.* J Infect Dis, 1990. **161**: p. 1148-1152.

129. Miwa, K., et al., *A novel blood purification therapy for the treatment of Gram-positive bacterial sepsis.* Jpn J Apher, 2005. **24**: p. 244-249.

130. Tsuchida, K., et al., *Blood purification for critical illness: cytokines adsorption therapy.* Therapeutic Apheresis and Dialysis, 2006. **10**(1): p. 25-31.

131. Sandeman, S.R., et al., *Inflammatory cytokine removal by an activated carbon device in a flowing system.* Biomaterials, 2008. **29**: p. 1638-1644.

132. Miwa, K., et al., *Preparation of a superantigen-adsorbing device and its superantigen removal efficacies in vitro and in vivo.* Int J Infect Dis, 2003. **7**: p. 21-28.

133. DiLeo, M.V., et al., *Selective improvement of TNF capture in a cytokine hemoadsorption device using immobilized anti-TNF*. J Biomed Mater Res B Appl Biomater, 2010. **In press**.

134. Weber, V., et al., *Efficient adsorption of tumor necrosis factor with an in vitro set-up of the microspheres-based detoxification system.* Blood Purification, 2007. **25**(2): p. 169-174.

135. Aderka, D., et al., *Stabilization of the bioactivity of tumor necrosis factor by its soluble receptors.* J. Exp. Med., 1992. **175**: p. 323-329.

136. Smith, R.A. and C. Baglioni, *The active form of tumor necrosis factor is a trimer.* J. Biological Chemistry, 1987. **262**(15): p. 6951-6954.

137. Froon, A.H., et al., *Increased plasma concentrations of soluble tumor necrosis factor receptors in sepsis syndrome: Correlation with plasma creatine values.* Crit Care Med, 1994. **22**: p. 803-809.

138. Seckinger, P. and J. Dayer, *Natural inhibitors of TNF*, in *Tumor Necrosis Factor. Structure, Function and Mechanism of Action*, B. Aggarwal and J. Vilcek, Editors. 1991: New York. p. 217-236.

139. Neilson, D.N., J.P. Kavanagh, and P.N. Rao, *Kinetics of circulating TNF-α and TNF soluble receptors following surgery in a clinical model of sepsis.* Cytokine, 1996. **8**: p. 938-943.

140. Alzani, R., et al., *Mechanism of suramin-induced deoligomerization of tumor necrosis factor α.* Biochemistry, 1995. **34**: p. 6344-50.

141. Margolles-Clark, E., et al., *Small-molecule costimulatory blockade: organic dye inhibitors of the CD40–CD154 interaction.* J Mol Med, 2009. **87**: p. 1133-43.

142. Stopa, B., et al., *Albumin binds self-assembling dyes as specific polymolecular ligands.* Int J Biol Macromol, 2006. **40**: p. 1-8.

143. Poiesi, C., et al., *Kinetic analysis of the TNF-α oligomer-monomer transition by surface plasmon resonance and immunochemical methods.* Cytokine, 1993. **5**: p. 536-45.

144. Loshkin, A., et al., *Mechanisms of growth stimulation by suramin in non-small-cell lung cancer cell lines.* Cancer Chemother Pharmacol, 1999. **43**: p. 341-7.

145. Valenti, I.E., *Characterization of a novel sorbent polymer for the treatment of sepsis*, in *Bioengineering*. 2010, University of Pittsburgh: Pittsburgh.